DYNAMICS AND REAL-TIME OPTIMAL CONTROL OF SATELLITE ATTITUDE AND SATELLITE FORMATION SYSTEMS

A Dissertation

by

HUI YAN

Submitted to the Office of Graduate Studies of
Texas A&M University
in partial fulfillment of the requirements for the degree of

DOCTOR OF PHILOSOPHY

August 2006

Major Subject: Aerospace Engineering

DYNAMICS AND REAL-TIME OPTIMAL CONTROL OF SATELLITE ATTITUDE AND SATELLITE FORMATION SYSTEMS

A Dissertation

by

HUI YAN

Submitted to the Office of Graduate Studies of
Texas A&M University
in partial fulfillment of the requirements for the degree of

DOCTOR OF PHILOSOPHY

Approved by:

Chair of Committee,	Kyle T. Alfriend
Committee Members,	Goong Chen
	John L. Junkins
	Srinivas R. Vadali
Head of Department,	Helen Reed

August 2006

Major Subject: Aerospace Engineering

ABSTRACT

Dynamics and Real-Time Optimal Control of Satellite

Attitude and Satellite Formation Systems. (August 2006)

Hui Yan, B.Eng., Beijing Institute of Technology;

M.Eng., Northwestern Polytechnical University;

D.Eng, Northwestern Polytechnical University

Chair of Advisory Committee: Dr. Kyle T. Alfriend

In this dissertation the solutions of the dynamics and real-time optimal control of magnetic attitude control and formation flying systems are presented. In magnetic attitude control, magnetic actuators for the time-optimal rest-to-rest maneuver with a pseudospectral algorithm are examined. The time-optimal magnetic control is bang-bang and the optimal slew time is about 232.7 seconds. The start time occurs when the maneuver is symmetric about the maximum field strength. For real-time computations, all the tested samples converge to optimal solutions or feasible solutions. We find the average computation time is about 0.45 seconds with the warm start and 19 seconds with the cold start, which is a great potential for real-time computations. Three-axis magnetic attitude stabilization is achieved by using a pseudospectral control law via the receding horizon control for satellites in eccentric low Earth orbits. The solutions from the pseudospectral control law are in excellent agreement with those obtained from the Riccati equation, but the computation speed improves by one order of magnitude.

Numerical solutions show state responses quickly tend to the region where the attitude motion is in the steady state.

Approximate models are often used for the study of relative motion of formation flying satellites. A modeling error index is introduced for evaluating and comparing the accuracy of various theories of the relative motion of satellites in order to determine the effect of modeling errors on the various theories. The numerical results show the sequence of the index from high to low should be Hill's equation, non- J_2, small eccentricity, Gim-Alfriend state transition matrix index, with the unit sphere approach and the Yan-Alfriend nonlinear method having the lowest index and equivalent performance. A higher order state transition matrix is developed using unit sphere approach in the mean elements space. Based on the state transition matrix analytical control laws for formation flying maintenance and reconfiguration are proposed using low-thrust and impulsive scheme. The control laws are easily derived with high accuracy. Numerical solutions show the control law works well in real-time computations.

TO

YONGXIA, YIHANG, LINDSEY

ACKNOWLEDGMENTS

I am deeply indebted to the esteemed Dr. Alfriend for all he did for me during these years. Indeed, this dissertation could not have been done at all without him. I have learned many things from Dr. Alfriend, not only in aerospace, but also in many other areas. I could only do this job under his intelligent guidance and moral support. Thank you Dr. Alfriend for all you did for me. It's my honor to be one of your students.

I am very grateful to Dr. Vadali for all his help. He is a very knowledgeable person with a very kind personality. I would like to thank the prestigious Dr. Junkins for his wonderful teaching and guidance. I was also impressed with his superb driving on the curved mountain highways in Maui, Hawaii. Thanks to Dr. Chen for his encouragement and support during my studies.

My special thanks go to Dr. Michael Ross from the Department of Mechanical and Astronautical Engineering at the Naval Postgraduate School. It is Mike who introduced and guided me to the amazing world of pseudospectral methods and real-time computations.

I had many constructive discussions and collaborations with Dr. Gim, Dr. Vaddi, Dr. Lee and Prasenjit Sengupta and I am grateful to them. I also thank the faculty, staff and graduate students of the Department of Aerospace Engineering for their help and cooperation. I have had a pleasant time with them. Special gratitude is reserved for Ms. Lisa Willingham for her assistance to my many travels.

Finally, my thanks and greetings go to my dear wife, Yongxia, my lovable kids, Yihang and Lindsey. Yongxia does most of the housework while pursuing her Ph.D. studies. It would have been a hard time here without her understanding and support. I really enjoy staying with my family. No words can explain my deep feeling about my parents. They gave me the life which is a valuable treasure and even more importantly, they taught me about the values of life and how to live.

TABLE OF CONTENTS

LIST OF FIGURES

FIGURE Page

FIGURE Page

FIGURE Page

LIST OF TABLES

CHAPTER I

INTRODUCTION

Optimal control of nonlinear systems is currently one of the most active research subjects in control theory. Although there has been considerable research in this area for many years, efficiently solving optimal control problems remains a challenge. In particular, obtaining optimal solutions in real time is a major challenge. The objective of this dissertation is the solution of the dynamics and real-time optimal control of some important nonlinear aerospace systems.

1.1 Numerical Solutions of Optimal Control

Optimal control establishes a general theory to the minimization of a performance index and the satisfaction of constraints, which is capable of dealing with a large class of nonlinear control problems. There are two methods, direct and indirect, for numerically solving optimal control problems. The indirect method is based on the calculus of variations and Pontryagin's minimum principle, and leads to a two point boundary value problem (TPBVP). The TPBVP occurs during the process of solving a single or a set of differential equations whose solution has to satisfy both the given initial and final boundary conditions. Shooting methods play a significant role in solving the TPBVP[1]. Shooting methods use Newton's method to adjust variables to satisfy the boundary

---

This dissertation follows the style of *Journal of Guidance, Control, and Dynamics*.

conditions. Obtaining solutions using shooting methods strongly depends on the initial guess of the costates, especially for optimal control problems, since the sensitivity of the Euler-Lagrange equation is inherent. Moreover it is extremely difficult to guess the initial costates that generally have no obvious physical meanings.

Direct methods for solving optimal control problems are based on discretizing the infinite dimensional optimization problem and transforming it to a finite-dimensional nonlinear programming (NLP) problem[1,2]. Our approach to discretization is achieved by dividing the time interval into subintervals whose endpoints are called *nodes*. The NLP variables are the values of the states and controls at these nodes. In the standard collocation techniques that use piecewise polynomials, the state equations are replaced by a set of difference constraints. In this manner the original optimal control problem is transcribed to an NLP which can then be solved by a variety of solvers. These methods provide solutions to a vast class of complex problems with a relatively wide radius of convergence and no reliance on satisfying the calculus of variation necessary conditions. In these two aspects, the direct methods avoid some of the pitfalls of the indirect methods, which are based on solving the necessary conditions derived from Pontryagin's minimum principle. The solution of the resulting TPBVP is not easy to obtain for all problems, for instance, for bounded controls with switches, it requires an a priori guess for the bang-bang control structure. In addition, the indirect methods suffer from a small radius of convergence: for most complex problems convergence to the optimal solution is obtained only with excellent initial guesses for the states and costates. Except for some simple dynamical models, finding an accurate guess for the costates that have no

physical interpretation is a hard task. Consequently, direct methods are often the choice for solving complex trajectory optimization problems.

Although the direct methods, in particular direct transcription methods, offer the aforementioned advantages over indirect methods, it is well known[1] that the direct solutions may not be as accurate as those obtained from the indirect methods, since we use a finite parametric representation to approximate continuous systems. From a practical point of view one is willing to forgo some level of accuracy. However, if the direct solutions yield feasible solutions that are far from optimal, it is often advantageous to determine the optimal solution, since the direct solutions can provide a good initial guess for the indirect methods. But the question remains: How does one know whether a direct solution is indeed sufficiently accurate? One possible answer would be to increase the number of nodes, but this approach can be flawed since it presumes convergence of the discretization scheme and convergence of the NLP solver. By the convergence of the discretization scheme we mean the convergence of the discretized problem to the optimal control problem as the number of nodes tends to infinity. The convergence of the NLP solver on the other hand, refers to the convergence of the NLP algorithm for a fixed number of nodes. In view of these two fundamentally distinct convergence issues, it is apparent that the NLP algorithm may fail due to possible ill-conditioning of the computed matrices and other challenges associated with iteration when there are a large number of variables. Thus, alternative approaches must be adopted to validate the accuracy of the direct solution. Yan, Fahroo and Ross[3]and Williams[4] have provided accuracy and computation efficiency comparisons of direct transcription methods.

1.2 Pseudospectral Methods

For a given problem, the accuracy of the direct solutions is dependent on several factors: the type and accuracy of the discretization scheme, the number and choice of the nodes, and the NLP solver. Further, the approximation of the original optimal control problem is achieved at two levels: one is the approximation of the continuous problem by the transcription method, and the other are the approximations performed by the NLP solver itself. In order to ensure convergence with a high degree of accuracy at both these levels one need to use an accurate discretization scheme, as well as a reliable, robust and accurate NLP solver. Convergence at both of these levels is dependent on the dimension of the NLP variable vector. Higher order discretization schemes, such as the Hermite-Simpson, offer a 4^{th} order local error as opposed to the trapezoidal rule which has a 2^{nd} order local error[5]. The use of higher order schemes allows using fewer NLP nodes for the same degree of accuracy. A smaller size NLP problem results in a more efficient and more robust solution. Herman and Conway[6] developed higher-order Gauss-Lobatto quadrature rules for use with collocation to get a higher order of accuracy. Elnagar et al [7,8] and Ross and Fahroo [9-13] employed the Legendre spectral collocation method for solving a variety of optimal control problems, and showed that highly accurate results can be obtained with a low degree of discretization. Qong, et al[14] showed pseudospectral methods offer Eulerian-like simplicity while providing very fast convergence rates known as spectral accuracy. The Legendre spectral collocation method is a fundamentally different transcription method where the nodes are fixed to be the

Legendre-Gauss-Lobatto (LGL) points. The LGL points offer the "best" discretization in the sense of minimal least-square error. The time derivative of the state vector is expressed in terms of the state vector at the collocation points by the use of a differentiation matrix. In this dissertation, we use a pseudospectral method to solve nonlinear optimal control problems, which has been implemented in the DIDO (Direct and Indirect Dynamic Optimization) [15] software. Over the last few years, DIDO has emerged as a new commercial software package for numerically solving optimal control problems.[9-13, 16-17] The software can be purchased from the website www.tomlab.biz.

1.3 Real-Time Optimal Control

Recently there has been significant interest in real-time optimal control due to its feedback property. From optimal control theory, the solved control is an open-loop function of time history. With no errors, the effect of the open loop optimal control is equivalent to a feedback control. Sometimes we may not need real-time optimization since we can schedule optimal control in advance or on the ground for aerospace applications. However, disturbances always exist and measurements are not perfect, so we should apply a receding horizon control (RHC) or model predictive control (MPC) to obtain real-time optimal control to reject disturbances. RHC is a form of control in which the current control sequence is obtained by solving a real-time optimal control with a finite horizon based on the current measurements, and the first control in the sequence is applied and the optimization is repeated at each subsequent time step to get a feedback control.[18] RHC and MPC have witnessed many successful applications in the

process industries where the plants controlled are sufficiently 'slow' to permit its implementation. Due to the complexity of solving the nonlinear optimal control problem in real-time, the computational time delay cannot be ignored. This is particularly important in aerospace applications, where the time scales of the spacecraft dynamics can be very short and comparable to the time required to solve a finite-horizon optimization problem.[19] However, it is not trivial to efficiently solve the optimal control problem, especially in a real-time manner. Junkins and Carrington in their pioneering work[20] developed time-optimal attitude maneuver formulations leading to a simple one-dimensional two-point boundary-value problem. In May 1981, the NOVA-1 spacecraft was launched, and several large-angle, minimum time maneuvers were carried out by using ground-based computers to generate the commands for the first near real-time implementation of an optimal control derived from indirect methods[21]. These seven to ten hour maneuver solution curve recomputed is about five minutes on the ground and uploaded to the spacecraft. It has been shown that direct methods can numerically solve optimal control problems efficiently and accurately, but solving the real-time optimal control problem has made little progress until recently because of the difficulties arising. Computing speed and the assurance of a reliable solution in real-time have been the major limiting factors in applying real-time optimal control.[22] Recent advancements in computational power and algorithms have made possible the exploitation of pseudospectral methods for real-time optimal control. What distinguishes pseudospectral methods from the other direct methods is the use of global orthogonal polynomials as the trial functions, such as Legendre and Chebyshev polynomials. This global orthogonality

and the use of Gaussian quadrature rules create simple rules for transferring an original underlying infinite dimension problem into a low finite dimension system of algebraic equations with spectral convergence rates. Recent developments have shown that pseudospectral methods have become a promising tool for performing real-time computations of optimal control problems.[23-29]

1.4 Pseudospectral Control Law

Orthogonal polynomials have been used extensively in solving optimal control problems. In particular, their use in solving linear time-varying (LTV) optimal problems has been widespread. Hwang and Chang[30] used shifted Legendre polynomials, whereas Chou and Horng[31] used Chebyshev polynomials for solving LTV problems. More recently, Razzaghi[32] employed a Fourier series method for solving this class of problems. The common approach in these papers is to first expand the state and control variables as a generalized Fourier series with the appropriate orthogonal functions as the basis functions. Then the orthogonality of these functions is used to arrive at simplified expressions for forward and backward integration matrices. These matrices, in turn, are used to express the state transition matrices in the optimal law in terms of unknown coefficients of expansion.

Another approach has been to use orthogonal polynomials in the context of pseudospectral methods.[7-17, 33] Through the use of a spectral differentiation matrix, the optimal control problem is transformed into a nonlinear programming problem. Thus, it is apparent that for linear systems with quadratic cost criteria, the optimal control

problem can easily be transformed to a quadratic programming (QP) problem (a quadratic cost function subject to linear algebraic constraints).[8] This method is in sharp contrast to prior work using orthogonal polynomials that rely on approximating the two point boundary value problem derived from the necessary conditions. Recently, Lu[34] approximated the related receding horizon problem for LTV systems to a QP problem. Based on Simpson –trapezoid approximations for the integral and Euler type approximations for the derivatives he approximated the LTV systems to a QP and then derived analytical control laws. Whereas Elnager et al[8] and Williams[35-36] chose to solve their QP problem numerically, Lu used the analytical solution. In both methods, by using a direct approach (avoiding the solution of the necessary conditions), one avoids the pitfalls of the indirect methods such as integrating the Riccati equation. However in Elnager's approach, the solution maybe not be as accurate as the indirect methods, and in Lu's method, finding higher order control laws for step by step replacements for the states can be too tedious.

Recently, Fahoo and Ross[37] proposed the indirect pseudospectral method for solving optimal control problems. In this method, the two point boundary value problem (TPBVP) arising from the necessary conditions is solved by spectral collocation. For general nonlinear problems the resulting set of algebraic equations that approximate the boundary-value problem are nonlinear and an iterative technique is necessary. However, for LTV systems with a quadratic cost function the algebra is linear. Thus, well-known methods from linear algebra can be used to solve the TPBVP. Ref. 38 compared pseudospectral techniques to Ricatti methods in solving LQR problems and showed that

there is a huge reduction in the number of equations to be solved and the required computer memory storage. Here we will show that this linear transformation is numerically very efficient and hence can be computed on-line. This generates a linear feedback law for the controls when the "initial" time t_0 is replaced by the current time t.[24,39-41]

1.5 Optimal Magnetic Attitude Control

Magnetic actuators have been used for momentum dumping of both low and high altitude satellites, and for the attitude control of momentum biased spacecraft, primarily those in low Earth orbit. Of late, magnetic actuators have also been proposed as a sole means for attitude control, particularly for small inexpensive spacecraft. Here we investigate the use of magnetic actuators for the time-optimal slew maneuver towards the goal of conducting a flight test for NPSAT1[42], an experimental satellite being built at the Naval Postgraduate School (NPS). We use pseudospectral methods with the aid of the reusable software package, DIDO, to solve the time-optimal slew maneuver using magnetic actuators in a real-time manner.[25] After the final attitude is reached, we apply the pseudospectral control law to also stabilize the attitude using magnetic torque.

1.6 Reconfiguration and Maintenance of Formation Flying

Formation flying control includes reconfiguration and maintenance. Reconfiguration means transferring from one formation configuration to another one. Usually formation configurations are designed to be stable or bounded, which can be done through the

choice of the formation initial conditions. The objective of maintenance is to maintain the formation configuration in the presence of measurement errors and perturbations, such as the Earth's gravitational field, atmospheric drag, etc. We choose projected circular orbits (PCO)[43] as examples and use the pseudospectral control law based on the state transition matrix (STM) to control the reconfiguration and reject disturbances.

1.7 Outline

Chapter II provides the basic mathematics background and procedure of using pseudospectral methods to solve real-time optimal control problems. For linear time-varying systems, the analytical pseudospectral control laws are derived for real-time implementation. The control laws can be used for tracking, targeting and rendezvous problems. In this chapter, several methods are introduced to reduce computation time for solving nonlinear optimal control problems, including warm start techniques, use of an analytical Jacobian matrix, model reductions and compensation techniques for time delay. RHC or MPC are described to implement real-time optimal control. An inverted pendulum problem is used to demonstrate real-time applications.

In Chapter III nonlinear magnetic attitude motion is set up and analyzed using a rotating Earth magnetic field. Based on the dynamic model, we investigate the use of magnetic actuators for the time-optimal slew maneuver using a pseudospectral algorithm implemented in the reusable software package, DIDO. After the final attitude is reached, we apply the pseudospectral control law to stabilize the attitude also using magnetic torque in circular and eccentric orbits. The parameters of the example problem

correspond to that of NPSAT1, a small satellite being built at the Naval Postgraduate School. Numerical experiments reveal that real-time optimal magnetic maneuvers and three-axis magnetic attitude stabilizations can be easily obtained.

Chapter IV focuses on the dynamics and control of formation flying. The dynamics models are described and propagated in the mean elements space to accommodate higher order gravity perturbations. Three kinds of periodic matching conditions are introduced in the chapter. The model index concept is proposed to compare and evaluate relative motion theories. The higher order state transition matrix is developed using unit sphere approach in the mean elements space. Based on the state transition, we propose analytical control laws for formation flying maintenance and reconfiguration.

Finally the conclusion remarks are in Chapter V.

CHAPTER II

SOLVING REAL-TIME OPTIMAL CONTROL USING PSEUDOSPECTRAL METHODS

The main feature of the direct methods is to use finite basis functions, which can be denoted by parameter variables, to approximate continuous systems. The major direct methods include pseudospectral methods[7-17], Hermite collocation[44,5-6], B-spline approximation[19] and Euler discretization[45-47]. We require the basis functions to be easily and efficiently operated for differentiation and integration. In this chapter we investigate pseudospectral methods, derive analytical feedback control laws for linear time-varying systems, and discuss real-time applications of pseudospectral methods. An inverted pendulum problem is used to demonstrate real-time implementation[26].

2.1 Solving Optimal Control Using Pseudospectral Methods

2.1.1 Pseudospectral Methods

Spectral methods, expansions based on global functions, are usually used to numerically approximate the solutions to partial or ordinary differential equations. Assume a general differential equation

$$\dot{X} = f(X(t), t) \tag{2.1}$$

The solution is then approximated using spectral methods[48]

$$X(t) \approx X^N(t) = \sum_{k=0}^{N} a_k \phi_k(t) \tag{2.2}$$

where the basis functions, $\phi_k(t)$, are smooth global functions. The function class that has proven to be the most successful by far is orthogonal polynomials of Jacobi type, with Legendre or Chebyshev orthogonal polynomials as the most important special cases. The polynomials have the following characteristics[48]:

- Gaussian integration formulas achieve a high accuracy by using zeros of orthogonal polynomials as nodes.
- Singular Sturm-Liouville eigensystems are well known to offer excellent bases for approximation. The Jacobi polynomials are the only polynomials that arise in this way.
- Truncated expansions in Legendre polynomials are optimal in the L^2 norm.

Using the approximation, the residual of the differential equation is

$$R_N(t) = \dot{X}^N(t) - f\left(X^N(t), t\right) \tag{2.3}$$

The three most common types of spectral methods are Galerkin, tau, and collocation. The spectral collocation is also considered to be a pseudospectral method. The pseudospectral methods require that the coefficients a_k be selected so that the boundary conditions are satisfied, and also make the residual zero at the collocation points. In this dissertation, we use pseudospectral methods to numerically solve optimal control problems, where the basis functions consist of Legendre polynomials. In the pseudospectral methods, the values of $X^N(t)$ are given exactly by the coefficients a_k at

the collocation points. This is helpful in the discretization of continuous systems and coding of the optimization problems.

2.1.2 Optimal Control Model

Consider the following optimal control problem. Determine the control function $U(t) \in R^m$, and the corresponding state trajectory $X(t) \in R^n$, that minimize the Bolza cost function:

$$J_1 = M[X(t_0 + T), t_0 + T] + \int_{t_0}^{t_0+T} L(X, U)dt \tag{2.4}$$

subject to the nonlinear state dynamics

$$\dot{X}(t) = f(X(t), U(t)), \qquad t \in [t_0, t_0 + T] \tag{2.5}$$

and boundary conditions

$$\psi_0[X(t_0), t_0] = 0, \tag{2.6}$$

$$\psi_1[X(t_0 + T), t_0 + T] = 0, \tag{2.7}$$

where $\psi_0 \in R^p$ with $p \le n$ and $\psi_1 \in R^q$ with $q \le n$, t_0 is initial time and T is the simulation time. Possible control inequality constraints are formulated as

$$g[U(t), t] \le 0, \qquad g \in R^r \tag{2.8}$$

2.1.3 Numerical Solutions of Optimal Control Using DIDO

Since direct methods are used to solve optimal control problems, we need to discretize the continuous model system. We use the Legendre pseudospectral method

which has been implemented in DIDO. The basic idea of this method is to seek polynomial approximations for the state, costate and control functions in terms of their values at the Legendre-Gauss-Lobatto (LGL) points. The LGL points offer the "best" discretization in the sense of minimal least-square error. The time derivative of the state vector is expressed in terms of the state vector at the collocation points by the use of a differentiation matrix. The NLP formulation for the spectral method is as follows. Set

$$a_l := X(\tau_l), \quad b_l := U(\tau_l) \tag{2.9}$$

where τ_l are the LGL points, *l=0,1,…N*.

Let $L_N(\tau)$ be the Legendre polynomial of degree N on the interval [-1, 1]. In the Legendre collocation approximation of Eq. (2.5), we use the LGL points, $\tau_l, l = 0,\cdots,N$ which are given by

$$\tau_0 = -1, \qquad \tau_N = 1, \tag{2.10}$$

and for $1 \le l \le N-1$, the τ_l are the zeros of $\dot{L}_N$, the derivative of the Legendre polynomial L_N. For approximating the continuous equations, we seek a polynomial approximation of the form

$$X^N(\tau) = \sum_{l=0}^{N} X(\tau_l)\phi_l(\tau) \tag{2.11}$$

where for $l = 0,1,\cdots,N$

$$\phi_l(\tau) = \frac{1}{N(N+1)L_N(\tau_l)} \frac{(\tau^2-1)\dot{L}_N(\tau)}{\tau-\tau_l} \tag{2.12}$$

are the Lagrange polynomials of order N. It can be shown that

$$\phi_l(\tau_k) = \delta_{lk} = \begin{cases} 1 & \text{if } l = k \\ 0 & \text{if } l \neq k \end{cases} \tag{2.13}$$

From this property of ϕ_l it follows that

$$X^N(\tau_l) = X(\tau_l) \tag{2.14}$$

Generally the approximations are expressed as

$$X(\tau) \approx X^N \tag{2.15}$$

but in this collocation method, as stated in the Eq. (2.14), the values of the approximate state are given exactly by the value of the continuous functions at these points.

To express the derivative $\dot{X}^N$ in terms of $X^N(\tau)$ at the collocation points τ_l, we differentiate Eq. (2.11), which results in a matrix multiplication of the following forms:

$$c_k = \dot{X}^N(\tau_k) = \sum_{l=0}^{N} D_{kl} a_l \tag{2.16}$$

where the D_{kl} are entries of the $(N+1)\times(N+1)$ differentiation matrix D

$$D = [D_{kl}] = \begin{cases} \dfrac{L_N(\tau_k)}{L_N(\tau_l)} \dfrac{1}{\tau_k - \tau_l} & k \neq l \\ -\dfrac{N(N+1)}{4} & k = l = 0 \\ \dfrac{N(N+1)}{4} & k = l = N \\ 0 & \text{otherwise} \end{cases} \tag{2.17}$$

The optimal control problem is discretized by the following NLP: Find the coefficients

$$a = (a_0, a_1, \cdots, a_N),\ b = (b_0, b_1, \cdots, b_N) \tag{2.18}$$

and possibly the final time $t_0 + T$ to minimize

$$J^N(a,b) = \frac{T}{2}\sum_{k=0}^{N} L(a_k, b_k) w_k + M(a_N, \tau_f) \tag{2.19}$$

subject to

$$\frac{T}{2} f(a_k, b_k) - c_k = 0, \qquad \mathrm{k} = 0,..., N \tag{2.20}$$

$$g(a_k, b_k) \le 0, \qquad k = 0, \cdots N, \tag{2.21}$$

$$\psi_0(a_0, \tau_0) = 0, \tag{2.22}$$

$$\psi_1(a_N, t_N) = 0. \tag{2.23}$$

where w_k are the weights given by

$$w_k = \frac{2}{N(N+1)} \frac{1}{[L_N(t_k)]^2} \qquad k = 0,1,...N \tag{2.24}$$

The above NLP model can be efficiently solved by DIDO.

2.2 Pseudospectral Control Laws

2.2.1 Linear Time-Varying Systems with Quadratic Criteria

Consider the linear time-varying system

$$\dot{X} = A(t)X(t) + B(t)U(t) \tag{2.25}$$

with the initial conditions

$$X(t_0) = X_0 \tag{2.26}$$

Here $X(t)$ and $U(t)$ are $n \times 1$ and $m \times 1$ state and control vectors respectively. $A(t)$ and $B(t)$ are $n \times n$ and $n \times m$ matrices respectively.

The problem is to determine the optimal control $U(t)$ and the corresponding state vector $X(t)$ satisfying Eqs. (2.25-2.26) while minimizing

$$J = \frac{1}{2} X^T(t_f) P_f X(t_f) + \frac{1}{2} \int_{t_0}^{t_f} \left[X^T(t) Q(t) X(t) + U^T(t) R(t) U(t) \right] dt \tag{2.27}$$

where P_f and $Q(t)$ are $n \times n$ weight symmetric semidefinite matrices, and $R(t)$ is a $m \times m$ weight symmetric positive definite matrix. This is the well known linear quadratic regulator (LQR) problem. The Hamiltonian for this system is

$$H = \frac{1}{2} [X^T(t) Q(t) X(t) + U^T(t) R(t) U(t)] + \lambda^T(t) [A(t) X(t) + B(t) U(t)] \tag{2.28}$$

where $\lambda(t)$ are costate vectors.

According to the calculus of variations, we have the costate equations

$$\dot{\lambda} = -\frac{\partial H}{\partial X} = -[Q(t) X(t) + A^T(t) \lambda(t)] \tag{2.29}$$

and the necessary optimality conditions

$$\frac{\partial H}{\partial U} = 0 \quad \text{or} \quad U(t) = F(t) \lambda(t) \tag{2.30}$$

where $F(t) = -R^{-1}(t) B^T(t)$

The transversality conditions are

$$\lambda(t_f) = P_f X(t_f) \tag{2.31}$$

Substituting Eq. (2.30) into Eq. (2.25), we have the following linear state and costate systems

$$\begin{bmatrix} \dot{X} \\ \dot{\lambda} \end{bmatrix} = \begin{bmatrix} A(t) & B(t) F(t) \\ -Q(t) & -A^T(t) \end{bmatrix} \begin{bmatrix} X \\ \lambda \end{bmatrix} \tag{2.32}$$

Analytical control laws will be obtained with the Legendre pseudospectral method by solving Eq. (2.32) with the conditions Eq. (2.26) and Eq. (2.31) .

2.2.2 Discretization of Linear Time-Varying Systems Using Pseudospectral Methods

The basic idea of this method is to seek polynomial approximations for the state, costate and control functions in terms of their values at the Legendre-Gauss-Lobatto (LGL) points. Then the linear time-varying systems with quadratic criteria are reduced to solving a system of algebraic equations. Based on the algebraic equations, the analytical control laws can be derived.

Since the problem presented in the previous section is formulated over the time interval $[t_0, t_f]$, and the LGL points lie in the interval [-1, 1], we use the following transformation to express the problem for $\tau \in [\tau_0, \tau_N] = [-1, 1]$:

$$\tau = \frac{2t - (t_f + t_0)}{t_f - t_0} \tag{2.33}$$

The use of the symbol τ_N (which maps t_f) will be apparent shortly. It follows that Eq. (2.32), Eq. (2.26) and Eq. (2.31) can be replaced by

$$\dot{X}(\tau) = \frac{t_f - t_0}{2}[A(\tau)X(\tau) + B(\tau)F(\tau)\lambda(\tau)] \tag{2.34}$$

$$\dot{\lambda}(\tau) = -\frac{t_f - t_0}{2}[Q(\tau)X(\tau) + A^T(\tau)\lambda(\tau)] \tag{2.35}$$

$$X(-1) = X_0 \tag{2.36}$$

$$\lambda(1) = SX(1) \tag{2.37}$$

Let $L_N(\tau)$ be the Legendre polynomial of degree N on the interval [-1, 1]. In the Legendre collocation approximation of Eqs. (2.34-37), we use the LGL points, $\tau_l, l = 0,\cdots,N$ which are given by

$$\tau_0 = -1, \qquad \tau_N = 1, \tag{2.38}$$

and for $1 \le l \le N-1$, the τ_l are the zeros of $\dot{L}_N$, the derivative of the Legendre polynomial L_N. There are no closed form expressions for these nodes, and they have to be computed numerically. For approximating the continuous equations, we seek a polynomial approximation of the form

$$X^N(\tau) = \sum_{l=0}^{N} X(\tau_l)\phi_l(\tau) \tag{2.39}$$

$$U^N(\tau) = \sum_{l=0}^{N} U(\tau_l)\phi_l(\tau) \tag{2.40}$$

$$\lambda^N(\tau) = \sum_{l=0}^{N} \lambda(\tau_l)\phi_l(\tau) \tag{2.41}$$

where for $l = 0,1,\cdots,N$

$$\phi_l(\tau) = \frac{1}{N(N+1)L_N(\tau_l)} \frac{(\tau^2-1)\dot{L}_N(\tau)}{\tau-\tau_l} \tag{2.42}$$

are the Lagrange polynomials of order N. It can be shown that

$$\phi_l(\tau_k) = \delta_{lk} = \begin{cases} 1 & \text{if } l = k \\ 0 & \text{if } l \ne k \end{cases} \tag{2.43}$$

From this property of ϕ_l it follows that

$$X^N(\tau_l) = X(\tau_l),\ U^N(\tau_l) = U(\tau_l),\ \ \lambda^N(\tau_l) = \lambda(\tau_l), \tag{2.44}$$

Generally the approximations are expressed as

$$X(\tau) \approx X^N, \quad U(\tau) \approx U^N, \quad \lambda(\tau) \approx \lambda^N, \tag{2.45}$$

but in this collocation method, as stated in Eq. (2.44), the values of the approximate state, control and costate functions are given exactly by the value of the continuous functions at these points.

To express the derivatives $\dot{X}^N$ and $\dot{\lambda}^N$ in terms of $X^N(\tau)$ and $\lambda^N(\tau)$ at the collocation points τ_l respectively, we differentiate Eq. (2.39) and Eq. (2.41), which results in a matrix multiplication of the following forms:

$$\dot{X}^N(\tau_k) = \sum_{l=0}^{N} D_{kl} X(\tau_l) \tag{2.46}$$

$$\dot{\lambda}^N(\tau_k) = \sum_{l=0}^{N} D_{kl} \lambda(\tau_l) \tag{2.47}$$

where the D_{kl} are entries of the $(N+1)\times(N+1)$ differentiation matrix D

$$D = [D_{kl}] = \begin{cases} \dfrac{L_N(\tau_k)}{L_N(\tau_l)} \dfrac{1}{\tau_k - \tau_l} & k \neq l \\ -\dfrac{N(N+1)}{4} & k = l = 0 \\ \dfrac{N(N+1)}{4} & k = l = N \\ 0 & \text{otherwise} \end{cases} \tag{2.48}$$

2.2.3 Analytical Feedback Control Law

We set

$$a = (a_0, a_1, \cdots, a_N) \tag{2.49}$$

$$b = (b_0, b_1, \cdots, b_N) \tag{2.50}$$

$$c = (c_0, c_1, \cdots, c_N) \tag{2.51}$$

and use the notation

$$a_l \coloneqq X(\tau_l), \quad b_l \coloneqq U(\tau_l), \quad c_l \coloneqq \lambda(\tau_l), \tag{2.52}$$

to rewrite Eqs. (2.32-2.34) in the form:

$$X^N(\tau) = \sum_{l=0}^{N} a_l \phi_l(\tau) \tag{2.53}$$

$$U^N(\tau) = \sum_{l=0}^{N} b_l \phi_l(\tau) \tag{2.54}$$

$$\lambda^N(\tau) = \sum_{l=0}^{N} c_l \phi_l(\tau) \tag{2.55}$$

Eqs. (2.34-2.35) and Eq. (2.30) are discretized and transformed into the following algebraic equations in terms of the coefficients a, b and c at the LGL nodes, t_k:

$$\sum_{l=0}^{N} D_{kl} a_l - \frac{\tau_f - \tau_0}{2}(A_k a_k + B_k F_k c_k) = 0 \tag{2.56}$$

$$\sum_{l=0}^{N} D_{kl} c_l + \frac{\tau_f - \tau_0}{2}(Q_k a_k + A_k^T c_k) = 0 \tag{2.57}$$

$$b_k - F_k c_k = 0 \tag{2.58}$$

$$k = 0,1,\cdots,N,$$

or

$$\tilde{A}\_a - \frac{\tau_f - \tau_0}{2}\tilde{G}c = 0 \tag{2.59}$$

$$\frac{\tau_f - \tau_0}{2}\tilde{Q}a + \tilde{A}_+ c = 0 \tag{2.60}$$

$$b - Mc = 0 \tag{2.61}$$

where

$\tilde{A}_-, \tilde{A}_+, \tilde{G}, \tilde{Q}$ and M are $[n\times(N+1)]\times[n\times(N+1)]$ matrices whose (ij)th blocks are $n\times n$ matrices of the following form

$$[\tilde{A}_-]_{ij} = \begin{cases} D_{ij} I_n & i \neq j \\ D_{ii} I_n - \dfrac{\tau_f - \tau_0}{2} A_i & i = j \end{cases} \tag{2.62}$$

$$[\tilde{A}_+]_{ij} = \begin{cases} D_{ij} I_n & i \neq j \\ D_{ii} I_n + \dfrac{\tau_f - \tau_0}{2} A_i^T & i = j \end{cases} \tag{2.63}$$

$$[\tilde{G}]_{ij} = \begin{cases} 0_n & i \neq j \\ B_i F_i & i = j \end{cases} \tag{2.64}$$

$$[\tilde{Q}]_{ij} = \begin{cases} 0_n & i \neq j \\ Q_i & i = j \end{cases} \tag{2.65}$$

$$[M]_{ij} = \begin{cases} 0_{\mathrm{n}} & i \neq j \\ F_i & i = j \end{cases} \tag{2.66}$$

In the above, I_n is a $n\times n$ unity matrix and 0_n is a $n\times n$ zero matrix.

The initial conditions are

$$a(0) = a_0 \tag{2.67}$$

The terminal constraints are forced for the stabilization of the receding horizon control[49].

$$a(N) = 0 \tag{2.68}$$

$$c(N) = 0 \tag{2.69}$$

The goal is to solve Eqs. (2.59-2.61) subject to the transversality conditions, Eqs. (2.67-2.69). Therefore, first we write the equations for the state and costate vectors a and c in block form to have the block matrix form

$$\begin{bmatrix} \tilde{A}_{-} & -\frac{\tau_f - \tau_0}{2}\tilde{G} \\ \frac{\tau_f - \tau_0}{2}\tilde{Q} & \tilde{A}_{+} \\ \tilde{P}_1 & \tilde{P}_2 \end{bmatrix} \begin{bmatrix} a \\ c \end{bmatrix} \equiv Vz = \begin{bmatrix} 0 \\ 0 \\ 0 \end{bmatrix} \tag{2.70}$$

In these equations,

$$a = [a_0^T, a_1^T, \cdots, a_N^T]^T, \quad c = [c_0^T, c_1^T, \cdots, c_N^T]^T, \quad z^T = [a^T, c^T] \tag{2.71}$$

and $\tilde{P}_1$ and $\tilde{P}_2$ are the following matrices

$$\tilde{P}_1 = \begin{bmatrix} O & I_n \\ O & 0_n \end{bmatrix} \tag{2.72}$$

$$\tilde{P}_2 = \begin{bmatrix} O & 0_n \\ O & I_n \end{bmatrix} \tag{2.73}$$

where O is a $n \times nN$ zero matrix. The matrix V in Eq. (2.70) is of dimension $n(2N+3) \times 2n(N+1)$. We partition V as $V = [V_0 \;\; V_e]$ such that

$$V_0 a_0 + V_e e = 0 \tag{2.74}$$

where vector e is of dimension $n(2N+1) \times 1$ and defined as

$$e = [a_1^T, a_2^T, \cdots, a_N^T, c_0^T, \cdots, c_N^T]^T \tag{2.75}$$

Thus, V_0 and V_e are $[n(2N+3)\times n]$, $[n(2N+3)\times n(2N+1)]$ block matrices of V, respectively. We can solve Eq. (2.74) for e using the method of least squares

$$e = -V_e \backslash V_0 a_0 = W a_0 \tag{2.76}$$

where the \ operator denotes the least-squares solution in MATLAB. As indicated in Eq. (2.76), $W \equiv -V_e \backslash V_0$ is a matrix of dimension $(2nN+n)\times n$. Since $z = \begin{bmatrix} a_0 \\ e \end{bmatrix}$ we get

$$z = \begin{bmatrix} a \\ c \end{bmatrix} = \begin{bmatrix} I_n \\ W \end{bmatrix} a_0 \equiv \begin{bmatrix} W_1 \\ W_2 \end{bmatrix} a_0 \tag{2.77}$$

where W_1 and W_2 are partitions of the $[I_n \;\; W]$ matrix, each of dimension $n(N+1)\times n$ so that we have,

$$a = W_1 a_0 \tag{2.78}$$

$$c = W_2 a_0 \tag{2.79}$$

From Eq. (2.61) we have

$$b = Mc = MW_2 a_0 \equiv W_3 a_0 \tag{2.80}$$

where W_3 is a matrix of dimension $n(N+1)\times n$.

If the initial states are known, the states, costates and controls at the LGL points can be solved from Eqs. (2.78-2.80) in the given horizon. It should be noticed that we obtained these solutions without any integrations. Regarding the current states as the new initial states, Eq. (2.80) constitutes a closed loop control law that can be rapidly performed in the receding horizon control manner.

2.3 Real-Time Optimal Control Planning

2.3.1 Receding Horizon Control (RHC)

With no errors the effect of open loop optimal control is equivalent to a feedback control. We may not need real-time optimization since we can schedule optimal control in advance or on the ground for aerospace applications. However, disturbances exist everywhere, so we try to obtain a numerical optimal control sequence at each sampling time, and just take the first control of the sequence to form a feedback control. This is done by RHC. At the current sampling time t_0, the state is estimated from the measurements,

$$X(0) = \hat{X}_{0/0} \tag{2.81}$$

Based on this initial condition we use the DIDO to numerically solve the optimal control model, Eqs. (2.4-2.8), to get the control sequence at the LGL points over the horizon T

$$U = \left(U_{k/k}, U_{k+1/k}, \cdots U_{(k+N)/k}\right)^T \tag{2.82}$$

Apply the first control of U to the system and repeat the procedure until the final time is reached.

2.3.2 Outer and Inner Loop Control

To enhance the robustness of real-time optimal control, we use two levels of the optimal control structure, outer loop and inner loop control. The outer loop control is defined by the model Eqs. (2.4-2.8). It is used to generate real-time trajectories to adapt to a large perturbation or varying mission goals. Since the model is nonlinear, it usually

takes significant CPU time to finish it. Also, it is more difficult to get convergent solutions when compared with linear optimal control. Adding inner loop control can alleviate the dependence of the system reliability on the outer loop. The inner optimal loop control is described as follows. If we just use the inner loop, then the model becomes a tracking problem using the LQR technique. When there is a large perturbation, it is difficult to track the original reference trajectory with the LQR. In case an immediate maneuver is required, the LQR tracking will not be able to track the reference trajectory. Using outer loop control, we can deal with the mentioned problems by updating the reference trajectory and tracking the new one. In each loop we use DIDO to solve the receding horizon control to obtain the control law. Also "warm start" approaches[50] are used in the numerical optimizations. One can see the challenge is how to obtain the real-time optimizations. Our effort is towards this direction.

To track the nonlinear optimal model, we linearize Eq. (2.5) and design the constrained linear time-varying system

$$\delta\dot{X} = A(t)\delta X(t) + B(t)\delta U(t) \tag{2.83}$$

which satisfies

$$\delta X(t_0) = \delta X_0 \tag{2.84}$$

$$U_{\min} - U \le \delta U \le U_{\max} - U \tag{2.85}$$

$A(t)$ and $B(t)$ are $n \times n$ and $n \times m$ matrices respectively, and

$$\delta X = X - X_{ref} \tag{2.86}$$

where X_{ref} is the solution from the nonlinear model. Then determine the optimal control $\delta U(t)$ and corresponding state vector $\delta X(\tau)$ satisfying Eqs. (2.83-2.85) while minimizing

$$J_2 = \frac{1}{2}\int_{t_0}^{t_0+T}\left[\delta X^T(t)Q\delta X(t) + \delta U^T(t)R\delta U(t)\right]dt \tag{2.87}$$

where Q and R are weight matrices and

$$A(t) = \frac{\partial f}{\partial X} \quad A(t) = \frac{\partial f}{\partial X} \tag{2.88}$$

Notice Eq. (2.85) ensures the total control applied to the system is within the limits. If the constraint Eq. (2.85) is absent, the inner control becomes the well known linear quadratic regulator, which can be solved by the pseudospectral control law. The major function of the inner loop is to track the outer loop trajectory. In case the outer loop control fails, the inner loop will track previous trajectories.

In the DIDO, we use SNOPT/TOMLAB[50] to solve the nonlinear programming problem in the outer loop and SQOPT/TOMLAB to obtain the solutions from the optimal tracking system in the inner loop. Fig. 2.1 shows the outer and inner control structure. The computational procedure is illustrated in Fig.2.2.

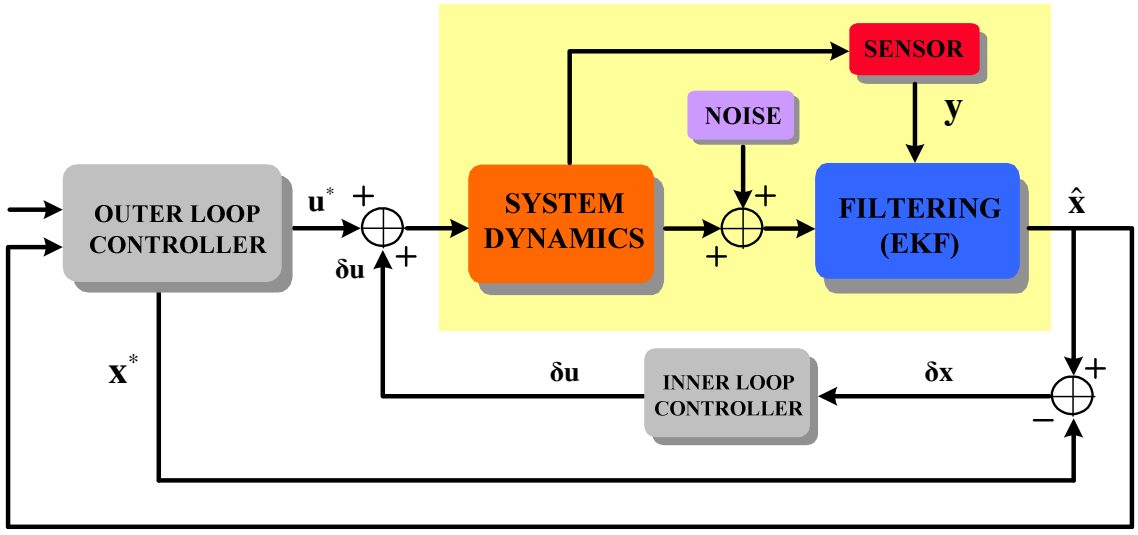

Fig. 2.1 Outer and Inner Loop Control

2.3.3 Speed Up Computations

Ways to improve the numerical optimization speed include a warm start technique, use of the analytical Jacobian matrix and scaling or balancing.

2.3.3.1 Warm Start

A warm start is a technique that starts codes based on the past history of iterations and function evaluations in the previous optimizations instead of arbitrary initial guesses or a cold start. Quite often an engineer needs to solve a slightly-altered version of the same base model. It makes sense in this scenario that the optimal solution of a previous version ought to serve as an excellent starting point for the current version of the model,

if the two versions of the model are similar. This is a warm start. In DIDO/TOMLAB, the warm start can be completed as described in Fig. 2.3:

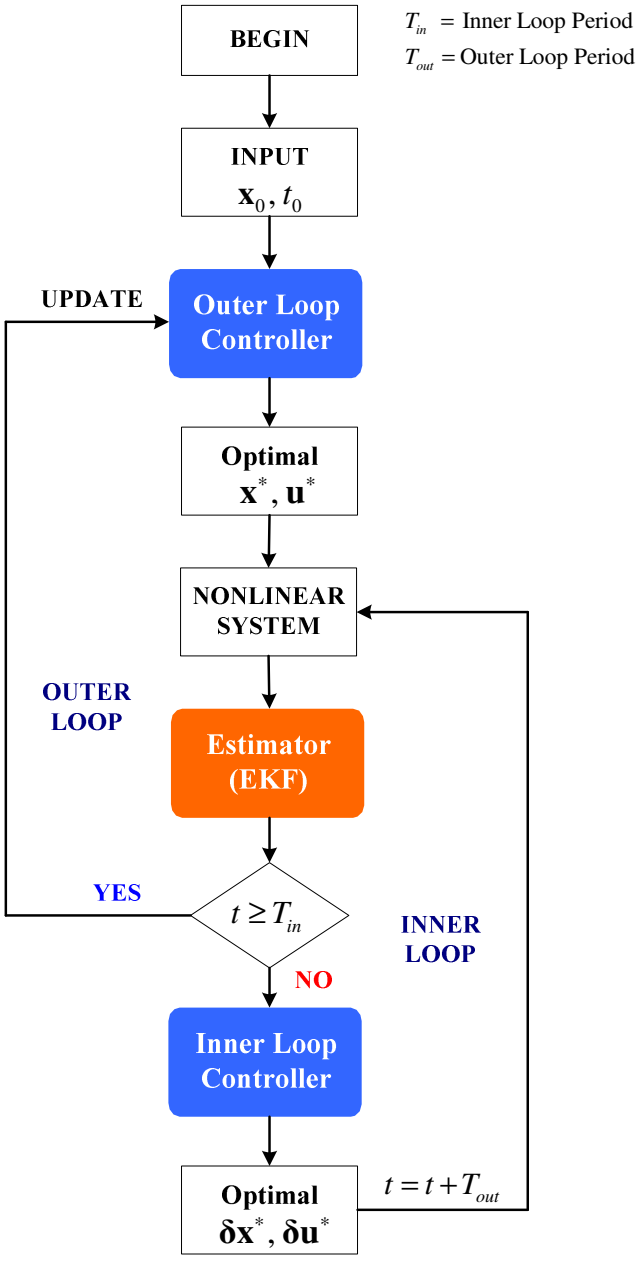

Fig. 2.2 Computational Procedure

Step 1: Define the first problem, call tomlab to solve the problem

Result = tomRun (‘snopt’, Prob);

Step 2: Use the warm start to solve similar problems

Set Result_previous = Result and revise the problem;

Prob = WarmDefSOL (‘snopt’, Prob_revised, Result_previous);

Result = tomRun (‘snopt’, Prob);

Fig. 2.3 Warm Start

2.3.3.2 Use of the Analytical Jacobian Matrix

The Jacobian matrix defines the search directions in the numerical optimizations. Use of the analytical Jacobian matrix greatly improves the computational speed of the numerical optimizations when compared with the numerically estimated Jacobian. The numerical accuracy is much less in the latter. Also it takes much more time to numerically estimate the Jacobian, since a lot of calls to the constraint function are required to estimate this Jacobian in numerical optimizations.

2.3.3.3 Scaling or Balancing Problems

Scaling plays an important role in numerical optimizations. It is necessary to scale models to make sure each variable weighs evenly. Here we suggest using the following procedure to scale models.

(1) Choose the basic units to assure the other units can be derived from the basic units.

(2) Scale the basic units to get the normalized model.

(3) Use the scale option in the DIDO/TOMLAB.

2.3.4 Time-Delay Considerations

Real-time optimal control means instantaneous control should be obtained once the measurement is received. Unfortunately, some time is required to solve for the optimal control. So there is a time delay in applying the optimal control to the system. A possible choice would be to use the previously optimized controls in an open loop manner, when the current optimal control is being solved. Obviously there exists a discontinuity at the conjunction of the previous and the current control. Also this does not make sense if the computational time is comparable with the horizon of the control. In our planning, we define the sampling period to be δ and the current time $t_k = k\delta$. Suppose the computational time for the optimal control takes less than *n* steps or $n\delta$ and

$$X(k-n) = X_{k-n} \tag{2.89}$$

is known from the measurement. Use Eq. (2.89) as the initial condition to integrate Eq. (2.5) to time t_k to get the predicted state $X_{k/k-n}$. The control U can be set as the reference control in the first horizon. Then use the predicted state $X_{k/k-n}$ as the initial

condition and solve the outer loop optimal control with DIDO, and get the control sequence

$$U_{outerloop} = \left(U_{k/k-n}, U_{k+1/k-n}, \cdots U_{(k+T/\delta)/k-n}\right)^T \tag{2.90}$$

If n is equal to zero, we have exact real-time optimal control. If solving the outer loop optimal control fails, we need to activate an alternative control. As the time arrives at t_k and the measurement at t_k is received, the estimated $\hat{X}_{k/k}$ is obtained from filtering theories. The inner loop control sequence is assumed to be solved in real-time

$$\delta U_{innerloop} = \left(\delta U_{k/k}, \delta U_{k+1/k}, \cdots \delta U_{(k+T/\delta)/k}\right)^T \tag{2.91}$$

The updated control is

$$U = U_{outerloop} + \delta U_{innerloop} \tag{2.92}$$

Apply the first control of U to the system and repeat the procedure until the final time is reached.

It is important to know the influence of all the perturbations before t_{k-n} is involved or reflected in the states X_{k-n} from the measurements in Eq. (2.89). The real-time open optimal control could reject the influence of the perturbations before t_{k-n}. This is much better than the reference control scheduled before missions, since it knows nothing about the perturbations. The disturbances between the time t_{k-n} and t_k can be rejected by the inner loop control in real-time.

2.4 Demonstrated Example: An Inverted Pendulum Problem

2.4.1 Description of the Inverted Pendulum Problem

The problem consists of designing the real-time numerical optimal control that provides the desired performance for an inverted pendulum attached on the top of a cart, as shown in Figure 2.4. The cart is only allowed to move in the positive and negative x-direction through the use of a linear actuator applying a force $U(t)$. The inverted pendulum is attached to the cart through a frictionless hinge joint. Furthermore, the cart position, $x(t)$, cart velocity $\dot{x}(t)$, pendulum angle, $\theta(t)$, and pendulum angular, $\dot{\theta}(t)$, can all be sensed for feedback.

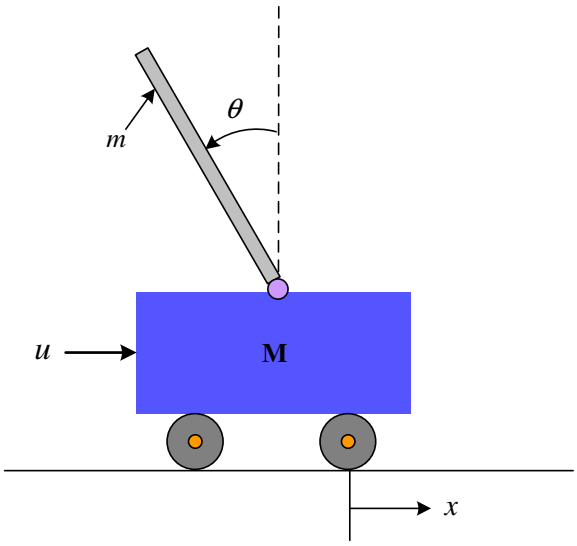

Figure 2.4 A Schematic of the Inverted Pendulum Attached on a Cart

The system dynamic equations of motion are

$$\dot{x} = v \tag{2.93}$$

$$\dot{v} = \frac{1}{c}\left(U - bv - \frac{1}{2} mL\omega^2 \sin(\theta) + \frac{3}{4} mg \cos(\theta)\sin(\theta) \right) \tag{2.94}$$

$$\dot{\theta} = \omega \tag{2.95}$$

$$\dot{\omega} = \frac{3}{2L}\left\{ \frac{\cos(\theta)}{c}\left(U - bv - \frac{1}{2} mL\omega^2 \sin(\theta) + \frac{3}{4} mg \cos(\theta)\sin(\theta) \right) + g \sin(\theta) \right\} \tag{2.96}$$

where $c = M + m - \frac{3}{4} m\cos(\theta)^2$

M	mass of the cart	0.5 kg
m	mass of the pendulum	0.5 kg
b	friction of the cart	0.1 N/m/sec
L	length of the pendulum	0.6 m
g	the acceleration of gravity	9.8m/sec/sec
U	applied force	[-3,3] N

Obviously the inverted pendulum can be considered as a simple attitude control problem. A more complicated case that is considered in this section is the attitude of the inverted pendulum when the pendulum is attached to a translating cart. In addition we address the constrained inverted pendulum, which means the control is subject to saturation. It is obvious that open loop optimal control does not work since any perturbations will cause the unstable pendulum to fall down. We implement the optimal control with receding horizon control so that closed loop optimal control is obtained. The inverted pendulum belongs to an infinite time problem, and we have no way to numerically solve infinite optimal control. So we need to use sequence finite horizon control to approximate the

infinite optimal control. To ensure the stability caused by the finite horizon approximation, we force terminal constraints at the end of each horizon.

2.4.2 Outer and Inner Loop Optimal Control

In this problem, assume the constraint

$$-3 \le U \le 3 \tag{2.97}$$

set in the outer loop. Once the optimal control U is determined, we force the $-3 \le \delta U + U \le 3$ constraint in the inner loop to make sure the total control is bounded before applied to the system. The sampling period for the outer loop is 0.5 seconds while 0.05 seconds for the inner loop. The number of LGL points is 32. The length of the fixed receding horizon is 10 seconds. The simulation time or the final time is also set as 10 seconds. So we have 20 updates for the outer loop and 200 updates for the inner loop. The initial pendulum angle is set as 15 degrees. The initial condition is

$$X(0) = [0,\ 0,\ 15\,\text{degree}, 0] \tag{2.98}$$

For the inverted pendulum, $X = [x,\ \dot{x},\ \theta,\ \dot{\theta}]$. We want to minimize

$$J = \frac{1}{2}\int_{t_0}^{t_0+T} \left[X^T(\tau)Q(\tau)X(\tau) + U^T(\tau)R(\tau)U(\tau)\right] d\tau \tag{2.99}$$

satisfying Eqs. (2.93-2.98) where $Q(\tau)$ is an $n \times n$ symmetric semidefinite matrix, $R(\tau)$ is a $m \times m$ symmetric positive definite matrix and T is the horizon. Obviously, the set point or equilibrium point is zero, which means we want the inverted pendulum and car to be static and the pendulum to be in the vertical direction.

The process noise for the dynamic model errors needs to be added to the acceleration terms in the state equations. The process noise matrix of the value $\mathbf{Q}_{dyn}$ takes the form

$$\mathbf{Q}_{dyn} = diag([0 \quad 0.1(m/s)^2 \quad 0 \quad 0.01(rad/s)^2]) \tag{2.100}$$

where the units are meters and radians. The following measurement errors were used

$$\mathbf{R}_{measure} = diag([0.0005(m^2) \quad 10^{-7}(m/s)^2 \quad 0.06(\deg^2) \quad 3\times10^{-6}(\deg/s)^2]) \tag{2.101}$$

An extended Kalman filter is used to estimate states to simulate real-time optimal control[51].

2.4.3 Numerical Results

Figs. 2.5-2.8 illustrate the numerical results.

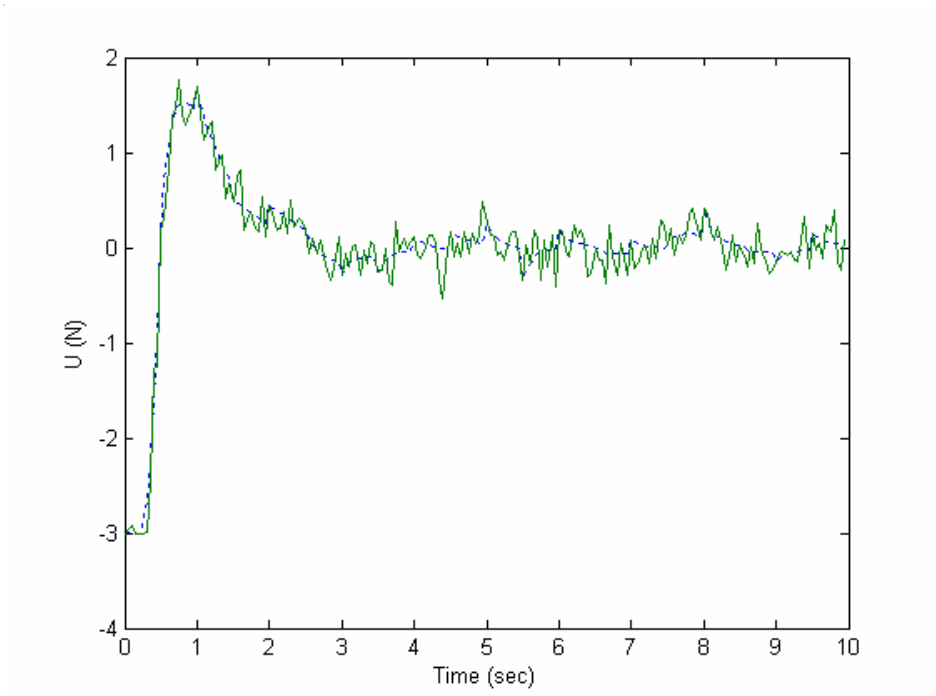

Fig. 2.5 Outer Loop Control

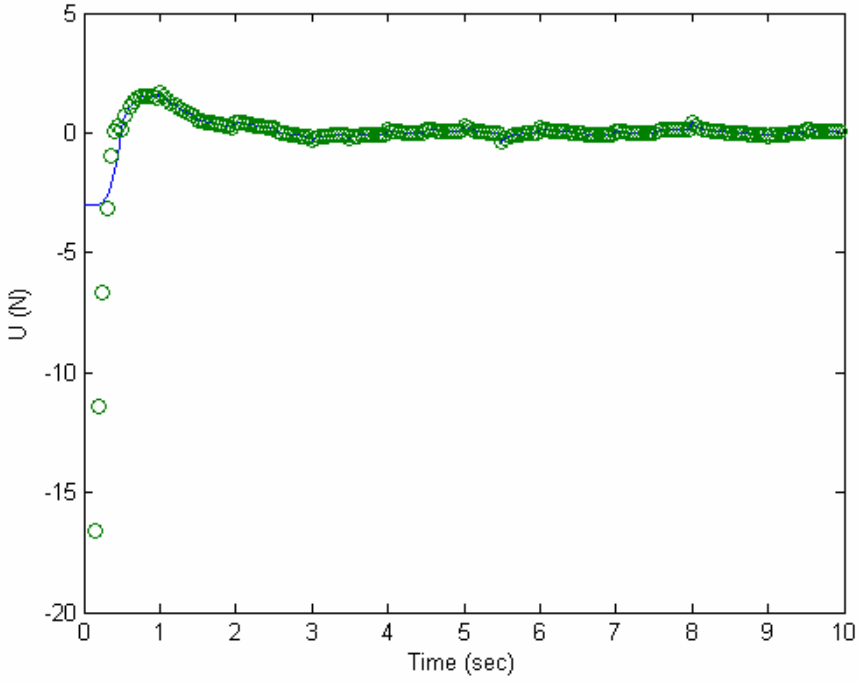

Fig. 2.6 Verify Outer Loop Control

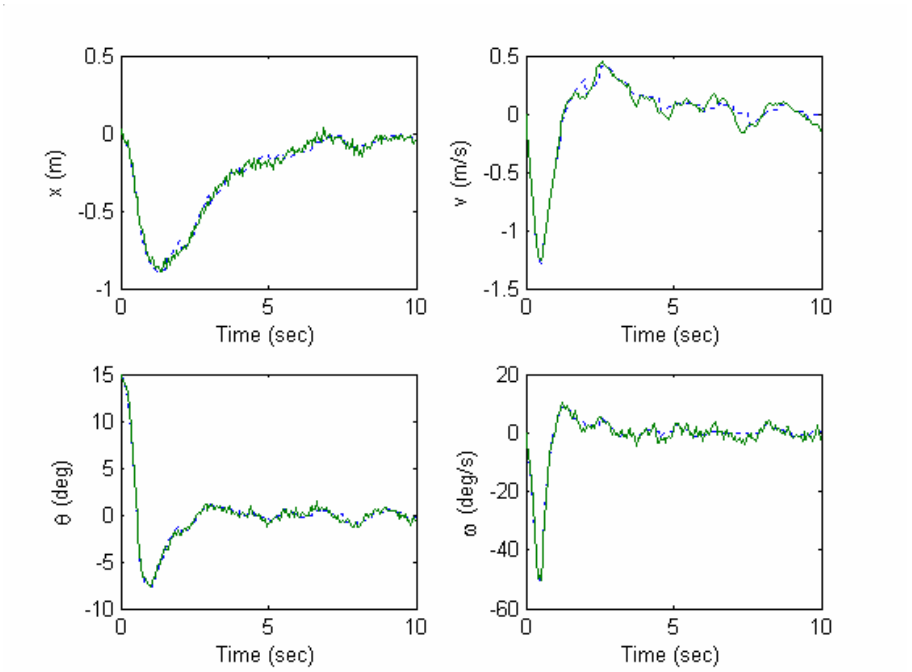

Fig. 2.7 Outer Loop States

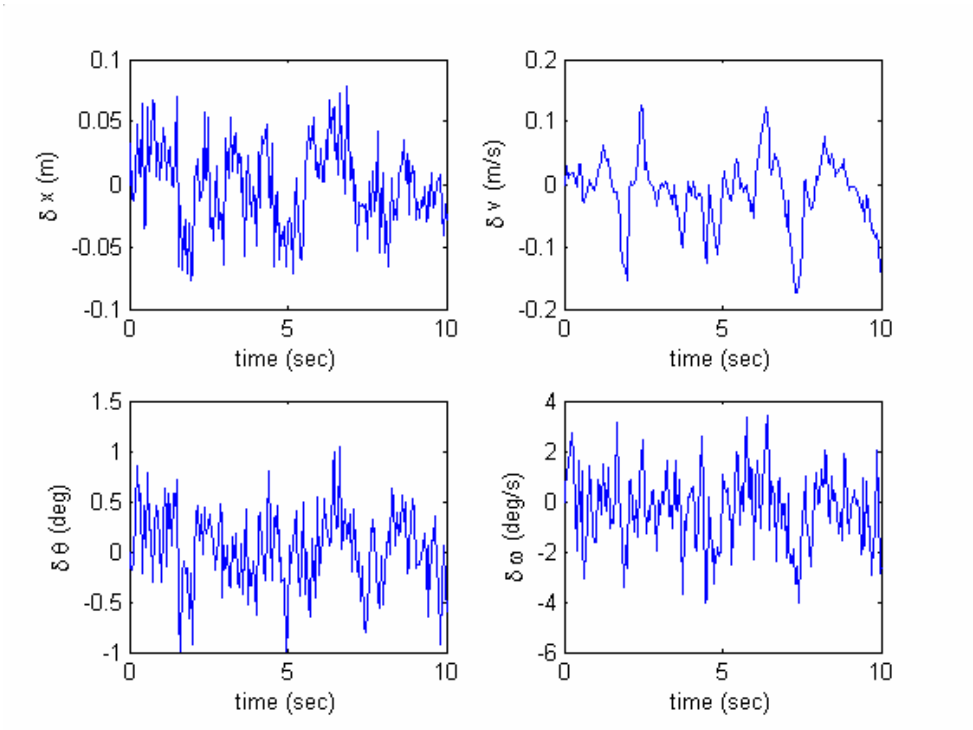

Fig. 2.8 Inner Loop States

The results show all the solutions are near optimal. In Fig. 2.5, the solid lines represent the total control $\delta U + U$ while the dot lines stand for the outer loop or reference control U from SNOPT. The control reaches the lower limit at the first stage in Fig. 2.5. This is because the maximum force should be applied in the reverse direction as soon as possible to prevent the pendulum from falling down. The solid lines represent the states obtained by integrating Eqs. (2.93-2.96) under the process noise and measurement error while the dot lines stand for the reference states from the outer loop in Fig. 2.7. The results show the actual trajectories (solid lines) follow the outer loop trajectories (dot lines) very well and the difference is illustrated in Fig. 2.8. Notice the outer loop trajectories in Fig. 2.7 are scheduled and updated in real-time when the new

measurements are received. Fig. 2.7 illustrates the inverted pendulum and cart are almost still and return to the zero position after 3 and 6 seconds, respectively.

We use the costate estimation[9] to verify the outer loop control. From optimal control theory, it can be shown that

$$U = \begin{cases} 3 & \Lambda \geq 3 \\ \Lambda & -3 < \Lambda < 3 \\ -3 & \Lambda \leq -3 \end{cases} \tag{2.102}$$

$$\Lambda = -\left(\lambda_v + 1.5L\cos\theta\lambda_\omega\right)/\left(Rc\right) \tag{2.103}$$

where R is a weighing factor and the value is one. λ_v and λ_ω are the costates corresponding to Eqs. (2.94) and (2.96), respectively. In Fig. 2.6, the solid line represents the outer loop control while the circles stand for the values of Λ. One can see that agreement between the outer loop control and Eqs. (2.102-2.103) is excellent.

2.4.3.1 Computation Speed

Table 2.1 lists CPU comparisons for the warm and cold start.

Table 2.1: CPU for Warm and Cold Start

Algorithm	*Warm Start (sec)*	*Cold Start (sec)*
Inner loop	*0.0348*	*0.172*
Outer loop	*0.4366*	*1.016*

In Table 2.1 all the initial guesses in the cold start are zeros.

2.4.3.2 Use of Analytical Jacobian Matrix

Our results indicate there is about a factor of 10 improvement when using the analytical Jacobian matrix instead of the numerical one, as shown in Table 2.2.

Table 2.2: CPU for Analytical and Numerical Jacobian Matrix

Jacobian Matrix	*Average CPU Used for Solving Outer Loop (second)*
Analytical	*0.425*
Numerical	*4.570*

2.4.3.3 Scaling or Balancing Problems

Scaling plays an important role in numerical optimizations. It is necessary to scale models to make sure each variable weighs evenly. Here we suggest using the following procedure to scale models.

(1) Choose the basic units to assure the other units can be derived from the basic units.

(2) Scale the basic units to get the normalized model.

(3) Use the scale option in the DIDO/TOMLAB.

2.4.3.4 Model Reductions

Simplify models: for instance, it is obvious that the computation speed of the linear model is much faster than that of nonlinear models. In our example, the CPU of the linear model is 0.0348 seconds, compared with 0.4366 seconds for the nonlinear model, as shown in Table 2.1.

2.4.3.5 Discretization Selection and Size

The use of higher order schemes allows using fewer discretization nodes for the same degree of accuracy. A smaller size discretization problem results in a more efficient and more robust solution. Recently Refs 7-17 employed the Legendre spectral collocation method for solving a variety of optimal control problems, and showed that highly accurate results can be obtained with a low degree of discretization.

Table 2.3: Effect of LGL Points on CPU

LGL Points	*Average CPU Used for Solving Out Loop (second)*	*Average CPU Used for Solving Inner Loop (second)*
16	*0.115*	*0.011*
24	*0.241*	*0.016*
32	*0.425*	*0.031*

Table 2.3 shows that as the number of LGL points is reduced the speed improves.

2.4.3.6 Computation Time Delay

To compute the effect of the time delay on the system, we input $U(\tau-\delta\tau)$ into the system instead of $U(\tau)$ at the time τ

$$U(\tau)=\begin{cases}0 & \tau \le \delta\tau \\ U(\tau-\delta\tau) & \tau > \delta\tau\end{cases} \tag{2.104}$$

where $\delta\tau$ is the computational time delay. In this case, set $\delta\tau_1 = 0.12$ and $\delta\tau_2 = 0.012$ seconds for the outer loop control and inner loop control. Choose 16 LGL points so that the computations are able to be completed in $\delta\tau_1$ and $\delta\tau_2$.

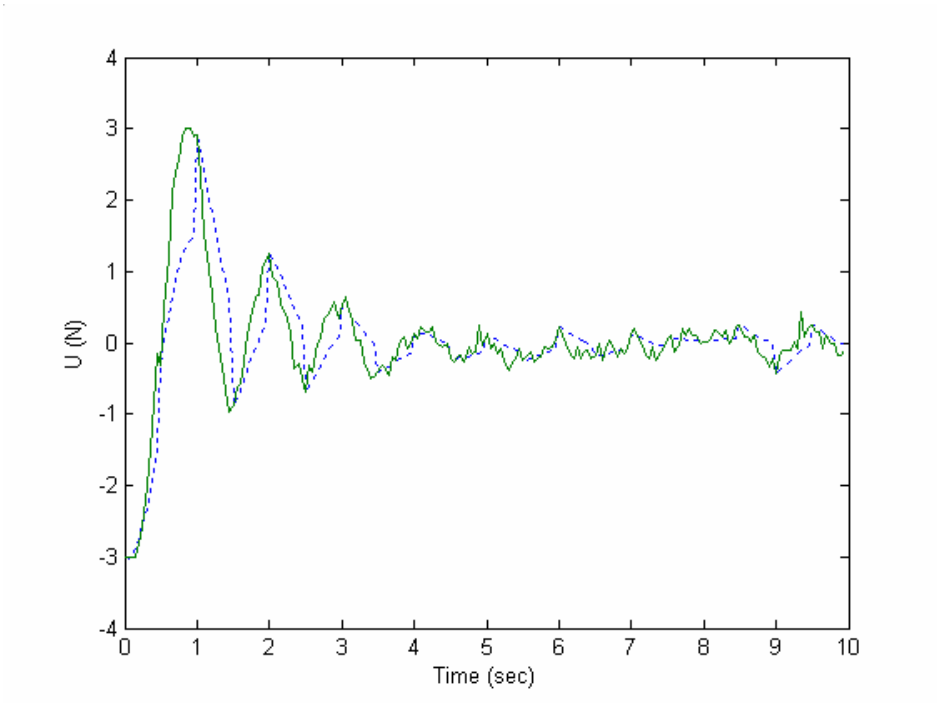

Fig. 2.9 Control Including Computational Delay Effects

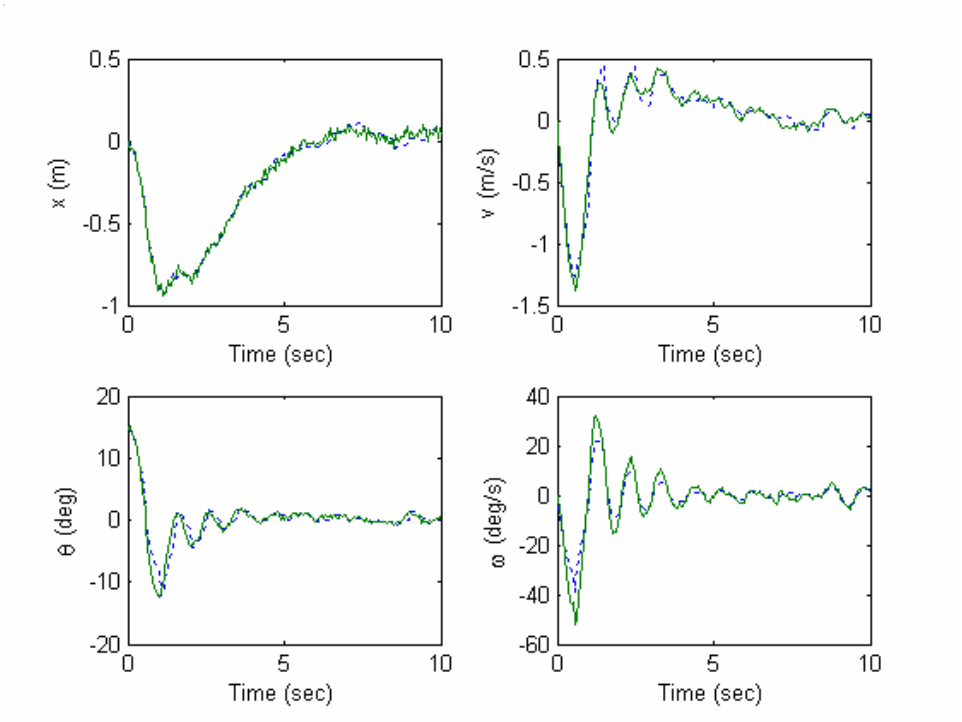

Fig. 2.10 States with Delay Effects

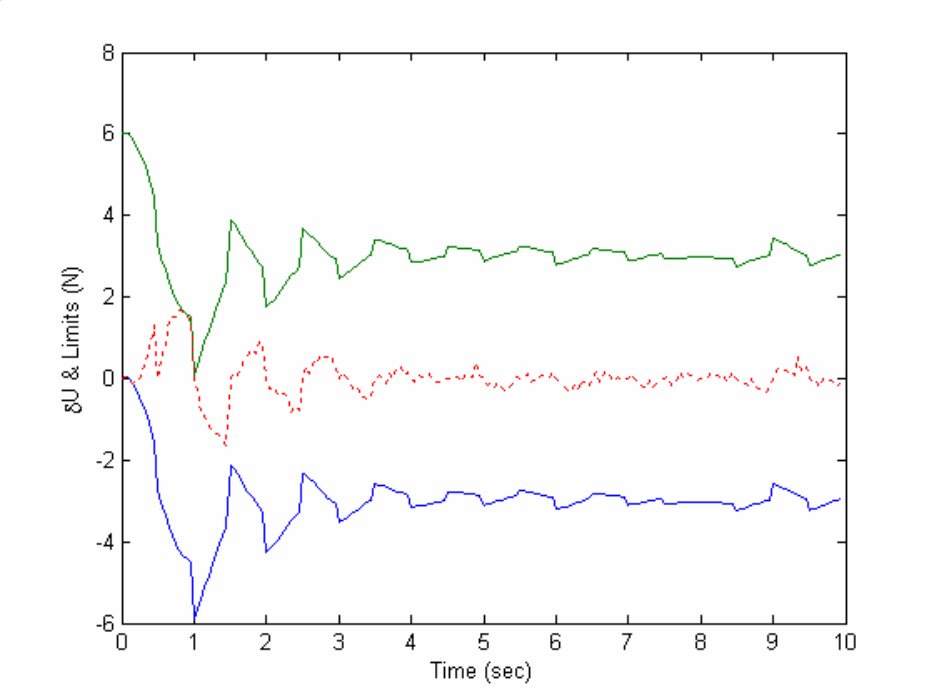

Fig. 2.11 Inner Loop Control Including Delay Effects

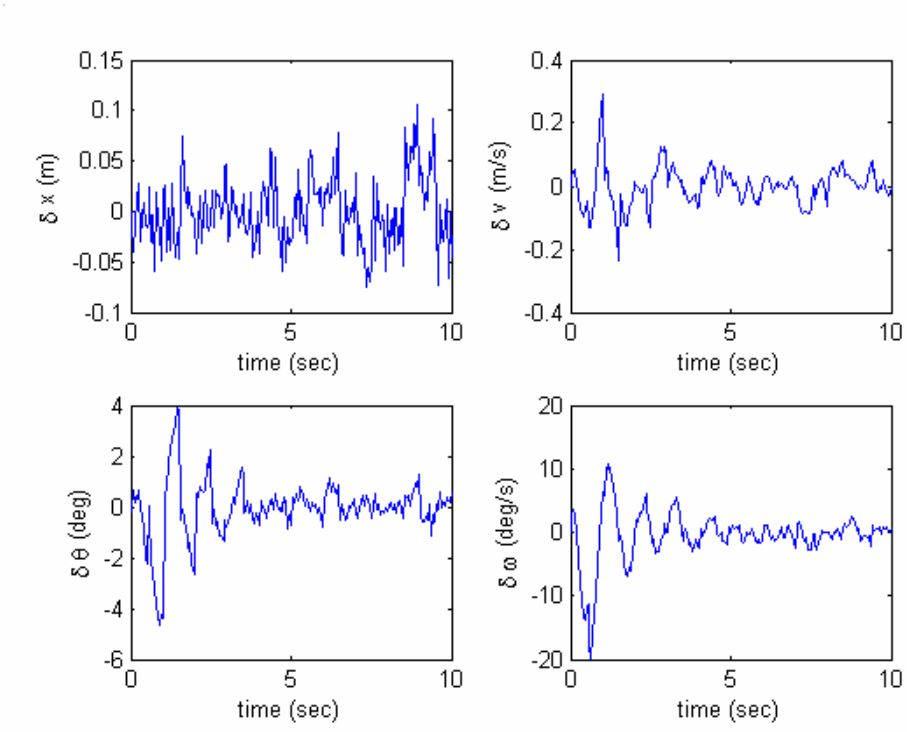

Fig. 2.12 Inner Loop States with Delay Effects

All the simulations were performed on a 1.7 GHz PENTIUM 4. The simulation results show the inverted pendulum can still be stabilized with the delay effects, which means we are able to control the inverted pendulum in real-time using a commercial computer to complete the computations. In Fig. 2.9, the solid lines represent the total control $\delta U + U$ while the dot lines stand for the outer loop or reference control U from SNOPT. In Fig. 2.10, the solid lines represent the states obtained by integrating Eqs. (2.93-2.96) with the process noise and measurement error while the dot lines stand for the states from the outer loop. Comparing Fig. 2.12 with Fig. 2.8, the time delay causes large perturbations in the states in the initial stages since the time delay has significant effects on the initial stages with fast dynamic response. The perturbations are rejected as

time increases. In Fig. 2.11, the dot lines represent the inner loop control while the solid lines stand for the control limits defined by Eq. (2.85). The figure shows the initial control of the inner loop is almost zero due to the Eq. (2.85) constraint since the lower limit is already reached in Fig. 2.9. From Figs. 2.9-2.12, one can see that the time delay in the system influences the fast dynamic part significantly, while it has little effect on the slow dynamic part.

2.4.4 Summary of the Demonstrated Example

We introduce a design structure for two levels of control, an outer loop and inner loop control, to implement real-time optimal control. The outer and inner loop optimal control problem is efficiently solved by DIDO. An extended Kalman filter is used to estimate states to simulate real-time optimal control. Several ways to improve computation speed were considered, including the analytical Jacobian matrix, warm start and algorithm selections. We used a classic constrained inverted pendulum problem to demonstrate our control approach. The results show the inverted pendulum can be stabilized very well in a real time manner.

CHAPTER III

OPTIMAL MAGNETIC ATTITUDE CONTROL

This chapter investigates the use of magnetic actuators for the time-optimal rest-to-rest maneuver using a pseudospectral algorithm implemented in the reusable software package, DIDO. The nonlinear attitude equations of motion are used. After the final attitude is reached in the orbit frame, the pseudospectral control law is applied to stabilize the attitude also using magnetic torque in circular and eccentric orbits. The parameters of the example problem correspond to that of NPSAT1, a small satellite being built at the Naval Postgraduate School. Numerical experiments reveal that real-time optimal magnetic maneuvers and three-axis magnetic attitude stabilizations can be easily obtained with onboard computation.

3.1 Coordinate Frames

3.1.1 Inertial Frame

The X_e axis points to the vernal point in the equatorial plane of the Earth. The Z_e axis is the axis of rotation of the Earth in a positive direction and Y_e is defined by the right-hand rule.

3.1.2 Magnetic Equator Frame

Assume the x_m axis is along the line of nodes between the magnetic equator plane and orbit plane, the z_m axis is perpendicular to the magnetic equator plane and points toward the northern hemisphere of the earth, and y_m is defined by the right-hand rule.

3.1.3 Orbit Frame

The origin is attached to the spacecraft. The z axis points from the spacecraft to the earth center, the y axis follows the negative normal direction the orbit plane and the x axis is defined by the right-hand rule, and points approximately along the velocity vector. We use this frame as the reference frame in spacecraft attitude control.

3.1.4 Body Frame

The attitude coordinates are chosen to be the (3-2-1) Euler angles: the body frame is first rotated about the z_1 axis by yaw angle ψ then about the rotated y_1 axis by pitch angle θ and finally about the rotated x_1 axis by roll angle ϕ. The x_1, y_1 and z_1 axis are chosen such that they are aligned with the principal body axes in a right-handed unit vectors.

3.2 Earth Magnetic Field Model and Magnetic Torque

3.2.1 Earth Magnetic Model

The magnetic field approximated by a dipole model is[60]

$$B = \frac{\mu_f}{|R|^3}\left[3(\hat{p}\cdot\hat{R})\hat{R} - \hat{p}\right] \tag{3.1}$$

where R is the position vector of the point at which the field is desired, $\hat{R}$ is the unit position vector. $\hat{p}$ is the vector dipole of the Earth's magnetic field, and the field's dipole strength is $\mu_f = 7.943\times10^{15}$ Wb-m. Notice this equation can be resolved in any coordinate system. The dipole vector, expressed in the geocentric inertial frame, is

$$\hat{p} = \begin{bmatrix} \sin\theta'_m \cos\alpha_m \\ \sin\theta'_m \sin\alpha_m \\ \cos\theta'_m \end{bmatrix} \tag{3.2}$$

$$\alpha_m = \alpha_{G0} + \frac{d\alpha_G}{dt}t + \phi'_m \tag{3.3}$$

where θ'_m is the coelevation of the dipole, ϕ'_m is the East longitude of the dipole, α_{G0} is the right ascension of the Greenwich meridian at some reference time (here we define the reference time $t = 0$ as the time when the satellite is at the ascending node of the satellite orbit), and $\frac{d\alpha_G}{dt}$ is the average rotation rate of the Earth.

Eq. (3.1) can be simplified if we express the equation in the orbit frame in the absence of the Earth rotation. First we set up the transformation matrix from the magnetic equator frame to the orbit frame

$$\begin{bmatrix} x \\ y \\ z \end{bmatrix} = \begin{bmatrix} -\sin(\omega_0 t - \eta_m) & \cos(\omega_0 t - \eta_m)\cos i_m & \cos(\omega_0 t - \eta_m)\sin i_m \\ 0 & \sin i_m & -\cos i_m \\ -\cos(\omega_0 t - \eta_m) & -\sin(\omega_0 t - \eta_m)\cos i_m & -\sin(\omega_0 t - \eta_m)\sin i_m \end{bmatrix} \begin{bmatrix} x_m \\ y_m \\ z_m \end{bmatrix} \tag{3.4}$$

where η_m is a phase angle measured from the ascending node of the orbit relative to the Earth equator to the ascending node of the orbit relative to the magnetic equator. The unit dipole vector in the magnetic equator frame is

$$\hat{p} = (0,0,-1)^T \tag{3.5}$$

Express it in the orbit frame

$$\hat{p} = \left(-\cos(\omega_0 t - \eta_m)\sin i_m, \cos i_m, \sin(\omega_0 t - \eta_m)\sin i_m\right)^T \tag{3.6}$$

The unit vector to the satellite in the orbit frame is

$$\hat{R} = (0,0,-1)^T \tag{3.7}$$

Substituting Eqs. (3.6-3.7) into Eq. (3.1) gives the magnetic field in the orbit frame,

$$\begin{bmatrix} B_x(t) \\ B_y(t) \\ B_z(t) \end{bmatrix} = \frac{\mu_f}{|R|^3} \begin{bmatrix} \cos(\omega_0 t - \eta_m)\sin i_m \\ -\cos i_m \\ 2\sin(\omega_0 t - \eta_m)\sin i_m \end{bmatrix} \tag{3.8}$$

where B_x, B_y and B_z are the components of the magnetic field B.

3.2.2 Magnetic Torque

A magnetic torque is caused by the interaction between the satellite magnetic field and the Earth magnetic field. The satellite magnetic field is produced by coils, rods and permanent magnets mounted on the satellite. The applied magnetic torque

$$M = m \times B \tag{3.9}$$

where m is the magnetic dipole moment of the torque rods and B is the Earth's magnetic field. In the body frame $m = (m_1, m_2, m_3)^T$ and $B = (B_1, B_2, B_3)^T$. From Eq. (3.9), one can see

the magnetic moments are orthogonal to the Earth magnetic field B, and no moments can be achieved along the direction of the field.

3.3 Time-Optimal Magnetic Attitude Control and Real-Time Computations

3.3.1 Introduction

Magnetic actuators have been used for momentum dumping of both low and high altitude satellites, and for the attitude control of momentum biased spacecraft, primarily those in low Earth orbit[52-53]. Of late, magnetic actuators have also been proposed as the sole means for attitude control[54,55,42], particularly for small inexpensive spacecraft. In this section, we investigate the use of magnetic actuators for the time-optimal slew maneuver towards the goal of conducting a flight test for NPSAT1[42], an experimental satellite being built at the Naval Postgraduate School (NPS). The minimum time required for a given spacecraft to perform a slew maneuver depends on the spacecraft orbital elements, its position in orbit as well as the actuator strength. Since the Earth's magnetic field is time-varying, the dynamical system is not autonomous. Junkins and Turner[21] developed time-optimal formulations leading to a simple one-dimensional two point boundary-value problem. Their numerical results suggested that the control structure was bang-bang. In May 1981, the NOVA-1 spacecraft was launched, and several large angle, minimum time maneuvers were carried out by using ground-based computers to generate the commands. In their pioneering work, Bilimoria and Wie[56] showed that eigenaxis maneuvers were not time-optimal. Further, they suggested that

significant improvements can be obtained by solving the full time optimal maneuver problem.

Recently, direct methods for solving optimal control problems have been successfully utilized. Shen and Tsiotras[57] and Yan, Fahroo and Ross[3] used direct methods to solve the time-optimal rigid spacecraft reorientation problem. Liang, Fuller and Chen applied RIOTS, a numerical optimal control software package, based on spline functions to approximate controls and Runge-Kutta methods to integrate state equations, to solve time-optimal magnetic attitude control problems[58]. They claimed the optimal control is bang-bang, and a computation time of 5 minutes on a Pentium 4 was required to solve the optimal control problem. In this section, we use the direct Legendre pseudospectral method and the corresponding software, DIDO developed by Ross and Fahroo, to numerically solve the time-optimal slew maneuver using magnetic torque. The basic idea of this method is to seek polynomial approximations for the state, costate and control functions in terms of their values at the Legendre-Gauss-Lobatto points, then solve the resulting parameter optimization problem. The parameters of the numerical example correspond to that of NPSAT1, a small satellite being built at the Naval Postgraduate School. For a benchmark 180-degree rest-to-rest maneuver, the minimum maneuver time was found to be 232.7 (sec). On a Pentium 4 the total computation time to obtain this solution was 7.2 (sec). Recent advancements in computational power and algorithms have made possible the exploitation of pseudospectral methods for real-time optimal control. What distinguishes pseudospectral methods from the other direct methods is the use of global orthogonal polynomials, such as Legendre and Chebyshev

polynomials, as the trial functions. This global orthogonality and the use of Gaussian quadrature rules create simple rules for transferring an original underlying infinite dimension problem into a low finite dimension system of algebraic equations with spectral convergence rates. Recent developments have shown that pseudospectral methods have become a promising tool to perform real-time computations of optimal control problems. In this chapter we use a warm start technique to test real-time computations. The numerical experiments reveal that real-time optimal solutions can be obtained.

3.3.2 Time-Optimal Magnetic Attitude Control

3.3.2.1 Equations of motion

The dynamic equations of angular motion are

$$\dot{\omega}_1 = \frac{M_1}{I_1} + \frac{I_2 - I_3}{I_1}\omega_2\omega_3 \tag{3.10}$$

$$\dot{\omega}_2 = \frac{M_2}{I_2} + \frac{I_3 - I_1}{I_2}\omega_3\omega_1 \tag{3.11}$$

$$\dot{\omega}_3 = \frac{M_3}{I_3} + \frac{I_1 - I_2}{I_3}\omega_1\omega_2 \tag{3.12}$$

The kinematic equations of angular motion are

$$\dot{q}_1 = 0.5(\omega_{1/O}q_4 - \omega_{2/O}q_3 + \omega_{3/O}q_2) \tag{3.13}$$

$$\dot{q}_2 = 0.5(\omega_{1/O}q_3 + \omega_{2/O}q_4 - \omega_{3/O}q_1) \tag{3.14}$$

$$\dot{q}_3 = 0.5(-\omega_{1/O} q_2 + \omega_{2/O} q_1 + \omega_{3/O} q_4) \tag{3.15}$$

$$\dot{q}_4 = 0.5(-\omega_{1/O} q_1 - \omega_{2/O} q_2 - \omega_{3/O} q_3) \tag{3.16}$$

where $(\omega_1, \omega_2, \omega_3)^T$ is the rotation rate of the body frame with respect to the inertial frame, expressed in the body frame, $(\omega_{1/O}, \omega_{2/O}, \omega_{3/O})^T$ is the rotation rate of the body frame with respect to the orbit frame, expressed in the body frame, and I_1, I_2, I_3 are the moments of inertia of the satellite about its principal axes, respectively. q_1, q_2, q_3, q_4 are the quaternion used to describe the orientation of the spacecraft in the orbit frame.

3.3.2.2 Rest-to-Rest Reorientation

We define rest-to-rest reorientation in the orbit frame. The rotational transformation from the orbit frame to the body frame is referred to as the direction cosine matrix (DCM). It is defined in terms of the quaternion vector as,

$$R_{bo} = \begin{bmatrix} q_1^2 - q_2^2 - q_3^2 + q_4^2 & 2(q_1 q_2 + q_3 q_4) & 2(q_1 q_3 - q_2 q_4) \\ 2(q_1 q_2 - q_3 q_4) & -q_1^2 + q_2^2 - q_3^2 + q_4^2 & 2(q_2 q_3 + q_1 q_4) \\ 2(q_1 q_3 + q_2 q_4) & 2(q_2 q_3 - q_1 q_4) & -q_1^2 - q_2^2 + q_3^2 + q_4^2 \end{bmatrix} \tag{3.17}$$

The DCM from the inertial frame to orbit frame is

$$R_{oe} = \begin{bmatrix} -\sin u \cos\Omega - \cos u \cos i \sin\Omega & -\sin u \sin\Omega + \cos u \cos i \cos\Omega & \cos u \sin i \\ -\sin i \sin\Omega & \sin i \cos\Omega & -\cos i \\ -\cos u \cos\Omega + \sin u \cos i \sin\Omega & -\cos u \sin\Omega - \sin u \cos i \cos\Omega & \sin u \sin i \end{bmatrix} \tag{3.18}$$

where u is the argument of latitude, Ω the longitude of the ascending node, and i the inclination of the orbit. Then the magnetic field components in the body frame are given by,

$$\begin{pmatrix} B_1 \\ B_2 \\ B_3 \end{pmatrix} = R_{bo} R_{oe} B \tag{3.19}$$

The rest-to-rest orientation is relative to the orbit frame, which is

$$\omega_{1/O}(t_0) = 0,\ \omega_{2/O}(t_0) = 0,\ \omega_{3/O}(t_0) = 0 \tag{3.20}$$

$$q_1(t_0) = q_2(t_0) = q_3(t_0) = 0,\ q_4(t_0) = 1 \tag{3.21}$$

and

$$\omega_{1/O}(t_f) = \omega_{2/O}(t_f) = \omega_{3/O}(t_f) = 0 \tag{3.22}$$

$$q_1(t_f) = q_2(t_f) = 0,\quad q_3(t_f) = \sin\frac{\beta}{2},\quad q_4(t_f) = \cos\frac{\beta}{2} \tag{3.23}$$

The angle β is the principal rotation angle[56]. t_0 is the initial time and t_f the final time.

The initial and final body angular velocities relative to the inertial frame are

$$\begin{pmatrix} \omega_1(t_0) \\ \omega_2(t_0) \\ \omega_3(t_0) \end{pmatrix} = \begin{pmatrix} \omega_{1/O}(t_0) \\ \omega_{2/O}(t_0) \\ \omega_{3/O}(t_0) \end{pmatrix} - \omega_0 \begin{pmatrix} 2(q_1(t_0)q_2(t_0) + q_3(t_0)q_4(t_0)) \\ -q_1^2(t_0) + q_2^2(t_0) - q_3^2(t_0) + q_4^2(t_0) \\ 2(q_2(t_0)q_3(t_0) - q_1(t_0)q_4(t_0)) \end{pmatrix} \tag{3.24}$$

$$\begin{pmatrix} \omega_1(t_f) \\ \omega_2(t_f) \\ \omega_3(t_f) \end{pmatrix} = \begin{pmatrix} \omega_{1/O}(t_f) \\ \omega_{2/O}(t_f) \\ \omega_{3/O}(t_f) \end{pmatrix} - \omega_0 \begin{pmatrix} 2(q_1(t_f)q_2(t_f) + q_3(t_f)q_4(t_f)) \\ -q_1^2(t_f) + q_2^2(t_f) - q_3^2(t_f) + q_4^2(t_f) \\ 2(q_2(t_f)q_3(t_f) - q_1(t_f)q_4(t_f)) \end{pmatrix} \tag{3.25}$$

where ω_O is the magnitude of the orbital angular velocity.

3.3.2.3 Time-Optimal Rest-to-Rest Reorientation

The problem addressed here is to find the optimal control vector for a spacecraft undergoing a rest-to-rest reorientation that minimizes the maneuver time using magnetic torques.

$$J = \int_{t_0}^{t_f} dt \tag{3.26}$$

subject to the state equations

$$\dot{X} = f\left(X(t), m(t), t\right) \tag{3.27}$$

or Eqs. (3.10-3.16) and the control constraints

$$m^l \le m_i \le m^u \qquad i = 1,2,3 \tag{3.28}$$

satisfying the initial and final conditions Eq (3.24)-Eq(3.25)

where

$$X = \left(\omega_1, \omega_2, \omega_3, q_1, q_2, q_3, q_4\right)^T \tag{3.29}$$

and m^l and m^u are the lower and upper limits, respectively. Notice the initial time t_0 and final time t_f are free in the formulation. The problem addressed here is a reorientation of an angle β about the yaw axis. This does not mean the rotation is necessarily about the yaw axis, but that the final orientation is equivalent to the angle β rotation.

The first step in solving the optimal control problem is to form the Hamiltonian. From optimal control theory, the Hamiltonian can be written as,

$$H = 1 + \lambda^T f \tag{3.30}$$

where the costates

$$\lambda = \left(\lambda_{\omega_1}, \lambda_{\omega_2}, \lambda_{\omega_3}, \lambda_{q_1}, \lambda_{q_2}, \lambda_{q_3}, \lambda_{q_4}\right)^T \tag{3.31}$$

Expressing the Hamiltonian, we have

$$\begin{aligned} H = {} & 1 + s_1 m_1 + s_2 m_2 + s_3 m_3 + 0.5\lambda_{q_1}\left(\omega_{1/O} q_4 - \omega_{2/O} q_3 + \omega_{3/O} q_2\right) + \\ & 0.5\lambda_{q_2}\left(\omega_{1/O} q_3 + \omega_{2/O} q_4 - \omega_{3/O} q_1\right) + 0.5\lambda_{q_3}\left(-\omega_{1/O} q_2 + \omega_{2/O} q_1 + \omega_{3/O} q_4\right) + \\ & 0.5\lambda_{q_4}\left(-\omega_{1/O} q_1 - \omega_{2/O} q_2 - \omega_{3/O} q_3\right) \end{aligned} \tag{3.32}$$

where the switching functions s_i are

$$s_1 = \frac{\lambda_{\omega_3}}{I_3} B_2 - \frac{\lambda_{\omega_2}}{I_2} B_3 \tag{3.33}$$

$$s_2 = \frac{\lambda_{\omega_1}}{I_1} B_3 - \frac{\lambda_{\omega_3}}{I_3} B_1 \tag{3.34}$$

$$s_3 = \frac{\lambda_{\omega_2}}{I_2} B_1 - \frac{\lambda_{\omega_1}}{I_1} B_2 \tag{3.35}$$

According to Pontryagin's Minimum Principle[61], the optimal control must minimize the Hamiltonian. The optimal control is

$$m_i = m^u \qquad \text{if } s_i < 0 \tag{3.36}$$

$$m_i = m^l \qquad \text{if } s_i > 0 \tag{3.37}$$

$$m_i = m_i^s \qquad \text{if } s_i \equiv 0 \tag{3.38}$$

where m_i^s are the singular controls.

3.3.3 The DIDO Discretization

Since direct methods are used to solve optimal control problems, we need to discretize the continuous model system. We use the DIDO discretization or Legendre pseudospectral method. Assume there are *N* LGL points. The NLP formulation for the spectral method is as follows. Set

$$a_l \coloneqq X(\tau_l), \quad b_l \coloneqq m(\tau_l) \tag{3.39}$$

where τ_l are the LGL points, *l=0,1,…N*. Using DIDO, the optimal control problem is discretized by the following NLP: Find the coefficients

$$a = (a_0, a_1, \cdots, a_N),\ b = (b_0, b_1, \cdots, b_N) \tag{3.40}$$

and the initial time t_0 and final time t_f to minimize

$$J^N(a,b) = t_f - t_0 \tag{3.41}$$

subject to

$$\frac{t_f - t_0}{2} f(a_k, b_k) - c_k = 0, \qquad \mathrm{k} = 0,..., N \tag{3.42}$$

$$m^l \le m_i(t_k) \le m^u \qquad i = 1,2,3 \qquad k = 0,..., N \tag{3.43}$$

$$\psi_0(a_0, t_0) = 0, \tag{3.44}$$

$$\psi_f(a_N, t_N) = 0. \tag{3.45}$$

where the w_i are the LGL weights, ψ_0 are the functions in terms of the initial states and initial time as shown in Eq. (3.24) and ψ_f are the functions in terms of the final states and final time as shown in Eq. (3.25).

3.3.4 Numerical Results

We consider a magnetically controlled small satellite as the simulation model. The satellite (NPSAT1) is being built by students and staff at the Naval Postgraduate School[5]. There are three rods, one along each axis in the satellite.

Table 3.1: Data for NPSAT1

Parameter & units	Value
Altitude ~km	560
Inclination ~deg	35.4
Right ascension ~deg	0
I_1 ~kg.m^2	5
I_2 ~kg.m^2	5.1
I_3 ~kg.m^2	2
$I_{12}=I_{13}=I_{23}$	0
Magnetic Torque Rod Saturation ~A.m^2	30

3.3.4.1 Earth Magnetic Field

The strength of the Earth magnetic field as observed by the satellite over one orbit is shown in Fig. 3.1. The figure is generated from the model Eqs. (3.1-3.3) and the values of θ_m', ϕ_m' and α_{G0} are from the Appendix H of Ref. 60.

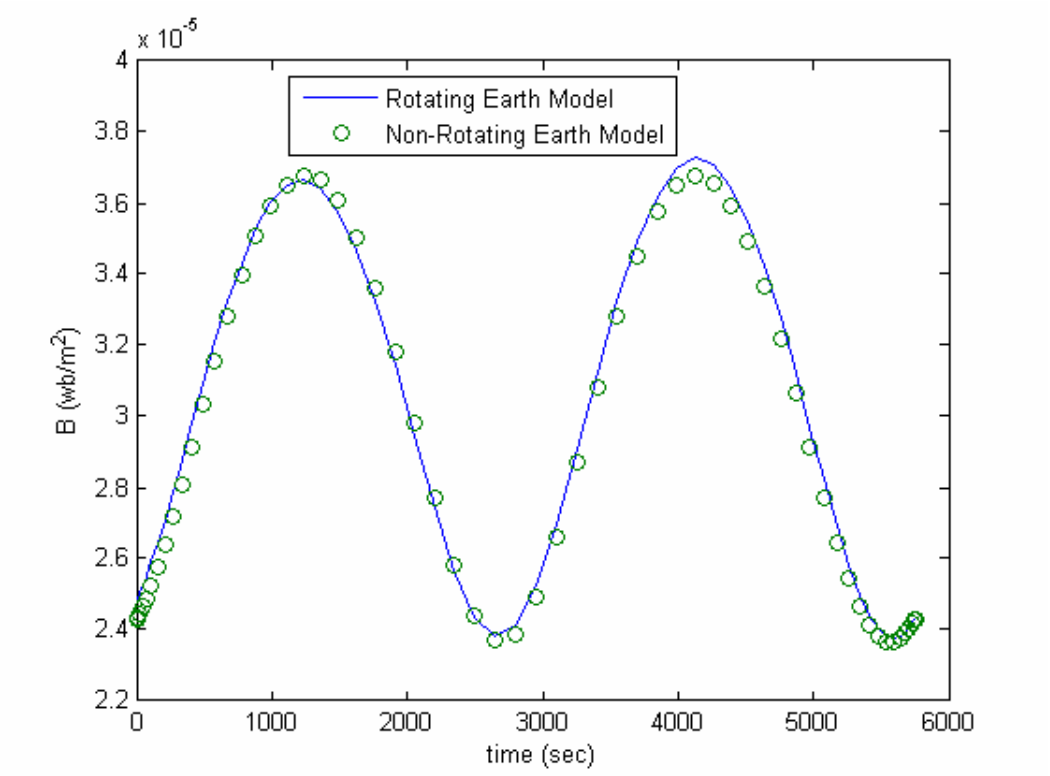

Fig. 3.1 Earth Magnetic Field

Fig. 3.1 indicates the Earth magnetic field is time-varying and there is little effect of the Earth rotation on the magnetic strength. Since we know the optimal slew maneuver times are about hundreds of seconds for the time-optimal magnetic maneuver of small satellites, as shown in Refs. 58 and 25, the starting maneuver times have a significant role in the fast maneuver.

3.3.4.2 Rest-to-Rest Time-Optimal Maneuver

Use DIDO to discretize Eqs. (3.10-16) to transfer the optimal control problem into a parameter optimization. Choose 32 LGL points. Given that the maximum possible rotation is 180 degrees, we consider this case for benchmarking the computational time. In addition, we consider rest-to-rest maneuvers as this is the only situation anticipated for NPSAT1. Maneuvers with an initial or final angular velocity could be solved with the same approach. The parameters of NPSAT1 are listed in Table 3.1. We claim that the bang-bang solution shown in Fig. 3.2 is time-optimal. Since the Legendre Pseudospectral Method, through its Covector Mapping Theorem[11], provides costate information at the nodes, we can evaluate the switching functions to check optimality according to Eqs. (3.36-38), as shown in Fig. 3.3 where the circles stand for the scaled switching functions and solid lines represent the optimal control results. From Fig. 3.3, we claim that the bang-bang control solution is time-optimal. The computation results demonstrate that there are no singular arcs.

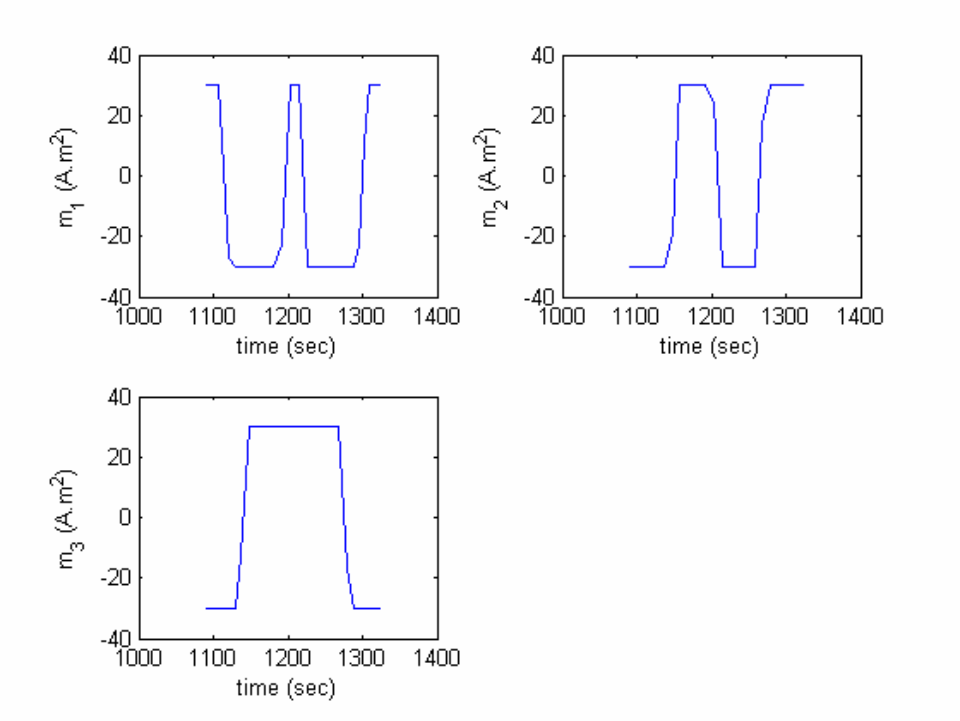

Fig. 3.2 Optimal Control

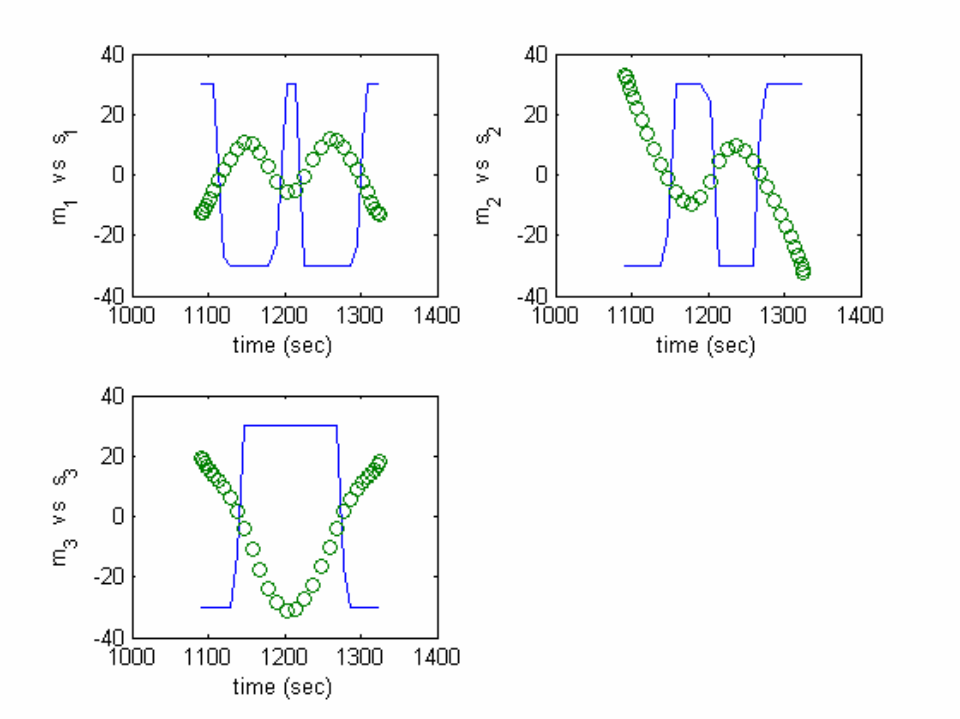

Fig. 3.3 Optimal Control and Switching Functions

As suggested in Ref. 15, the control solution is propagated through a separate ODE 45 dynamics simulator to verify that the candidate solution drives the dynamic system from the initial state to the final state. Figs. 3.4-3.5 illustrate the angular velocity relative to the orbit frame and quaternion time histories. In these figures, the circles represent the optimal solutions at the node points while the solid lines are the solutions obtained from integrating Eqs. (3.10-16) with the control from DIDO. Clearly, the solutions from DIDO are agreeable with the integration results and Eqs. (3.20-23) are satisfied. The Euler angle time history is shown in Fig. 3.6.

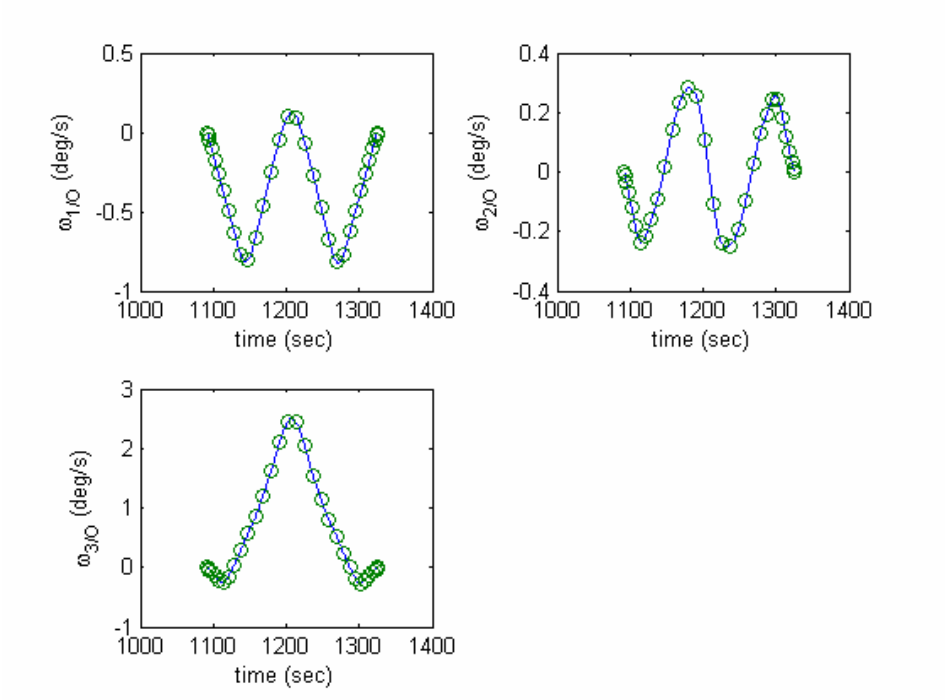

Fig. 3.4 Angular Velocity Time History

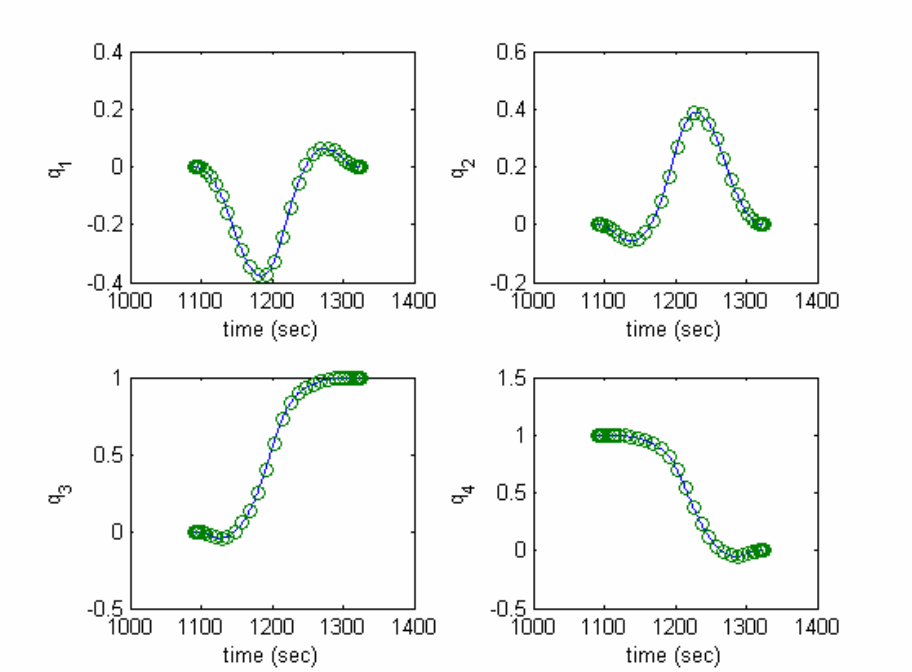

Fig. 3.5 Quaternion Time History

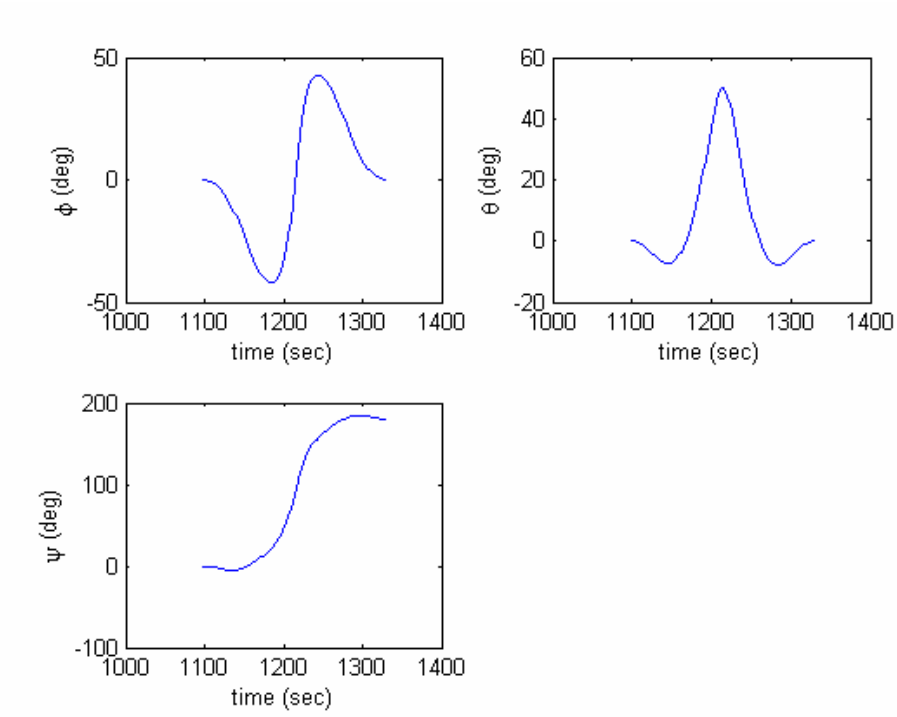

Fig. 3.6 Euler Angle Time History

Fig. 3.6 indicates there is a net angle change of 180 degree about the yaw axis. The minimum time is found to be 232.7 seconds while the computation time on a PENTIUM 4 was about 9 seconds. The maneuver is clearly not an eigenaxis slew. This is evident from both the variation in the quaternions q_1 and q_2 and the non-zero angular rates of $\omega_{1/0}$ and $\omega_{2/0}$.

The starting time of the minimum slew maneuver time is about 1098.4 seconds. From Fig. 3.1 the starting time corresponds to the maximum strength of the Earth magnetic field. The strength of the Earth magnetic field can be described from Eq. (3.8)

$$|B| = \frac{\mu_f}{|R|^3}\sqrt{1+3\sin^2(\omega_0 t-\eta_m)\sin^2 i_m} \tag{3.46}$$

Given the orbital elements, the first maximum strength time should be from *t = 0*

$$t_1 = \frac{\pi}{2\omega_0}+\frac{\eta_m}{\omega_0} \tag{3.47}$$

The phase angle η_m can be solved using spherical geometry

$$\eta_m = a\tan\left(\frac{\sin(\Omega-\alpha_m)}{\cos(\Omega-\alpha_m)\cos i+\sin i\,\mathrm{ctg}\,i_{me}}\right) \tag{3.48}$$

where i_{me} is the angle between the Earth equator and magnetic equator. Then we obtain t_1 is about 1211.2 seconds. One can see the optimal slew maneuver period is almost symmetric to t_1. This is easy to understand since the stronger the Earth magnetic field, the more powerful the magnetic torques. Thus, the start time occurs when the maneuver

is symmetric about the maximum field strength and this takes maximum advantage of the magnetic field.

3.3.4.3 Extreme Field Map

The magnetic torque equals the dipole moment crossed by the magnetic field, as shown in Eq. (3.9). We investigate if the direction of the control vector, the dipole moment *m,* should be perpendicular to the magnetic filed *B* to take the maximum advantage of the magnetic torque. For the full dimension rotations, it is difficult to find a simple extreme field map. Fig. 3.7 shows the time history of the angle between the control vector and the local magnetic field for the minimum slew maneuver time.

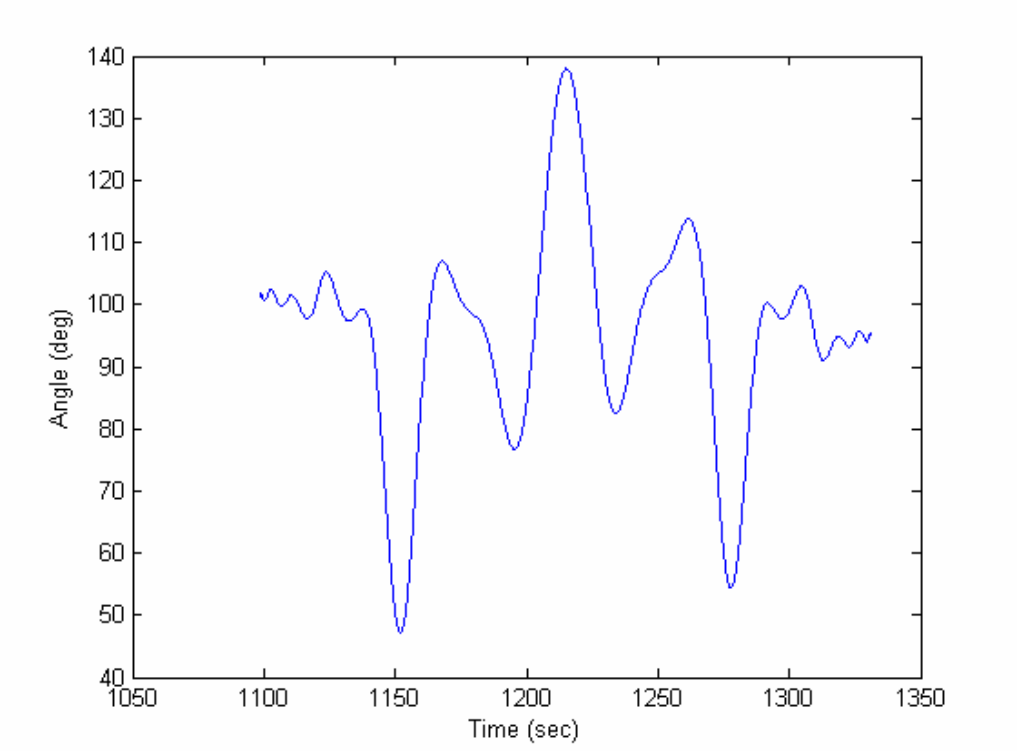

Fig. 3.7 Angle Between Control Vector and Magnetic Field

Fig. 3.7 shows there are several sharp changes at the control switching point in the angle time history since the control values are switched from one bound to another one. The average value of the angle is about 95 deg.

3.3.4.4 Local Minimums

We always wonder if the numerical solutions from direct methods converge to optimal control solutions. Actually, there are two fundamentally distinct convergence issues. One is the convergence of the discretization scheme and the other is nonlinear programming (NLP) convergence. The former means the convergence of the discretized problem to the optimal control problem as the number of nodes tends to infinity. The convergence of the NLP solver on the other hand, refers to the convergence of the NLP algorithm for a fixed number of nodes. The convergence of pseudospectral discretizations has been verified by Dr. Ross's research group[11,14]. The convergence of the NLP solver in fact belongs to applied mathematics problems.

Usually NLP problems are specified by a set of constraints. Any solutions satisfied with the constraints are called the feasible solutions. A feasible solution that minimizes object functions is called an optimal solution. In general, there will be several local minima and maxima, where a *local minimum* x^* is defined as a point such that for some $\delta > 0$ and all x around x^* such that all of the objective function value are less than or equal to the value at that point. It is easy to find local minima — additional facts about the problem (e.g. the function being convex) are required to ensure that the solution found is a global minimum.

Many popular NLP solvers use a sequential quadratic programming (SQP) method, such as NPSOL, FMINCOM, SNOPT. While they reportedly provide "accurate" results for most problems, the resulting solutions should be thoroughly checked. The need for this check arises from the fact that the NLP solutions satisfy the Karush-Kuhn-Tucker (KKT) conditions up to a prescribed degree of computational tolerance. Even for an accurate discretization scheme, these conditions converge to the first order necessary conditions of Pontryagin only in the limit. This convergence is not always uniform with respect to the degree of discretization and the choice of initial guesses. Therefore, the optimality of these solutions is dependent on the prescribed tolerance, the initial guesses for the NLP variable and the size of the NLP variables. In most cases, the SQP algorithm can only guarantee convergence to a local minimum, and several different initial guesses should be chosen to ensure that the obtained solution is indeed the "optimal" one. In some problems, different initial guesses may results in different optimal solutions (with the same value for the cost function).

Now we assume the starting time is 1098.4 seconds, arbitrarily choose 100 sets of initial guesses (cold starts). The optimal slew times are shown in Fig. 3.8.

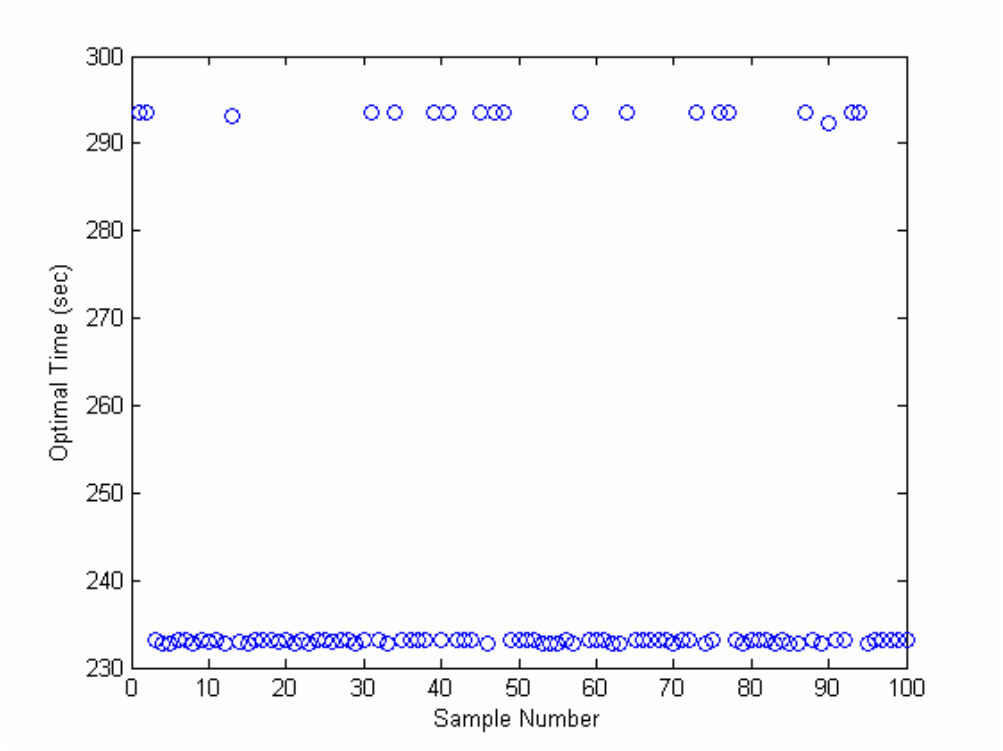

Fig. 3.8 Optimal Slew Times

From Fig. 3.8 we conclude the global optimal time should be about 232.7 seconds. The optimal values 293.7 seconds in Fig. 3.8 could be claimed as local minimums. Figs. 3.9-3.12 illustrate the solutions of the local minimum.

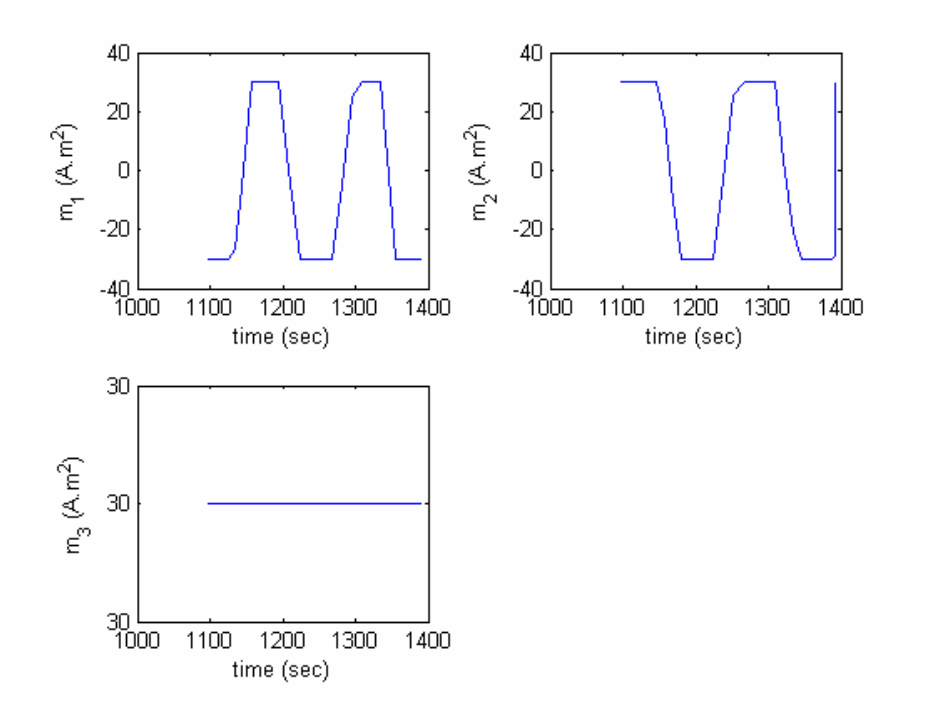

Fig. 3.9 Optimal Control Solutions (Local Minimum)

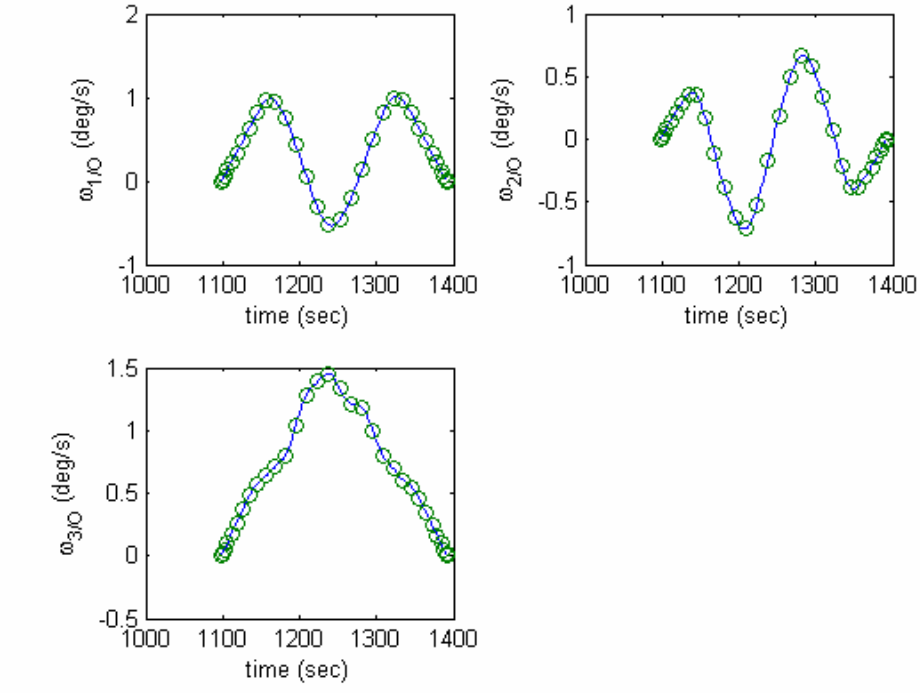

Fig. 3.10 Angular Velocity Time History (Local Minimum)

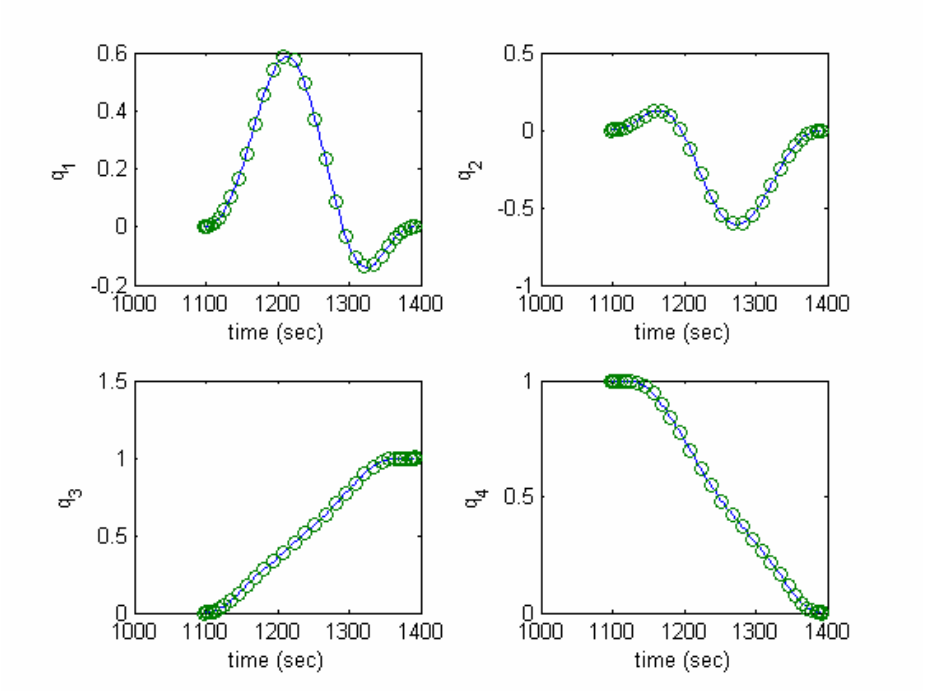

Fig. 3.11 Quaternion Time History (Local Minimum)

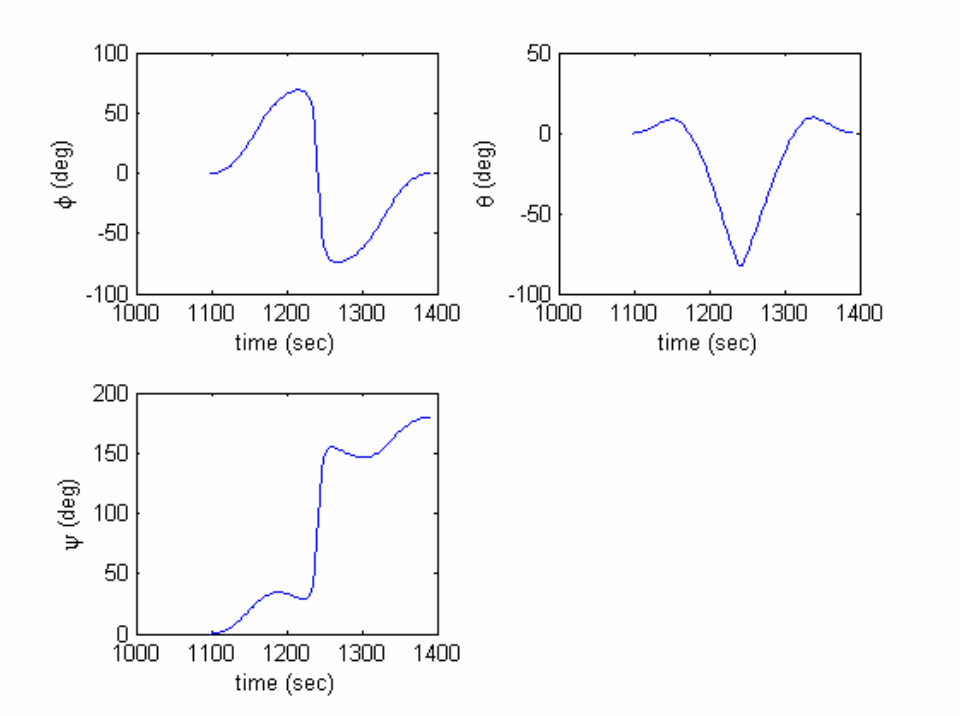

Fig. 3.12 Euler Angle Time History (Local Minimum)

In the Figs. 3.10-3.11, the circles represent the optimal solutions at the node points while the solid lines are the solutions obtained from integrating the state equations with the control from the pseudospectral methods. Obviously, the solutions from pseudospectral methods are in agreement with the integration results. Compared with Fig. 3.2, the different control switching structure is founded in the Fig. 3.9 for the local minimum solution. The similar situation is also shown in Ref. 56 where it was called as multiple minima. Fig. 3.6 and Fig. 3.12 indicate the rotations about the roll and pitch axis are in the inverse directions for two cases, respectively.

3.3.4.5 Real-Time Computation Considerations

First we test the DIDO convergence or robustness. We still use the 180 degree time-optimal rest-to-rest reorientation with 32 LGL points as an example, but the initial time is not a variable in the optimization. We choose 1000 starting times of the optimal slew evenly along about one orbit period, or we select sample starting points separated by about five seconds. We use cold starts to start the optimizations and all the initial guesses are evenly selected between 0 and 1 for the scaled optimal model. The results are shown in Fig. 3.13. Almost all the solutions are optimal, except about 1.1 percent of the 1000 samples are feasible solutions, which satisfy all the constraints but may not be optimal. The average computation time is about 19 seconds. As expected from the earlier discussion the optimal slew maneuver times do vary with the starting slew times because the magnetic field strength varies around the orbit. Fig. 3.13 shows the change of the

optimal slew times is unsmooth along the orbit, since the cold starts may lead to local minimums and we did not use any global optimization algorithms. However, the results do show the better solutions should be a smooth curve osculating to the lower limits of the optimal results from the cold starts.

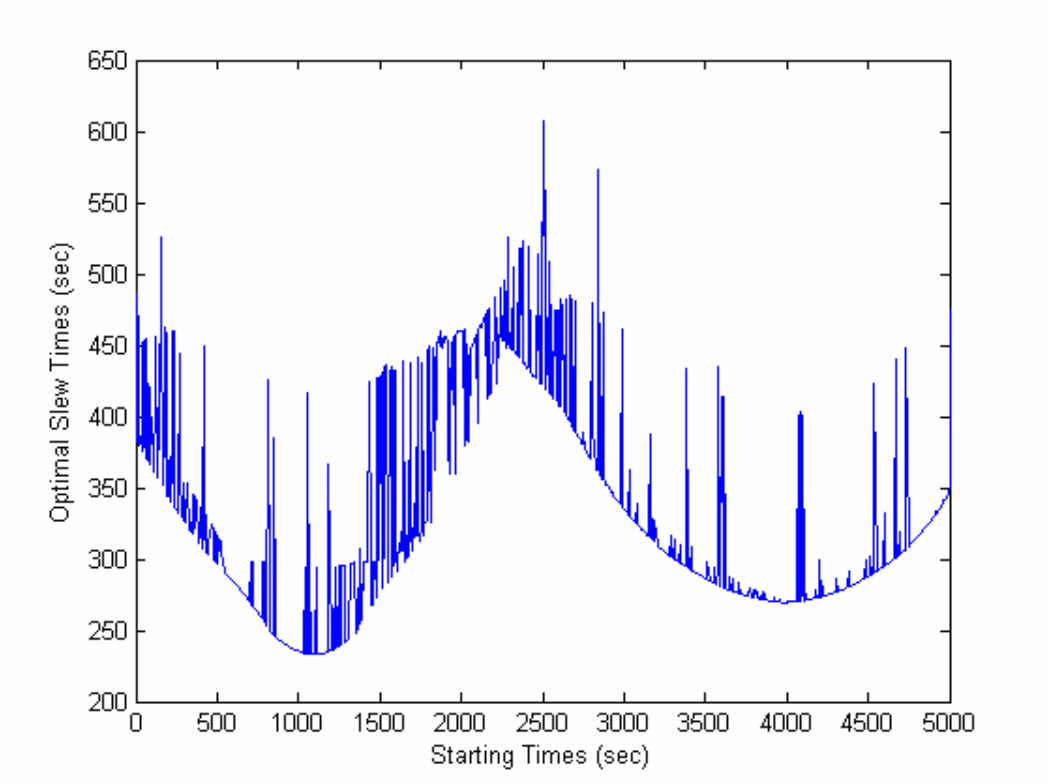

Fig. 3.13 Optimal Slew Times with Cold Starts

Although direct methods may not require good initial guesses for convergence, an educated initial guess does improve convergence rates and reliability. A warm start is a technique that starts codes based on the past history of iterations and function evaluations in the previous optimizations instead of arbitrary initial guesses or cold start. Quite often we need to solve many slightly-changed versions of the same base model. It

makes sense in this situation that the optimal solution of a previous version ought to serve as an excellent warm start starting point for the current version of the model, if the two versions of the model are similar. We solve the same problem but the warm start technique is used for initial guesses. Our solutions indicate all the solutions are optimal ones except about 0.8 percent which are feasible solutions. The average computation time is about 0.45 seconds. The results show there is a big computation time reduction using a warm start technique, which is a great potential for real-time computations. The optimal solutions with the warm start are illustrated in Fig. 3.14. In the figure, one can see the optimal slew maneuver times vary from as low as 232 seconds to as high as 450 seconds, dependent on different starting times. Comparing Fig. 3.14 with Fig. 3.1, there is an inverse relationship between the Earth magnetic strength and optimal slew times.

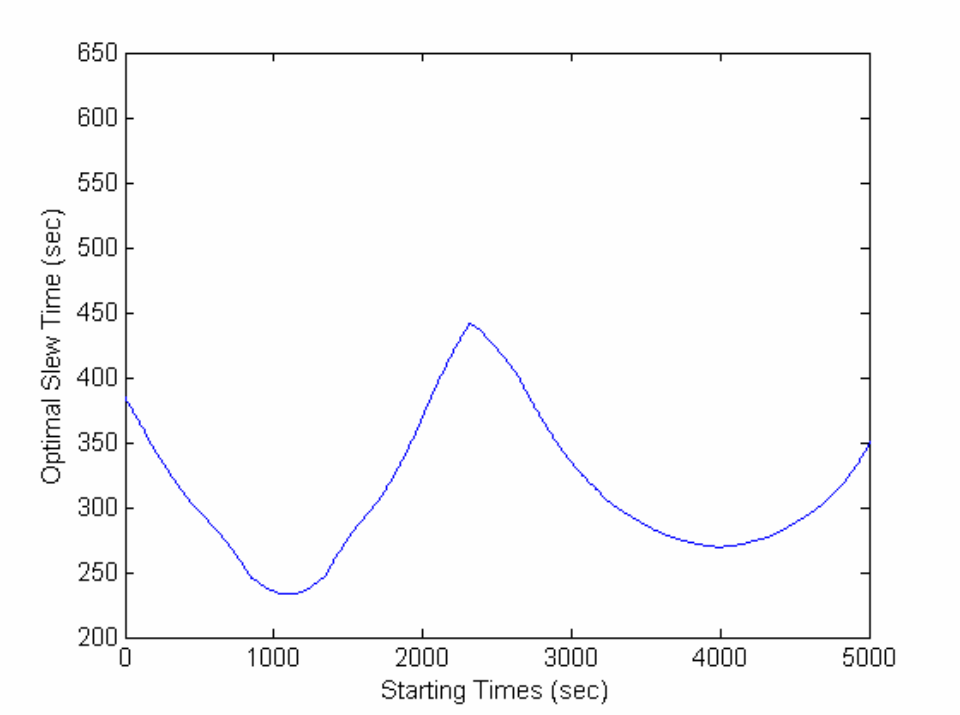

Fig. 3.14 Optimal Slew Times with Warm Start

Fig. 3.15 shows the optimal solutions with the warm start technique and optimal results using the cold starts. In the figure the circles represent the solutions from the warm start while the solid lines stand for the ones from the cold starts.

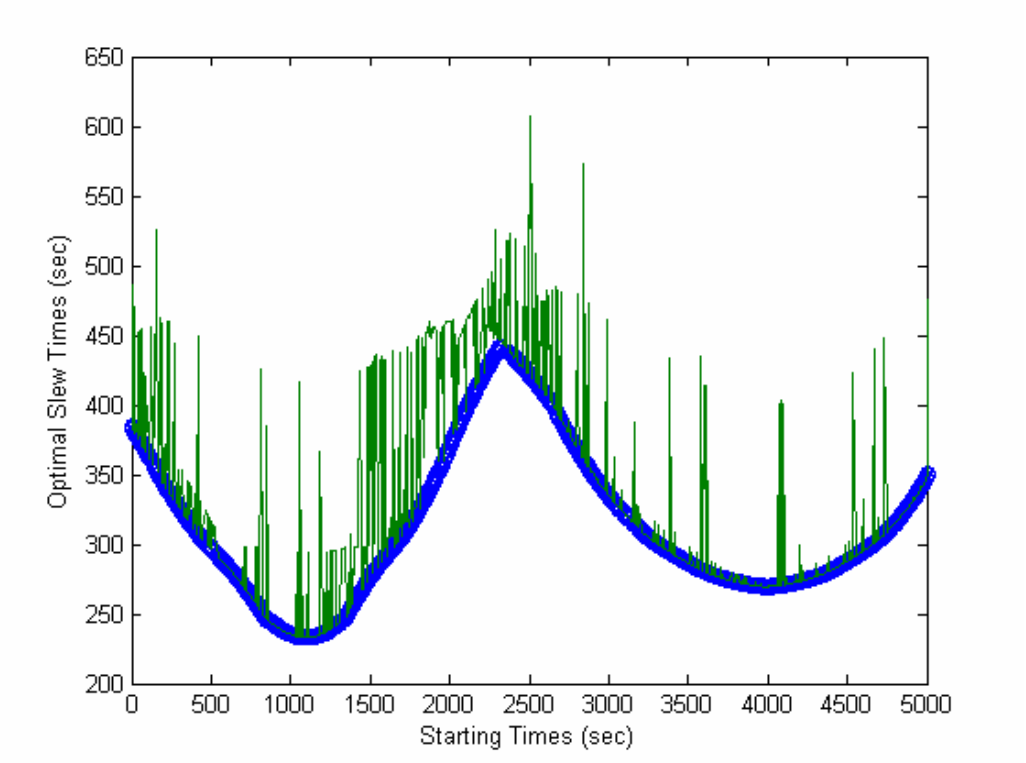

Fig. 3.15 Comparisons for Optimal Slew Time

The comparison results in Fig. 3.15 suggest the solutions from the warm start are tangential to the lower limits of the optimal results from the cold starts, which means the former solutions are better than the latter ones. As warm start techniques offer a faster convergence rate and better solutions compared with bad initial guesses, we would like to note warm start techniques should be used for slightly-altered version situations.

3.3.5 Remarks

The time optimal attitude rest-to-rest attitude maneuver for a satellite in low Earth orbit with magnetic control has been solved. The feasibility of the solutions has been verified by numerical integration while the necessary conditions resulting from the Minimum Principle are checked for optimality. The time-optimal magnetic control is bang-bang. The optimal maneuver is not an eigenaxis slew. The optimal slew time is about 232.7 seconds. The start time occurs when the maneuver is symmetric about the maximum field strength. For real-time computations, all the tested samples converge to optimal solutions or feasible solutions. We find the average computation time is about 0.45 seconds with the warm start and 19 seconds with the bad initial guess, which is a great potential for real-time computations. The optimal solutions from the warm start are better than those from the bad initial guess. The results show that DIDO is a very robust algorithm in solving optimal control problems.

3.4 Three-Axis Magnetic Attitude Control Using Pseudospectral Control Law in Eccentric Orbits

3.4.1 Introduction

Attitude stabilization systems play an important role in spacecraft attitude control. In general, they are classified as active and passive. The simplicity and low cost of active magnetic control make it an attractive option for small satellites in low Earth orbit (LEO) when precise attitude control is not a requirement.

There are many published papers concerned with active magnetic attitude stabilization[55,62-65]. Both linear and nonlinear methods have been investigated. For linearized magnetic systems most of the models can be formulated as linear quadratic regulators (LQR). A key challenge is the fact that the magnetic torque can only be produced in a plane perpendicular to the local Earth field vector, therefore the satellite is not controllable when considered at a fixed time[62]. However, for orbits which are inclined to the Earth's magnetic equator the direction of the field vector changes and it is possible to use this changing direction to stabilize motion over the entire orbit[65]. Solving the LQR with linear time varying (LTV) systems requires an efficient solution of the Ricatti equation. Solving Ricatti equations is time expensive in real-time. To reduce this computational burden, the steady-state periodic solutions were obtained by averaging the periodic matrix in the Riccati equations[55,62]. The difference caused by using the average is considered an additional external disturbance torque acting on the satellite.

In general the operating orbits for Earth pointing satellites in low earth orbit (LEO) are restricted to near circular orbits. However, there are some missions in which an eccentric orbit is desirable. Since the angular velocity and hence, angular momentum, are time-varying in eccentric orbits there is a time varying gravity gradient pitch torque that is proportional to the eccentricity. Thus, to maintain the satellite attitude, which is usually nadir pointing, some kind of passive or active control is required. As we know, the gravity gradient torque can be used to passively stabilize the attitude of a satellite. However, even if the gravity gradient torque stabilizes the spacecraft some active control may still be required. For this stabilization to be effective the main requirement is a

favorable inertia distribution. There are two stable satellite's inertia distributions for the case of a circular orbit. One is a satellite's minor axis is vertical and the major axis is normal to the orbit. In this case the Hamiltonian is positive definite at the nadir pointing equilibrium point. Hence, it is Liapunov stable[66]. In the second case the intermediate axis is aligned with the local vertical, and the minor axis is normal to the orbit. In this case the system is being stabilized by the gyroscopic forces and the Hamiltonian is indefinite at the equilibrium point. Since the rotation is about the minor axis, any slight damping or disturbance will result in instability and drift away from the equilibrium point. Consequently, the second case is impractical for passive attitude control. In eccentric orbits the gravity gradient disturbance due to the eccentricity can make a satellite that is in the circular orbit gravity gradient stable configuration tumble. The orbit eccentricity at which the satellite begins to tumble varies with the spacecraft shape, but is generally between 0.05 and 0.2[67].

Active attitude stabilization in eccentric orbits was widely investigated in the 60-70's[68-71]. The control methods focused on momentum exchange devices and cold gas plants. Magnetic attitude control has been utilized extensively since the 70's for momentum bias LEO satellites[72-73]. Seldom were only magnetic torques proposed until the 1990's when several papers appeared that proposed three-axis magnetic attitude stabilization for non-momentum bias satellites in circular orbits[55,62-65]. Each of these was for a small satellite.

One challenge of magnetic attitude stabilizations in eccentric orbits is the Earth magnetic field and gravity gradient torque are time-varying since they are related to the

orbital elements of the eccentric orbits. Another problem comes from the specific direction of the magnetic torque, which is perpendicular to the Earth magnetic field. Consequently, there is no way to totally reject the attitude librations due to the eccentricity using only magnetic torques.

We apply the pseudospectral control law to magnetic attitude control in eccentric orbits. Pseudospectral methods have been used very effectively in solving a wide variety of nonlinear optimal control problems as illustrated in Refs. 11-12, 7. The basic idea of this method is to seek polynomial approximations for the state, costate and control functions in terms of their values at the Legendre-Gauss-Lobatto (LGL) points. Thus it is apparent that the LQR problems can easily be transformed to a quadratic programming (QP) problem (a quadratic cost function subject to linear algebraic constraints)[8]. Ref. 38 compared pseudospectral techniques to Ricatti methods in solving LQR problems and showed that there is a huge reduction in the number of equations to be solved and the required computer memory storage. While Refs. 8, 35-36 and 38 solved their QP numerically, we derived the analytical solutions as shown in Ref. 39. Compared with another analytical control law using step by step replacements for the states in Ref. 34, our approach is easy to derive and implement.

Based on the analytical solutions we propose a closed form control law to apply to receding horizon control problems. In the receding horizon control, an optimal control is determined on-line over a finite horizon in terms of current time and states. The first move of the optimal control sequence is then implemented until the next measurements of the states are available. Repeating this procedure, the receding horizon control can be

considered as a feedback control. Our results show three-axis magnetic attitude stabilization is achieved by using the pseudospectral control law via the receding horizon control in eccentric orbits. The residual librations errors are within 1 degree for an eccentricity of 0.1.

3.4.2 Magnetic Attitude Dynamic Model

The dynamic equations of angular motion are

$$\dot{\omega}_1 = \frac{M_1 + G_1}{I_1} + \frac{I_2 - I_3}{I_1}\omega_2\omega_3 \tag{3.49}$$

$$\dot{\omega}_2 = \frac{M_2 + G_2}{I_2} + \frac{I_3 - I_1}{I_2}\omega_1\omega_3 \tag{3.50}$$

$$\dot{\omega}_3 = \frac{M_3 + G_3}{I_3} + \frac{I_1 - I_2}{I_3}\omega_1\omega_2 \tag{3.51}$$

where I_1, I_2, I_3 are the moments of inertia of the satellite about its principal axes, respectively. $(\omega_1, \omega_2, \omega_3)^T$ is the rotation rate of the body frame with respect to the inertial frame, expressed in the body frame. The gravity gradient moments are[74]

$$G = 1.5\frac{\mu}{R^3}\begin{pmatrix} (I_3 - I_2)\cos^2\theta\sin 2\phi \\ -(I_1 - I_3)\cos\phi\sin 2\theta \\ -(I_2 - I_1)\sin\phi\sin 2\theta \end{pmatrix} \tag{3.52}$$

and $G = [G_1 \quad G_2 \quad G_3]^T$.

The body angular velocity relative to the orbit frame expressed in the body frame is

$$\omega_{B/O} = \begin{bmatrix} -\sin\theta & 0 & 1 \\ \sin\phi\cos\theta & \cos\phi & 0 \\ \cos\phi\cos\theta & -\sin\phi & 0 \end{bmatrix} \begin{bmatrix} \dot{\psi} \\ \dot{\theta} \\ \dot{\phi} \end{bmatrix} \tag{3.53}$$

We have

$$\omega_{B/E} = \omega_{B/O} + R_{BO} \begin{bmatrix} 0 \\ -\omega_0 \\ 0 \end{bmatrix} \tag{3.54}$$

where ω_0 is the orbital velocity and the transformation matrix is

$$R_{BO} = \begin{bmatrix} \cos\theta\cos\psi & \cos\theta\sin\psi & -\sin\theta \\ \sin\phi\sin\theta\cos\psi - \cos\phi\sin\psi & \sin\phi\sin\theta\sin\psi + \cos\phi\cos\psi & \sin\phi\cos\theta \\ \cos\phi\sin\theta\cos\psi + \sin\phi\sin\psi & \cos\phi\sin\theta\sin\psi - \sin\phi\cos\psi & \cos\phi\cos\theta \end{bmatrix} \tag{3.55}$$

Linearizing for small angles and rates gives,

$$\omega_{B/E} = \begin{bmatrix} \dot{\phi} - \omega_0\psi \\ \dot{\theta} - \omega_0 \\ \dot{\psi} + \omega_0\phi \end{bmatrix} \tag{3.56}$$

Differentiating gives

$$\dot{\omega}_{B/E} = \begin{bmatrix} \ddot{\phi} - \omega_0\dot{\psi} - \dot{\omega}_0\psi \\ \ddot{\theta} - \dot{\omega}_0 \\ \ddot{\psi} + \omega_0\dot{\phi} + \dot{\omega}_0\phi \end{bmatrix} \tag{3.57}$$

Substituting Eqs. (3.56-57) into Eqs. (3.49-51) and linearizing again gives

$$\dot{X} = AX + Gm + F_d \tag{3.58}$$

$$X = \left[\phi\ \theta\ \psi\ \dot{\phi}\ \dot{\theta}\ \dot{\psi}\right]^T \tag{3.59}$$

where

$$F_d = \begin{bmatrix} 0 & 0 & 0 & 0 & \dot{\omega}_0 & 0 \end{bmatrix}^T \tag{3.60}$$

$$A = \begin{bmatrix} 0 & 0 & 0 & 1 & 0 & 0 \\ 0 & 0 & 0 & 0 & 1 & 0 \\ 0 & 0 & 0 & 0 & 0 & 1 \\ -\left(3\frac{\mu}{R^3} + \omega_0^2\right)\sigma_1 & 0 & \dot{\omega}_0 & 0 & 0 & \omega_0(1-\sigma_1) \\ 0 & 3\frac{\mu}{R^3}\sigma_2 & 0 & 0 & 0 & 0 \\ -\dot{\omega}_0 & 0 & \omega_0^2\sigma_3 & -\omega_0(1+\sigma_3) & 0 & 0 \end{bmatrix} \tag{3.61}$$

$$G = \begin{bmatrix} 0 & 0 & 0 \\ 0 & 0 & 0 \\ 0 & 0 & 0 \\ 0 & \frac{B_3}{I_1} & -\frac{B_2}{I_1} \\ -\frac{B_3}{I_2} & 0 & \frac{B_1}{I_2} \\ \frac{B_2}{I_3} & -\frac{B_1}{I_3} & 0 \end{bmatrix} \tag{3.62}$$

$$\sigma_1 = (I_2 - I_3)/I_1\,,\ \ \sigma_2 = (I_3 - I_1)/I_2\ ,\ \sigma_3 = (I_1 - I_2)/I_3 \tag{3.63}$$

Note that the gravity gradient torque is included in Eq. (3.61).

3.4.3 Control Law Design

We can see there is a forced term in Eq. (3.58). The term can be expressed as

$$T_d = I_2\dot{\omega}_0 \tag{3.64}$$

where

$$\dot{\omega}_0 = \frac{K}{I_2}\sin f \tag{3.65}$$

and

$$K = -2I_2 e\frac{\mu}{R^3} \tag{3.66}$$

where f is the true anomaly and e is the eccentricity. T_d can be considered as a known disturbance. A standard way of minimizing the effect of a known disturbance torque is to feed forward the estimate of the torque to the control system so that the system does not have to wait to respond to the effect of the torque. Since a feed forward is an open loop, a linear quadratic regulator (LQR) is used coincidently together with the feed forward control to compensate for the latter's inaccuracies and track reference trajectories.

3.4.3.1 Feed Forward Control Design

Magnetic torques are used to reject the known disturbance. The magnetic control torques are

$$T_{f1} = \overline{m}_2 B_3 - \overline{m}_3 B_2 \tag{3.67}$$

$$T_{f2} = \overline{m}_3 B_1 - \overline{m}_1 B_3 \tag{3.68}$$

$$T_{f3} = \overline{m}_1 B_2 - \overline{m}_2 B_1 \tag{3.69}$$

where $\overline{m}_1, \overline{m}_2, \overline{m}_3$ are the components of the dipole vector $\overline{m}$ in the body frame. Since the known disturbance is along the pitch direction, Eqs. (3.67-69) indicate we can't totally reject the disturbance due to magnetic interaction. To minimize the known disturbance effects, we introduce the following performance index

$$J_f = T_{f1}^2 + \left(T_{f2} - T_d\right)^2 + T_{f3}^2 \tag{3.70}$$

The magnetic control torque

$$T_f = \overline{m} \times B \tag{3.71}$$

One can see from Eq. (3.71) that the minimum $\|\overline{m}\|$ occurs when[75]

$$\overline{m} \cdot B = 0 \tag{3.72}$$

since a magnetic moment generated in the direction parallel to the magnetic field has no influence on the attitude control. The augmented performance after adding Eq. (3.72) to Eq. (3.70) and substituting for the control torques gives

$$\bar{J}_f = \left(\overline{m}_2 B_3 - \overline{m}_3 B_2\right)^2 + \left(\overline{m}_3 B_1 - \overline{m}_1 B_3 - K \sin f\right)^2 + \left(\overline{m}_1 B_2 - \overline{m}_2 B_1\right)^2 + \xi \overline{m} \cdot B \tag{3.73}$$

where ξ is a Lagrange multiplier. Taking the partials for optimal solutions gives

$$\left(B_2^2 + B_3^2\right)\overline{m}_1 - B_1 B_2 \overline{m}_2 - B_1 B_3 \overline{m}_3 + B_3 K \sin f + 2\xi B_1 = 0 \tag{3.74}$$

$$-B_2 B_1 \overline{m}_1 + \left(B_1^2 + B_3^2\right)\overline{m}_2 - B_2 B_3 \overline{m}_3 + 2\xi B_2 = 0 \tag{3.75}$$

$$-B_1 B_3 \overline{m}_1 - B_2 B_3 \overline{m}_2 + \left(B_1^2 + B_2^2\right)\overline{m}_3 - B_1 K \sin f + 2\xi B_3 = 0 \tag{3.76}$$

Solving Eqs. (3.74-76) with Eq. (3.72) gives

$$\overline{m}_1 = -\frac{B_3}{B^2} K \sin f \tag{3.77}$$

$$\overline{m}_2 = 0 \tag{3.78}$$

$$\overline{m}_3 = \frac{B_1}{B^2} K \sin f \tag{3.79}$$

where $B^2 = B_1^2 + B_2^2 + B_3^2$. Substituting Eqs. (3.77-79) into Eq. (3.70), we have

$$J_f = \frac{B_2^2}{B^2}\left(K \sin f\right)^2 \tag{3.80}$$

which is much less than one would have if there was no feed forward control.

3.4.3.2 LQR Control Design

Considering the feed forward control term, Eq. (3.58) becomes

$$\dot{X} = AX + G(m - \overline{m}) + F_d \tag{3.81}$$

with the initial conditions

$$X(t_0) = X_0 \tag{3.82}$$

The problem is to determine the optimal control $m(t)$ and the corresponding state vector $X(t)$ satisfying Eqs. (3.81-82) while minimizing

$$J = \frac{1}{2} X^T(t_f) P_f X(t_f) + \frac{1}{2} \int_{t_0}^{t_f} \left[X^T(t) Q(t) X(t) + m^T(t) R(t) m(t) \right] dt \tag{3.83}$$

where P_f and $Q(t)$ are $n \times n$ weight symmetric semidefinite matrices, and $R(t)$ is a $m \times m$ weight symmetric positive definite matrix. The matrices are set as unit ones.

The Hamiltonian for this system is

$$H = \frac{1}{2} [X^T(t) Q(t) X(t) + m^T(t) R(t) m(t)] + \lambda^T(t) (AX + Gm - G\overline{m} + F_d) \tag{3.84}$$

where $\lambda(t)$ are costate vectors. According to the calculus of variations, we have the costate equations

$$\dot{\lambda}(t) = -\frac{\partial H}{\partial X} = -[Q(t) X(t) + A^T(t) \lambda(t)] \tag{3.85}$$

and the necessary optimality conditions

$$\frac{\partial H}{\partial m} = 0 \quad \text{or} \quad m(t) = F(t) \lambda(t) \tag{3.86}$$

where $F(t) = -R^{-1}(t) G^T(t)$

The transversality conditions are

$$\lambda(t_f) = P_f X(t_f) \tag{3.87}$$

Substituting Eq. (3.86) into Eq. (3.81), we have the following linear TPBVP.

$$\begin{bmatrix} \dot{X} \\ \dot{\lambda} \end{bmatrix} = \begin{bmatrix} A(t) & G(t)F(t) \\ -Q(t) & -A^T(t) \end{bmatrix} \begin{bmatrix} X \\ \lambda \end{bmatrix} + \begin{bmatrix} -G(t)\overline{m} + F_d \\ O_n \end{bmatrix} \tag{3.88}$$

where O_n is a $n \times 1$ zero vector. Analytical control laws will be obtained with the Legendre pseudospectral method by solving Eq. (3.88) with the conditions Eq. (3.82) and Eq. (3.87) .

3.4.4 Pseudospectral Method with the Known Disturbance

The basic idea of this method is to seek polynomial approximations for the state, costate and control functions in terms of their values at the Legendre-Gauss-Lobatto (LGL) points. Then the LTV systems with quadratic criteria are reduced to solving a system of algebraic equations. Based on the algebraic equations, the analytical control laws can be derived.

Since the problem presented in the previous section is formulated over the time interval $[t_0, t_f]$, and the LGL points lie in the interval [-1, 1], we use the following transformation to express the problem for $\tau \in [\tau_0, \tau_N] = [-1, 1]$:

$$t = \frac{(t_f - t_0)\tau + (t_f + t_0)}{2} \tag{3.89}$$

The use of the symbol τ_N (which maps to t_f) will be apparent shortly. It follows that Eq. (3.88), Eq. (3.82) and Eq. (3.87) can be replaced by

$$\dot{X}(\tau) = \frac{t_f - t_0}{2}[A(\tau)X(\tau) + G(\tau)F(\tau)\lambda(\tau) - G(\tau)\bar{m} + F_d] \tag{3.90}$$

$$\dot{\lambda}(\tau) = -\frac{t_f - t_0}{2}[Q(\tau)X(\tau) + A^T(\tau)\lambda(\tau)] \tag{3.91}$$

$$X(-1) = X_0 \tag{3.92}$$

$$\lambda(1) = SX(1) \tag{3.93}$$

Let $L_N(\tau)$ be the Legendre polynomial of degree N on the interval [-1, 1]. In the Legendre collocation approximation of Eqs. (3.90-93), we use the LGL points, $\tau_l, l = 0, \cdots, N$ which are given by

$$\tau_0 = -1, \qquad \tau_N = 1, \tag{3.94}$$

and for $1 \le l \le N-1$, τ_l are the zeros of $\dot{L}_N$, the derivative of the Legendre polynomial L_N. There are no closed form expressions for these nodes, and they have to be computed numerically. For approximating the continuous equations, we seek a polynomial approximation of the form

$$X^N(\tau) = \sum_{l=0}^{N} X(\tau_l)\phi_l(\tau) \tag{3.95}$$

$$m^N(\tau) = \sum_{l=0}^{N} m(\tau_l)\phi_l(\tau) \tag{3.96}$$

$$\lambda^N(\tau) = \sum_{l=0}^{N} \lambda(\tau_l)\phi_l(\tau) \tag{3.97}$$

where for $l = 0,1,\cdots,N$

$$\phi_l(\tau) = \frac{1}{N(N+1)L_N(\tau_l)} \frac{(\tau^2 - 1)\dot{L}_N(\tau)}{\tau - \tau_l} \tag{3.98}$$

are the Lagrange polynomials of order N. It can be shown that

$$\phi_l(\tau_k) = \delta_{lk} = \begin{cases} 1 & \text{if } l = k \\ 0 & \text{if } l \neq k \end{cases} \tag{3.99}$$

From this property of ϕ_l it follows that

$$X^N(\tau_l) = X(\tau_l),\ m^N(\tau_l) = m(\tau_l),\ \ \lambda^N(\tau_l) = \lambda(\tau_l), \tag{3.100}$$

Generally the approximations are expressed as

$$X(\tau) \approx X^N, \quad m(\tau) \approx m^N, \quad \lambda(\tau) \approx \lambda^N, \tag{3.101}$$

but in this collocation method, as stated in Eq. (3.100), the values of the approximate state, control and costate functions are given exactly by the value of the continuous functions at these points.

To express the derivatives $\dot{X}^N$ and $\dot{\lambda}^N$ in terms of $X^N(\tau)$ and $\lambda^N(\tau)$ at the collocation points τ_l respectively, we differentiate Eq. (3.95) and Eq. (3.97), which results in a matrix multiplication of the following forms:

$$\dot{X}^N(\tau_k) = \sum_{l=0}^{N} D_{kl} X(\tau_l) \tag{3.102}$$

$$\dot{\lambda}^N(\tau_k) = \sum_{l=0}^{N} D_{kl} \lambda(\tau_l) \tag{3.103}$$

where the D_{kl} are the entries of the $(N+1)\times(N+1)$ differentiation matrix D

$$D = [D_{kl}] = \begin{cases} \dfrac{L_N(\tau_k)}{L_N(\tau_l)} \dfrac{1}{\tau_k - \tau_l} & k \neq l \\ -\dfrac{N(N+1)}{4} & k = l = 0 \\ \dfrac{N(N+1)}{4} & k = l = N \\ 0 & \text{otherwise} \end{cases} \tag{3.104}$$

3.4.5 Analytical Feedback Control Law for the Known Disturbance

We set

$$a = (a_0, a_1, \cdots, a_N) \tag{3.105}$$

$$b = (b_0, b_1, \cdots, b_N) \tag{3.106}$$

$$c = (c_0, c_1, \cdots, c_N) \tag{3.107}$$

and use the notation

$$a_l \coloneqq X(\tau_l), \quad b_l \coloneqq m(\tau_l), \quad c_l \coloneqq \lambda(\tau_l), \tag{3.108}$$

to rewrite Eqs. (3.95-97) in the form:

$$X^N(\tau) = \sum_{l=0}^{N} a_l \phi_l(\tau) \tag{3.109}$$

$$m^N(\tau) = \sum_{l=0}^{N} b_l \phi_l(\tau) \tag{3.110}$$

$$\lambda^N(\tau) = \sum_{l=0}^{N} c_l \phi_l(\tau) \tag{3.111}$$

Eqs. (3.90-91) and Eq. (3.86) are discretized and transformed into the following algebraic equations in terms of the coefficients a, b and c at the LGL nodes, t_k:

$$\sum_{l=0}^{N} D_{kl} a_l - \frac{\tau_f - \tau_0}{2}(A_k a_k + G_k F_k c_k) = \frac{\tau_f - \tau_0}{2}\left(F_{dk} - G_k \overline{m}_k\right) \tag{3.112}$$

$$\sum_{l=0}^{N} D_{kl} c_l + \frac{\tau_f - \tau_0}{2}(Q_k a_k + A_k^T c_k) = 0 \tag{3.113}$$

$$b_k - F_k c_k = 0 \tag{3.114}$$

$$k = 0,1,\cdots,N,$$

or

$$\tilde{A}_{-} a - \frac{\tau_f - \tau_0}{2}\tilde{G} c = V_f \tag{3.115}$$

$$\frac{\tau_f - \tau_0}{2}\tilde{Q} a + \tilde{A}_{+} c = 0 \tag{3.116}$$

$$b - Pc = 0 \tag{3.117}$$

where

$\tilde{A}_{-}, \tilde{A}_{+}, \tilde{G}, \tilde{Q}$ and P are $[n\times(N+1)]\times[n\times(N+1)]$ matrices whose (ij) th blocks are $n\times n$ matrices of the following form

$$[\tilde{A}_{-}]_{ij} = \begin{cases} D_{ij} I_n & i \neq j \\ D_{ii} I_n - \dfrac{\tau_f - \tau_0}{2} A_i & i = j \end{cases} \tag{3.118}$$

$$[\tilde{A}_{+}]_{ij} = \begin{cases} D_{ij} I_n & i \neq j \\ D_{ii} I_n + \dfrac{\tau_f - \tau_0}{2} A_i^T & i = j \end{cases} \tag{3.119}$$

$$[\tilde{G}]_{ij} = \begin{cases} 0_n & i \neq j \\ \overline{B}_i F_i & i = j \end{cases} \tag{3.120}$$

$$[\tilde{Q}]_{ij} = \begin{cases} 0_n & i \neq j \\ Q_i & i = j \end{cases} \tag{3.121}$$

$$[P]_{ij} = \begin{cases} 0_n & i \neq j \\ F_i & i = j \end{cases} \tag{3.122}$$

In the above, I_n is the $n \times n$ unity matrix and 0_n is the $n \times n$ zero matrix. V_f is a $[n \times (N+1)] \times 1]$ vector and

$$\left[V_f\right]_i = \frac{\tau_f - \tau_0}{2}\left(F_{di} - G_i \overline{m}_i\right) \tag{3.123}$$

The initial conditions are

$$a(0) = a_0 \tag{3.124}$$

The terminal constraints are forced for the stabilization of the receding horizon control[49].

$$a(N) = 0 \tag{3.125}$$

$$c(N) = 0 \tag{3.126}$$

The goal is to solve Eqs. (3.115-117) subject to the transversality conditions Eqs. (3.124-126). Therefore, first we write the equations for the state and costate vectors a and c in block form to have the block matrix form

$$\begin{bmatrix} \tilde{A}_- & -\frac{\tau_f - \tau_0}{2}\tilde{G} \\ \frac{\tau_f - \tau_0}{2}\tilde{Q} & \tilde{A}_+ \\ \tilde{P}_1 & \tilde{P}_2 \end{bmatrix} \begin{bmatrix} a \\ c \end{bmatrix} \equiv Vz = \begin{bmatrix} V_f \\ 0 \\ 0 \end{bmatrix} \equiv V_w \tag{3.127}$$

In these equations,

$$a = [a_0^T, a_1^T, \cdots, a_N^T]^T, \quad c = [c_0^T, c_1^T, \cdots, c_N^T]^T, \quad z^T = [a^T, c^T] \tag{3.128}$$

and $\tilde{P}_1$ and $\tilde{P}_2$ are the following matrices

$$\tilde{P}_1 = \begin{bmatrix} O & I_n \\ O & 0_n \end{bmatrix} \tag{3.129}$$

$$\tilde{P}_2 = \begin{bmatrix} O & 0_n \\ O & I_n \end{bmatrix} \tag{3.130}$$

where O is a $n \times nN$ zero matrix. The matrix V in Eq. (3.127) is of dimension $n(2N+3) \times 2n(N+1)$. We partition V as $V = [V_0 \;\; V_d]$ such that

$$V_0 a_0 + V_d d = V_w \tag{3.131}$$

where vector d is of dimension $n(2N+1) \times 1$ and defined as

$$d = [a_1^T, a_2^T, \cdots, a_N^T, c_0^T, \cdots, c_N^T]^T \tag{3.132}$$

Thus, V_0 and V_e are $[n(2N+3) \times n]$, $[n(2N+3) \times n(2N+1)]$ block matrices of V, respectively. We can solve Eq. (3.131) for d using the method of least squares

$$e = -\left(V_d^T V_d\right)^{-1} V_d^T \left(V_0 a_0 - V_w\right) = W a_0 + W_v V_w \tag{3.133}$$

where $W_v = \left(V_d^T V_d\right)^{-1} V_d^T$ and $W = -W_v V_0$. Since $z = \begin{bmatrix} a_0 \\ d \end{bmatrix}$ we get

$$z = \begin{bmatrix} a \\ c \end{bmatrix} = \begin{bmatrix} I_n \\ W \end{bmatrix} a_0 + \begin{bmatrix} O_n \\ W_v V_w \end{bmatrix} \equiv \begin{bmatrix} W_1 \\ W_2 \end{bmatrix} a_0 + \begin{bmatrix} W_3 \\ W_4 \end{bmatrix} \tag{3.134}$$

where W_1 and W_2 are partitions of the $[I_n \quad W]^T$ matrix, each of dimension $n(N+1) \times n$, W_3 and W_4 are partitions of the $[O_n \quad W_v V_w]^T$ matrix, each of dimension $n(N+1) \times n$ so that we have,

$$a = W_1 a_0 + W_3 \tag{3.135}$$

$$c = W_2 a_0 + W_4 \tag{3.136}$$

From Eq. (3.117), we have

$$b = Pc = PW_2 a_0 + PW_4 \equiv W_5 a_0 + PW_4 \tag{3.137}$$

where W_5 is a matrix of dimension $n(N+1)\times n$.

If the initial states and disturbances are known, the states, costates and controls at the LGL points can be solved from Eqs. (3.135-137) in the given horizon. It should be noticed that we obtained these solutions without any integrations. As shown in Eq. (3.135) and Eq. (3.137), the solutions of the states consist of a natural response and forced response. One can see the states and control are not zeros even if the initial conditions are zeros due to the forced term or the known disturbance. Regarding the current states as the new initial states, Eq. (3.137) constitutes a hybrid close loop control law that can be rapidly performed in the receding horizon control manner.

3.4.6 Simulation Results

We consider a magnetically controlled small satellite as the simulation model. The satellite (NPSAT1) is being built by students and staff at the Naval Postgraduate School[5]. There are three rods, one along each axis. Table 3.2 lists the simulation parameters for eccentric orbits.

Table 3.2: Simulation Parameters

Parameter & units	Value
Eccentricity	0.1
Semimajor axis ~km	560
Inclination ~deg	35.4
Inertia ~kg.m^2	5.1, 5, 2
Magnetic Torque Rod Saturation ~A.m^2	30

3.4.6.1 Compare Pseudospectral Control Law with Riccati Solutions

Here we take a circular orbit with a 560 km radius as an example. Assume the initial Euler angles errors are about 30 deg and angular velocities 0.03 deg/s on all three axes. Obtaining control laws using the Riccati equation involves: (1) integrating the Riccati equation backward in time, (2) storing this solution, and then (3) integrating the state equations in forward.

Fig. 3.16 shows comparisons between the pseudospectral solutions and the Riccati solutions.

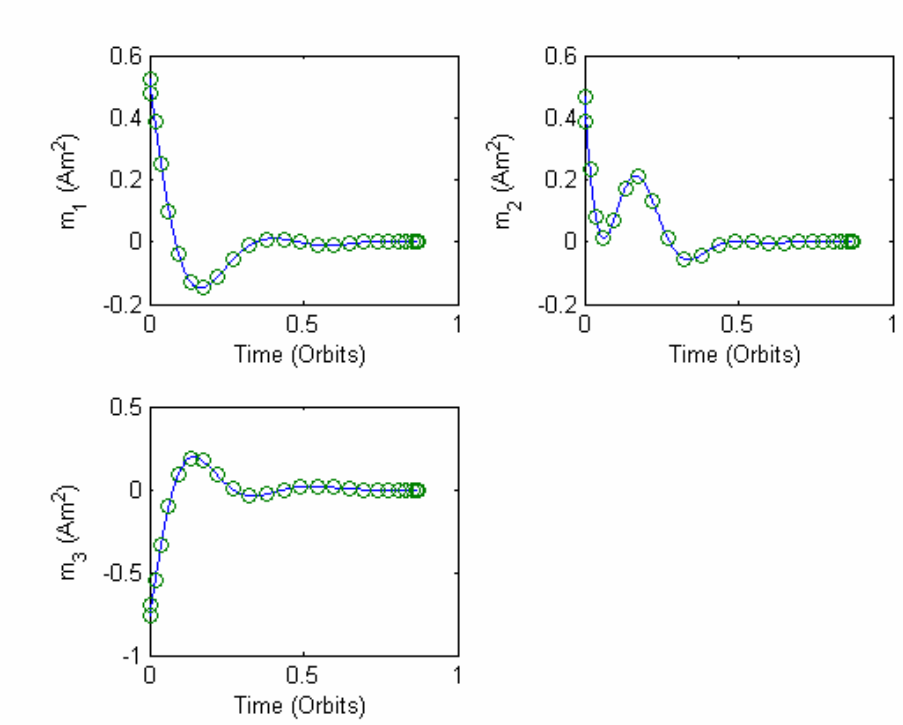

Fig. 3.16 Pseudospectral Control Law vs. Riccati Solutions

In the figure, the solid lines represent the solutions from the Riccati equation while the circles stand for those from the pseudospectral control law. The number of LGL points used is 30. From this figure one can see that the comparison between the pseudospectral and Riccati solutions is excellent. The computation time for the pseudospectral control law is about 0.3 seconds, while obtaining the control law and gains from the Riccati solutions takes about 4 seconds. There is one order of magnitude improvement in the computation time using the pseudospectral control law and the results are the same as those from the Riccati equations. The elliptic orbit introduces parametric excitations and forced terms not present in circular orbits. As shown in Ref. 40, the initial conditions have no effect on the long-term behavior of the solutions, the

first terms in the right sides of Eqs. (3.135-137) will tend to zero and the solutions approaches the forced response as time increases.

3.4.6.2 Magnetic Attitude Control in Eccentric Orbits

3.4.6.2.1 Feed Forward Control

The known torque disturbance can be found in Eq. (3.64). Using the feed forward control, Eq. (3.80) stands for the total torque of the remaining torque disturbance and undesired magnetic torque. Fig. 3.17 shows the total torque of the remaining disturbance and undesired magnetic torque is much less than the torque disturbance if there was no feed forward control.

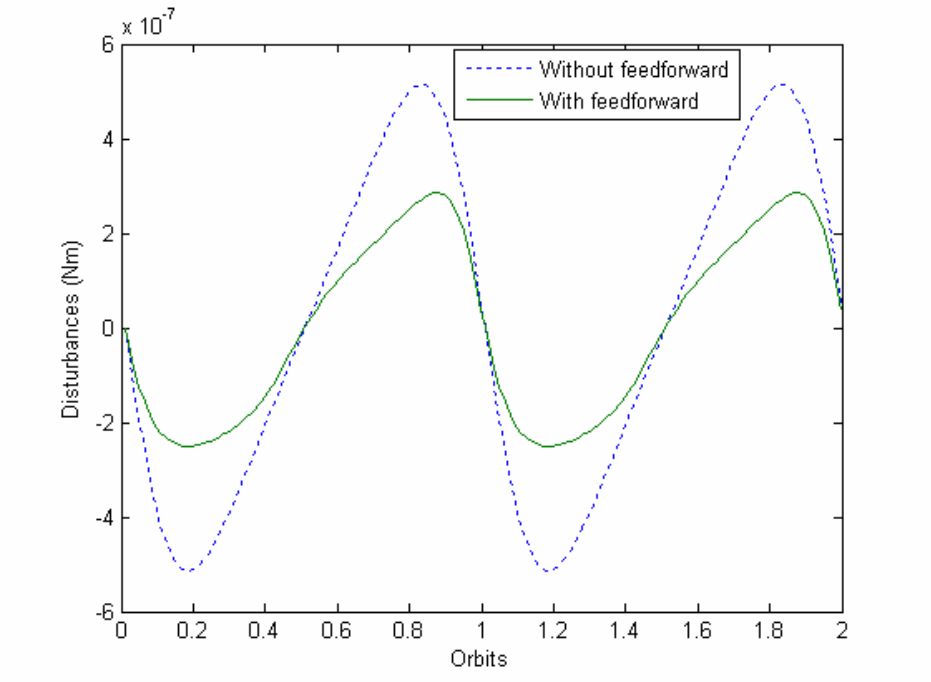

Fig. 3.17 Disturbance Comparison

3.4.6.2.2 Pseudospectral Control Law via Receding Horizon Control Implementation

Choose 30 LGL points. The horizon is selected as one orbit period. Starting at the initial time, we take the sampling for the current states every 50 seconds. The total samples are 1000. Once the control law, Eq. (3.137), is obtained with the initial conditions over the given horizon, the actual trajectory is then computed with the nonlinear dynamics governed by the system Eqs. (3.49-51, 3.53-54) plus the feed forward control. The next state conditions δX are generated from $\delta X = X - X^*$, where X is the state response from system Eqs. (3.49-51, 3.53-54) and the asterisk denotes the reference value, which should be zero for stabilization. In other words, the δX are the actual values, not those generated from the linear equations, Eqs. (3.81). Repeat this procedure to form the receding horizon control.

Assume all the initial conditions are zeros. Considering the following inertia distributions:

Case 1

$$I_2 > I_1 > I_3$$

Case 2

$$I_1 > I_3 > I_2$$

In Case 1, I_1=5 kgm^2, I_2=5.1 kgm^2, I_3=2 kgm^2 while in Case 2 I_1=5.1 kgm^2, I_2=2 kgm^2, I_3=5 kgm^2. Figs. (3.18-3.21) show the magnetic control and Euler angle time histories for the two cases.

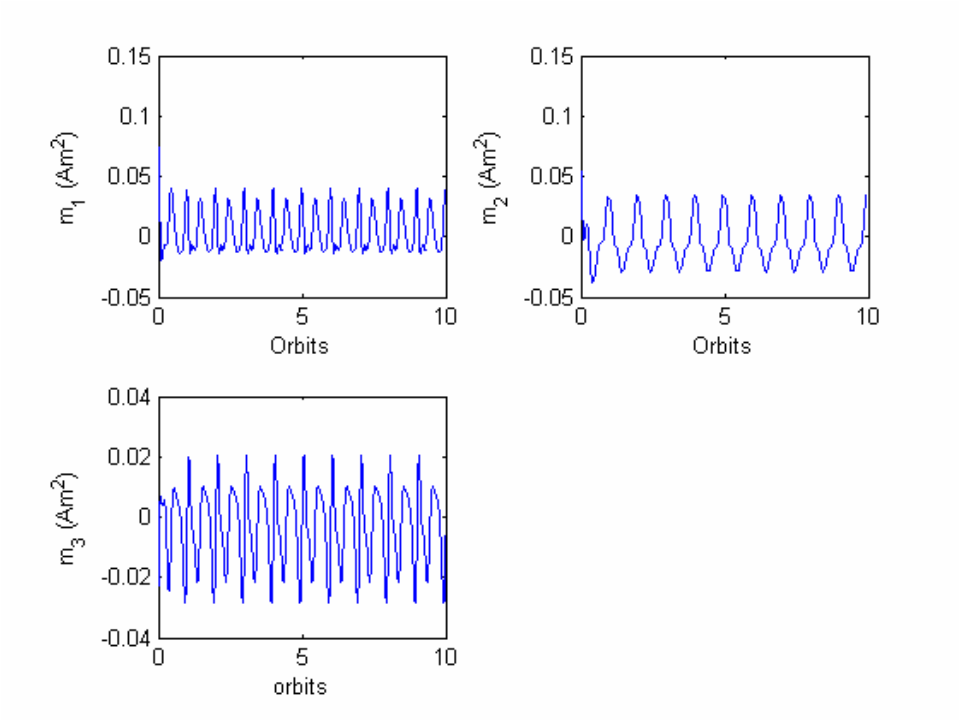

Fig. 3.18 Case 1: Magnetic Dipole Moments

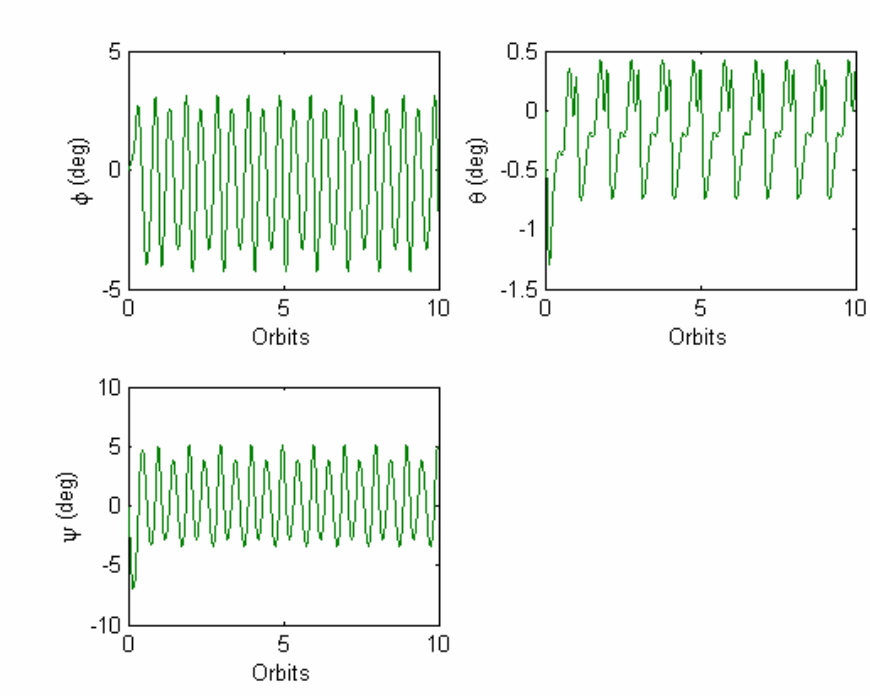

Fig. 3.19 Case 1: Euler Angles

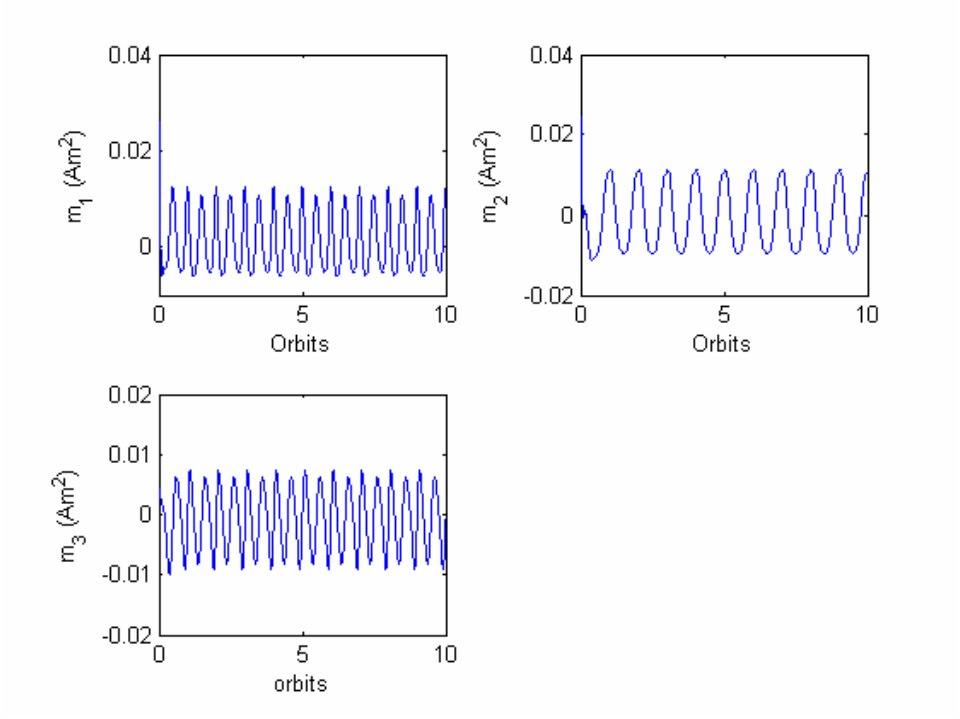

Fig. 3.20 Case 2: Magnetic Dipole Moments

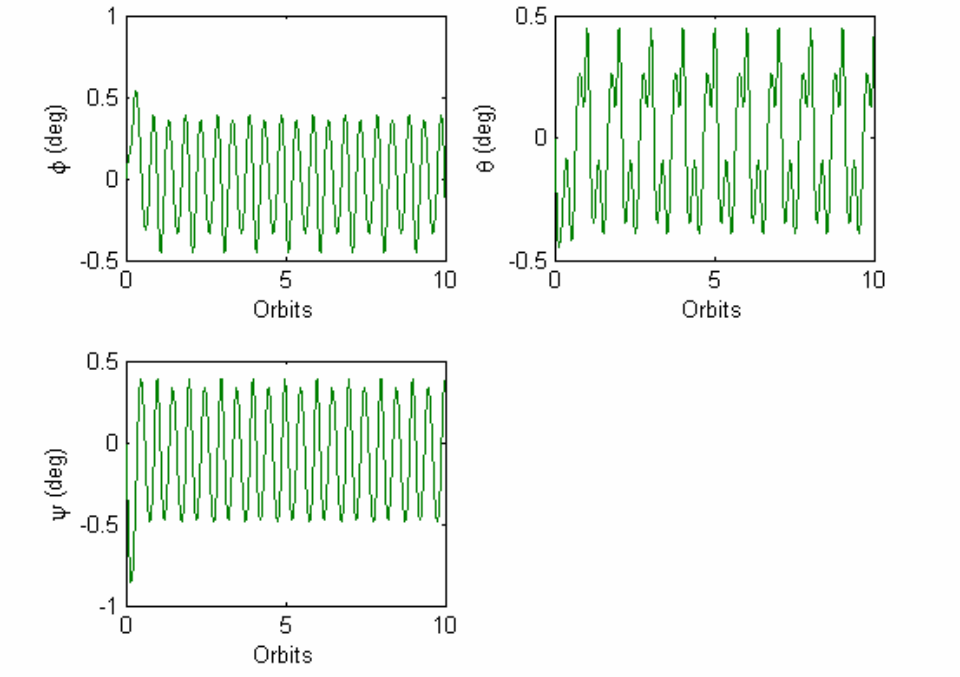

Fig. 3.21 Case 2: Euler Angles

Case 1 represents static stabilization while Case 2 is statically unstable[66]. In general the stable gravity gradient attitude system works better than the unstable system in the circular orbit. But comparing Fig. 3.19 with Fig. 3.21, the Euler angles in Case 2 are much smaller than those in Case 1. A comparison of Fig. 3.18 and Fig. 3.20 shows that the magnetic control effort is also less in Case 2. This result is caused by the different disturbance angular accelerations due to different inertia ratios while the unstable gravity gradient torque is a trivial matter in the forced steady state. Substituting Eqs. (3.77-79) into Eqs. (3.67-69), we obtain the undesired torques or disturbance.

$$T_{d1} = -\frac{B_1 B_2}{B^2} K \sin f \tag{3.138}$$

$$T_{d2} = -\frac{B_2^2}{B^2} K \sin f \tag{3.139}$$

$$T_{d3} = -\frac{B_2 B_3}{B^2} K \sin f \tag{3.140}$$

The disturbance angular accelerations in the roll, pitch and yaw axes after substituting Eq. (3.66) into Eqs. (3.138-140) are

$$a_{d1} = -2ek_1 \left(\frac{B_1 B_2}{B^2} \right) \left(\frac{\mu}{R^3} \right) \sin f \tag{3.141}$$

$$a_{d2} = -2e \left(\frac{B_2^2}{B^2} \right) \left(\frac{\mu}{R^3} \right) \sin f \tag{3.142}$$

$$a_{d3} = -2ek_3 \left(\frac{B_2 B_3}{B^2} \right) \left(\frac{\mu}{R^3} \right) \sin f \tag{3.143}$$

where

$$k_1 = \frac{I_2}{I_1} \tag{3.144}$$

$$k_3 = \frac{I_2}{I_3} \tag{3.145}$$

From Eqs. (3.141-145), one can see there is a big difference in the disturbance angular accelerations due to the different inertia ratios for Cases 1 and 2. For example, $k_3 = 2.55$ in Case 1 while $k_3 = 0.4$ in Case 2, which means the disturbance acceleration of Case 1 is 6.375 times more than that of Case 2 in the yaw axis and 2.601 times in the roll axis.

3.4.6.2.3 Effects of Inertia Distributions

As we observe there is a significant effect of the inertia distributions on the performance of magnetic attitude control. Fig. 3.22 illustrates the simulation results from random inertia distribution samples. In the figure the circles represent the solutions where the maximum Euler angles are less than 1 degree at the final stage. The stars stand for the ones where the maximum Euler angles are over 1 degree.

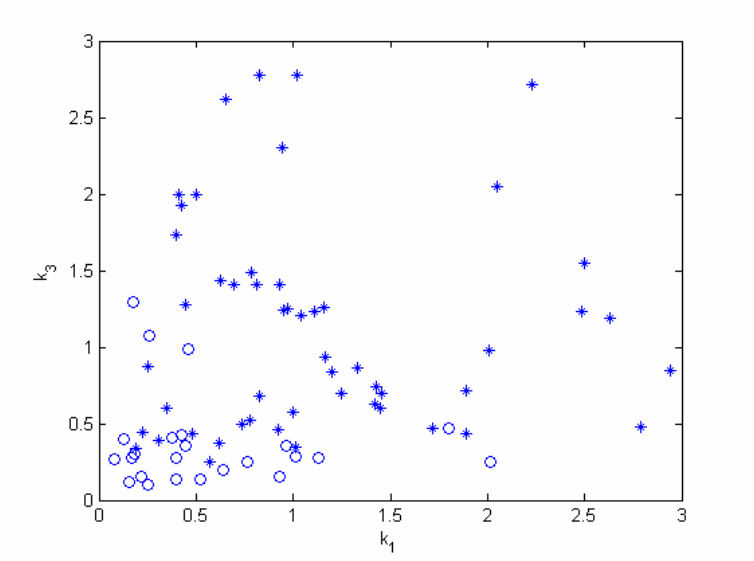

Fig. 3.22 Effects of Inertia Distributions

From Fig. 3.22 one can see most of the solutions satisfy the 1-degree accuracy requirement if k_1 and k_3 are less than 0.5. Another possible choice is k_1 or k_3 less than 0.2. According to Fig. 3.22 we need to set the maximum inertia axis as the roll or yaw axis instead of the pitch axis to reduce effects of the disturbance from eccentric orbits as show in Eq. (3.144) and Eq. (3.145). Fig. 3.22 shows that in this case the effects of the disturbance torque are minimized when the maximum inertia matrix is either the roll or yaw axis.

3.4.6.2.4 Consider Initial Perturbations

Assume the initial Euler angles errors are about 30 deg and the angular velocities are zero on all three axes. The simulations were performed using the nonlinear dynamic model input with the pseudospectral control laws. The results show that the

pseudospectral control law works well for the magnetic attitude stabilization in eccentric orbits. Figs. 3.23-3.24 show Euler angles time histories for Cases 1 and 2.

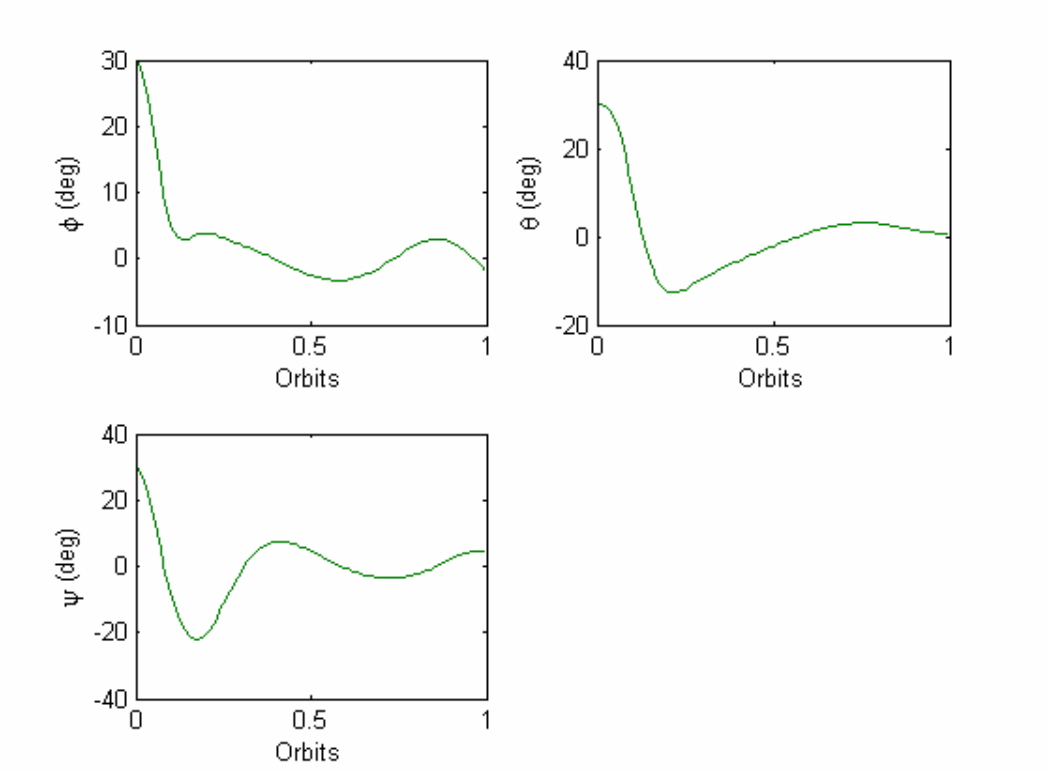

Fig. 3.23 Euler Angles (Case 1)

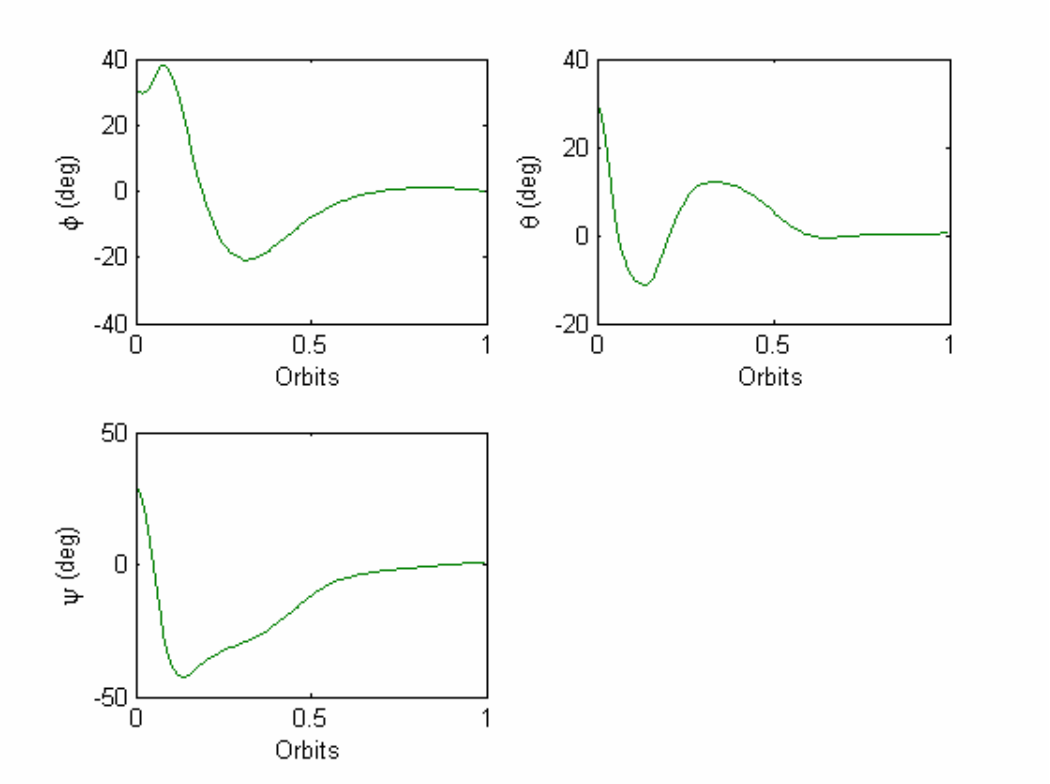

Fig. 3.24 Euler Angles (Case 2)

The initial errors are rejected and the attitude is stabilized in less than one orbit period, as shown in Figs. 3.23-3.24. The transient responses demonstrate good performance and fast decays with one or two oscillations to the equilibrium where the magnetic torques and the disturbance torques balance. The transient responses of Case 1 are much better than that of Case 2, as a result of the stable gravity gradient torque in Case 1. In the initial phase the gravity gradient torque plays a major rule and dominates the known disturbance. As the initial large angle error is nullified the gravity gradient torque becomes small and the primary torque is the pitch disturbance torque that is proportional to eccentricity. For the best magnetic attitude control in eccentric orbits,

favorable inertial distributions should be static gravity gradient stabilization in the initial phase, then satellites make 90 degree fast slew maneuver as illustrated in Ref. 25. It is better to have the roll or yaw axis as the maximum inertia to minimize the angular disturbance accelerations caused by the eccentricity in steady phase.

3.4.6.2.5 Use LQR Only

Here we just apply the LQR to reject the known disturbances[61]. We set in Eq. (3.81)

$$\overline{m} = 0 \tag{3.146}$$

The reason for using the feed forward control is to reduce the larger known disturbance so that the LQR could work better for the smaller known disturbance. Figs. 3.25-3.26 illustrate the magnetic dipole moments and Euler time histories without the feed forward control for the Case 2.

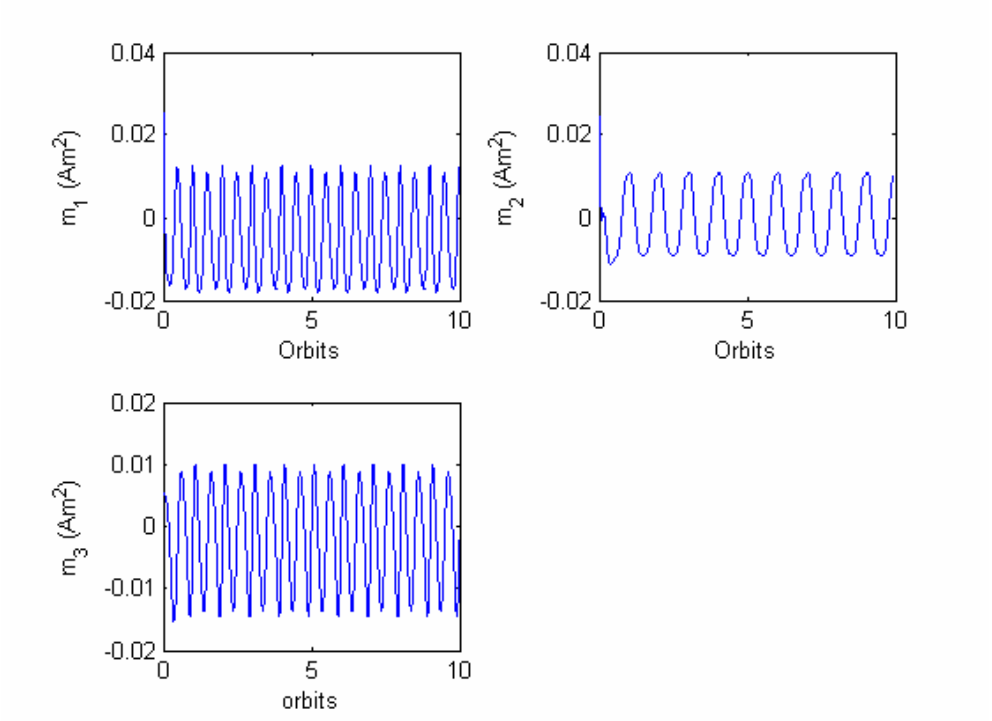

Fig. 3.25 Magnetic Dipole Moments (Without Feed Forward Control)

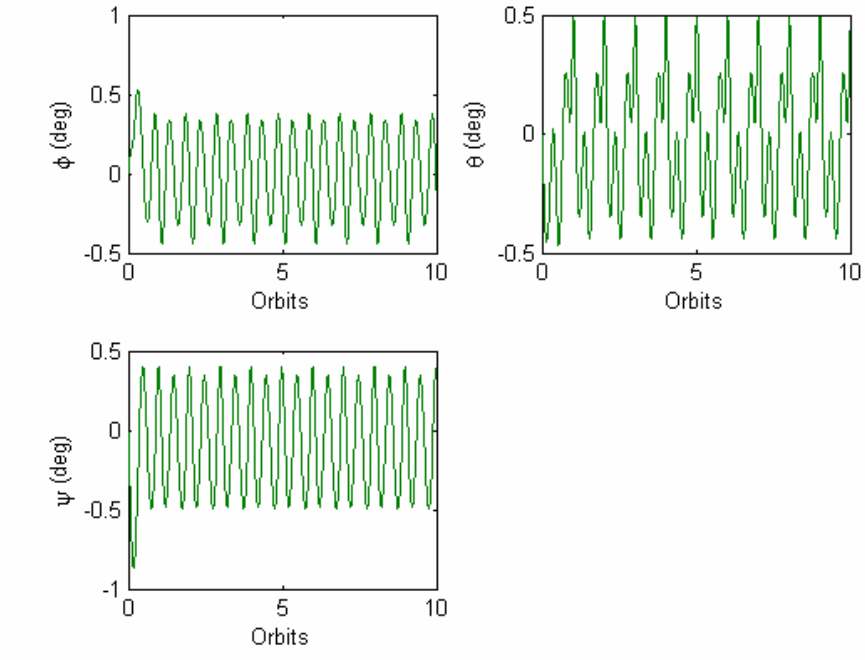

Fig. 3.26 Euler Angle (Without Feed Forward Control)

Fig. 3.21 and Fig. 3.26 show there is little difference in the Euler angle residual errors with the feed forward control and without it. Comparing Fig. 3.20 with Fig. 3.25, we find the dipole moments with the feed forward control are less than the moments without the feed forward control. This is because the disturbance in the former is reduced by the feed forward control, as shown in Fig. 3.17. But if adding the dipole moment $\overline{m}$ from the feed forward control to the moments m from the LQR in Fig. 3.20, we have

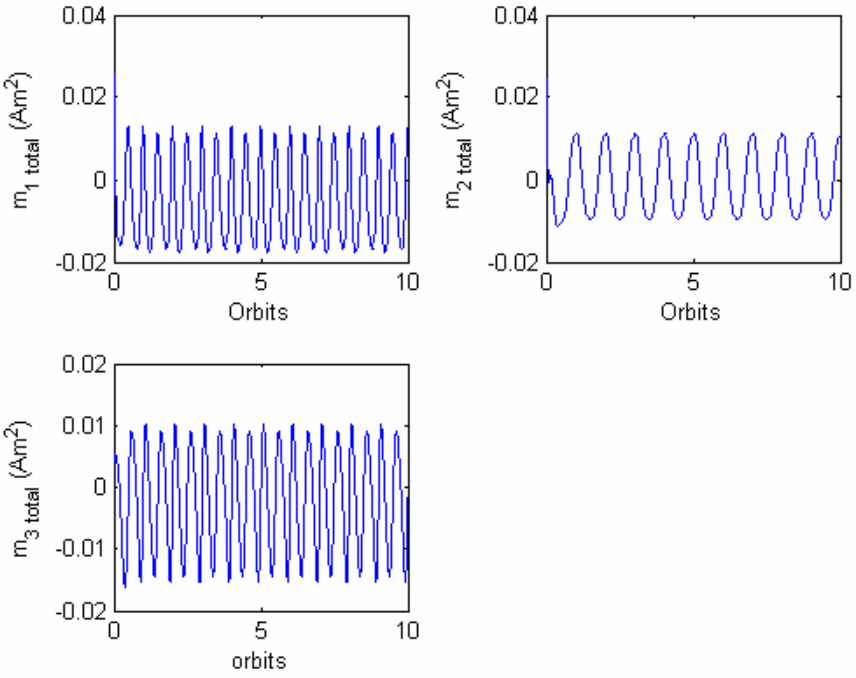

Fig. 3.27 Total Magnetic Dipole Moments (Case2)

Fig. 3.27 indicates the total control effort is almost the same as the magnetic dipole moments in Fig. 3.25.

3.4.7 Remarks

Three-axis magnetic attitude stabilization is achieved by using a pseudospectral control law via the receding horizon control for satellites in eccentric low Earth orbits. The solutions from the pseudospectral control law are in excellent agreement with those obtained from the Riccati equation, but the computation speed improves by one order of magnitude. The control law indicates the solutions consist of natural and forced responses. The known disturbance is greatly rejected by using a feed forward control. Numerical solutions show natural responses quickly tend to the region where the attitude motion is in the steady state. It is better to set the maximum inertia axis as roll or yaw axis and the residual librations errors are within 1 degree for the eccentricity 0.1.

CHAPTER IV

FORMATION FLYING DYNAMICS AND REAL-TIME OPTIMAL CONTROL*

In recent years, the concept of using a group of spacecraft flying in a close, precise formation has been considered for various missions. Since the missions generally last a long time, the main interest is how to maintain and reconfigure the relative motion orbits of the satellite formations with various perturbations. This chapter focuses on the dynamics and control of formation flying. The dynamic models are described and propagated in the mean elements space to accommodate higher order gravity perturbations. Three kinds of periodic matching conditions for minimizing secular drift are introduced in the chapter. The model error index concept is proposed to compare and evaluate relative motion theories. A higher order state transition matrix is developed using the unit sphere approach[108] in the mean elements space. Based on the state transition, we propose analytical control laws for formation maintenance and reconfiguration.

4.1 Approximate Theories of Relative Motion

Since relative motion of formation flying is very complicated, much effort has been devoted to simplifying the dynamic models of formation flying to better understand and

* Part of the data reported in this chapter is reprinted with permission from "Evaluation and Comparison of Relative Motion Theories" by Kyle T. Alfriend and Hui Yan, 2005. *Journal of Guidance, Control, and Dynamics*, Volume 28, Pages 254-261. Copyright © 2004 by Texas A&M University.

control relative motion. The first published study in the US for the relative motion of close or neighboring satellites was performed by Clohessy and Wiltshire[76], hence the often used name, the Clohessy-Wiltshire (C-W) equations. However, the approach of using the rotating reference frame for relative motion dates back to the 1800's to the work by Hill[77] in his development of the lunar theory, hence the other name of Hill's equations that is often used. These equations assume that motion is about a spherical Earth, the reference orbit or target is in a circular orbit and the distance between the satellites is small compared to the orbit radius so that the equations of motion can be linearized. Since the C-W equations were derived for rendezvous, which is a short-term process with intermittent thrusting, these assumptions are valid for rendezvous. They also provide a good basis for identifying potential relative motion orbits for satellites in near-circular orbits. However, the modeling errors introduced by these assumptions can have a significant effect on fuel consumption if they are used for determining the initial conditions for bounded or periodic relative motion orbits. Thus, better models for the motion of the reference point and the relative motion are needed. Tschauner and Hempel[79] obtained a solution for the relative motion that included the reference orbit eccentricity. Incorporation of the eccentricity for the reference orbit was also obtained by Lawden[78]. Improved forms of the Lawden solution with the reference orbit eccentricity are also found in Carter[93]. How[88] investigated the effects of neglecting the reference orbit eccentricity when establishing the relative motion initial conditions. References 94-95 and 80 were attempts to obtain corrections to the initial conditions to account for the nonlinear terms for the periodic relative motion orbits. They did not consider the general

solution to the nonlinear equations. Alfriend[91,92] developed a new approach to the nonlinear problem using differential orbital elements. As a first step to including the non-spherical Earth effects Gim and Alfriend[86] obtained the state transition matrix for the relative motion that includes the absolute and differential J_2 effects. For $J_2 = 0$ this solution reduces to another form for the state transition matrix for eccentric orbits. A different approach was used in that the solution was obtained by considering differential orbital elements and then transforming into the Cartesian relative motion frame. Thus, the differential relative equations of motion did not have to be solved.

4.1.1 Approximate Equations

4.1.1.1 Hill's Equations

We investigate the relative motion of two or more satellites, and one satellite is defined as the Chief, the others are called Deputies. In the relative motion, the Deputy is with respect to the Chief. Hill's equations are established in the Chief centered local vertical local horizontal (LVLH) frame by making the assumptions of a circular Chief orbit, spherical Earth, linearizing the differential gravity accelerations and neglecting all other perturbations[76-77]. The LVLH frame is based on the orbit plane and attached to the spacecraft. The axis x points from the Earth center to the spacecraft, the axis z follows the normal direction to the orbit plane, and the axis y is defined by the right-hand rule and points approximately along the velocity vector. Hill's equations are

$$\ddot{x} - 2n\dot{y} - 3n^2 x = 0 \tag{4.1}$$

$$\ddot{y} + 2n\dot{x} = 0 \tag{4.2}$$

$$\ddot{z} + n^2 z = 0 \tag{4.3}$$

where x, y and z are the LVLH Cartesian coordinates, and $\dot{x}$, $\dot{y}$ and $\dot{z}$ are the relative velocity components in the rotating LVLH frame. The mean motion n is given by $n = \sqrt{\mu/a^3}$, μ is the gravitational parameter and a is the semi-major axis. Hill's equations have an analytical solution, so it can easily be used to approximate relative motions. It is

$$x(t) = (\dot{x}_0/n)\sin nt - (2\dot{y}_0/n + 3x_0)\cos nt + (2\dot{y}_0/n + 4x_0) \tag{4.4}$$

$$y(t) = (2\dot{x}_0/n)\cos nt + (4\dot{y}_0/n + 6x_0)\sin nt + (y_0 - 2\dot{x}_0/n) - (3\dot{y}_0 + 6nx_0)t \tag{4.5}$$

$$z(t) = z_0 \cos nt + (\dot{z}_0/n)\sin nt \tag{4.6}$$

Eq. (4.5) shows there is a secular drift in the in-track y direction which will grow infinitely large as $t \to \infty$. All other terms are either periodic terms or constant biases. If we set the drift term $3\dot{y}_0 + 6nx_0 = 0$, the periodic in-plane motion reduces to a 2-1 ellipse with the long axis in the y direction.

4.1.1.2 Lawden's Equations

The equations of motion that include the effect of the eccentricity on Hill's equations derived by Lawden and other people are.

$$\ddot{x} - 2\dot{\theta}\dot{y} - \ddot{\theta}^2 x - 2(\mu/r_c^3)x = 0 \tag{4.7}$$

$$\ddot{y} + 2\dot{\theta}\dot{x} + \ddot{\theta}x - \dot{\theta}^2 y + (\mu/r_c^3)y = 0 \tag{4.8}$$

$$\ddot{z} + (\mu/r_c^3)z = 0 \tag{4.9}$$

where θ is the argument of latitude and r_c is the orbit radius of the Chief. Eqs. (4.7-9) can be solved analytically, see Refs. 78-79.

4.1.1.3 Vaddi, Vadali and Alfriend's Equations

Vaddi, Vadali and Alfriend developed a method to accommodate nonlinearity and eccentricity perturbations in Hill's equations[80]. They first derived equations with nonlinearity (consider quadratic term) without eccentricity, then combined with Lawden or Melton's solutions using perturbation methods to include the effect of the nonlinearity and eccentricity on Hill's equations.

4.1.1.4 Schweighart and Sedwick's Equations

Schweighart and Sedwick obtained equations of motion that incorporate the effect of the 1st order gravitational perturbation J_2 for circular orbits on Hill's equations[81].

$$\ddot{x} - 3n^2 x - 2n\dot{y} = -k\left(1 - 3\sin^2 i \sin^2\theta\right) \tag{4.10}$$

$$\ddot{y} + 2n\dot{x} = -2k\sin^2 i \sin\theta\cos\theta \tag{4.11}$$

$$\ddot{z} + n^2 z = -2k\sin i\cos i\sin\theta \tag{4.12}$$

where $k = \frac{3}{2}\frac{\mu J_2 R_E^2}{r^4}$, i is the inclination , R_E is the Earth radius, r is the position vector. The analytical solutions can be found in Ref. 81.

4.1.1.5 Orbital Elements Approach

The characteristic of the above approaches is to linearize the nonlinear equations of motion in the Cartesian frame in order to obtain an approximate analytical solution. Garrison et al[82] used a novel method to relate the states in the Cartesian LVLH frame to orbital element differences. The linear approximation using the differential orbital elements is more accurate than that using the Cartesian or curvilinear coordinates as shown in Ref. 83. Moreover, using the differential orbital elements automatically includes the reference or Chief orbit eccentricity, which is not included in Hill's equations. Notice this method does not require the solution of differential equations. In mean space, we have[84]

$$\dot{\lambda} = \frac{1}{L^3} + \frac{3\varepsilon}{4L^7\eta^4}\left[(1+\eta) - (5+3\eta)\cos^2 i\right] \tag{4.13}$$

$$\dot{\omega} = \frac{3\varepsilon}{4L^7\eta^4}\left(1 - 5\cos^2 i\right) \tag{4.14}$$

$$\dot{\Omega} = \frac{3\varepsilon}{2L^7\eta^4}\cos i \tag{4.15}$$

where $L = \sqrt{\mu a}$, $\eta = \sqrt{1-e^2}$. ω is the argument of perigee and Ω is the longitude of ascending node. The mean argument of latitude $\lambda = l + \omega$ and l is the mean anomaly. Then

$$\begin{bmatrix} a(t) \\ e(t) \\ i(t) \\ \Omega(t) \\ \omega(t) \\ \lambda(t) \end{bmatrix} = \begin{bmatrix} a(t_0) \\ e(t_0) \\ i(t_0) \\ \Omega(t_0) \\ \omega(t_0) \\ \lambda(t_0) \end{bmatrix} + \begin{bmatrix} 0 \\ 0 \\ 0 \\ \dot{\Omega} \\ \dot{\omega} \\ \dot{\lambda} \end{bmatrix} t \tag{4.16}$$

Using differential orbital elements, Alfriend et al[85] described relative motion in terms of mean elements, incorporating 1st order J_2 and eccentricity effects in the equations. Gim and Alfriend[86] developed an accurate state transition matrix for the perturbed non-circular reference orbit using a geometrical method. Realizing the Deputy relative motion is a result of small changes in the orbital elements of the Chief, they used differential orbital elements and then transformed into the LVLH coordinates. Notice this method does not require the solution of differential equations. The state transition matrix is

$$X(t) = \{A(t) + \alpha B(t)\} \delta e \tag{4.17}$$

or

$$X(t) = \{A(t) + \alpha B(t)\} D(t) \bar{\phi}_e(t, t_0) D^{-1}(t_0) \{A(t_0) + \alpha B(t_0)\}^{-1} X(t_0) \tag{4.18}$$

where $X = [x\ \dot{x}\ y\ \dot{y}\ z\ \dot{z}]$ is the relative motion coordinate vector, $\alpha = 3J_2 R_e^2$. The matrix $B(t)$ contains only the terms perturbed by J_2. $\bar{\phi}_e(t)$ is the state transition matrix for the relative mean elements, and $D(t)$ is the Jacobian of the mean to osculating element transformation.

A modeling error index is introduced for evaluating and comparing the accuracy of various theories of the relative motion of satellites in order to determine the effect of modeling errors on the various theories by Alfriend and Yan[87].

4.1.2 Analytical Periodic Matching Conditions

If we set

$$\dot{y}_0 = -2nx_0 \tag{4.19}$$

periodic motions in the relative motion will be identified in Hill's eqs. (4.1-6). These periodic motions include in-plane, out-of-plane, and combinations of these two motion types. The ideal in formation flying is that the satellites will remain close over a long period of time without using any control effort. Inspired by designing bounded relative motion, Inalhan and How[88] derived the periodic matching conditions for an eccentric chief orbit based on Eqs. (4.7-9),

$$\dot{y}_0 = -\frac{n(2+e)}{(1+e)^{1/2}(1-e)^{3/2}} x_0 \tag{4.20}$$

The periodic matching conditions considering J_2 perturbations in circular orbits are[81]

$$\dot{y}_0 = -2n\sqrt{1+sx_0} \quad \dot{x}_0 = \frac{n(1-s)}{2\sqrt{1+s}} \tag{4.21}$$

where $s = \frac{3}{8} J_2 \left(\frac{R}{a}\right)^2 (1+3\cos 2i)$. Using these conditions does not eliminate the secular growth experienced in the cross-track direction due to J_2. To consider nonlinearity and

eccentricity effects on the Hill's bounded conditions, Vaddi, Vadali and Alfriend[80] obtained the following periodic matching conditions

$$\dot{y}_0 = -\frac{n\rho \sin\alpha_0 (2+e)}{2(1+e)^{1/2}(1-e)^{3/2}} - \left(\frac{3\mu}{a^4}\right)\left(\frac{\rho^2}{48n}\right)(12+6\cos 2\alpha_0) \tag{4.22}$$

where ρ is the relative orbit size and α_0 is the initial phase angle.

As we mentioned above, use of differential orbital elements has the unique advantage of incorporating eccentricity and J_2 perturbations. Without J_2 perturbations, the bounded condition can be simply expressed in the nonlinear sense as

$$\delta a = 0 \tag{4.23}$$

which means the orbital periods of Chief and Deputy are the same.

Schaub and Alfriend[89] proposed J_2 invariant relative orbits for formation flying. In Ref. 89, two drift rate constraints were applied among spacecraft in mean space

$$\delta\dot{\lambda} + \delta\dot{\omega} = 0 \tag{4.24}$$

$$\delta\dot{\Omega} = 0 \tag{4.25}$$

The first constrains secular drift in the in-track direction and the 2nd constrains drift in the out-of-plane direction. With these constraints the spacecraft will not drift apart over time under the influence of J_2 in mean space. Since the difference of semi-major axis, eccentricity and inclination should satisfy Eqs. (4.24-25), one of them can be independently chosen. This greatly limits formation flying mission designs. Based on Gim and Alfriend STM, Ref. 90 presented an in-track constraint periodic matching condition

$$\delta\dot{\lambda} + \delta\dot{\Omega}\cos i = 0 \tag{4.26}$$

If the out-of-plane constraint, Eq. (4-25) is not satisfied the in-plane constraint, Eq. (4-24) is replaced with Eq. (4-26). To accommodate nonlinearity in this condition, Refs. 91-92 expanded Eq. (4.26) to the second order and included a term J_2^2.

4.1.3 Generalized Periodic Matching Conditions

Considering all the perturbations the constraint is

$$X_T = X_0 \tag{4.27}$$

where $X = \begin{pmatrix} x & \dot{x} & y & \dot{y} & z & \dot{z} \end{pmatrix}^T$ is the relative motion coordinate vector. X_0 and X_T are the initial state and state after one orbit period. Eq. (4.27) only has numerical solutions for periodic matching conditions and may need control effort.

4.2 An Orbital Elements Approach to the Nonlinear Formation Flying Problems

4.2.1 Introduction

In this section a new approach is presented. We begin with the differential orbital elements rather than the C-W equations. This is done for several reasons. First, the linear approximation using differential orbital elements is more accurate than the Cartesian or curvilinear coordinates with the C-W equations as was shown in Ref. 83. Secondly, using differential orbital elements automatically includes the eccentric reference orbit, which is not available using the C-W equations. Also, relative motion

periodic orbits are well defined using differential orbital elements and the first order solutions have been obtained.

First we start with a discussion of the nonlinear effects and their magnitude in relation to the other modeling errors. We then develop the approach for including the nonlinear terms when using differential orbital elements. The condition for suppressing the secular drift in the in-track direction, called the period matching condition, is discussed and the constraints for satisfying this constraint are developed. Finally, results are presented.

4.2.2 Formations and Orbital Elements

Before proceeding to the nonlinear theory consider the design of relative motion orbits in orbital element space. From Ref. 86, we have

$$\begin{aligned} x &= R\left[\frac{\delta a}{a}+\left(\frac{R}{p}\right)\left(q_1\sin\theta-q_2\cos\theta\right)\delta\theta-2\left(\frac{a}{p}\right)\left(q_1\delta q_1+q_2\delta q_2\right)-\left(\frac{R}{p}\right)\left(\delta q_1\cos\theta+\delta q_2\sin\theta\right)\right] \\ y &= R\left(\delta\theta+\delta\Omega\cos i\right) \\ z &= R\left(\delta i\sin\theta-\delta\Omega\sin i\cos\theta\right) \end{aligned} \tag{4.28}$$

where θ is the true argument of latitude, $q_1 = e\cos\omega, q_2 = e\sin\omega$, and the orbital elements are those of the chief or reference satellite and δ represents the difference in the elements between the two satellites. First consider $J_2 = 0$ and $\delta a = 0$ so that there are no secular terms. We are not restricting the chief orbit to be circular. From the last of Eq. (4.28)

$$z_{\max} \le R_a\left[\left(\delta i\right)^2 + \left(\delta\Omega \sin i\right)^2\right]^{1/2}, R_a = a\left(1+e\right) \tag{4.29}$$

When $\delta i = 0$ the maximum out-of-plane separation occurs at the equator, when $\delta\Omega = 0$ the maximum occurs at the anti-node. We will adopt the quantity in Eq. (4.29) as a measure of the maximum out-of-plane separation, realizing that the maximum will probably be less than this depending on the location of perigee.

Now consider the in-plane motion and two scenarios. The first is a constant in-track separation angle that is accomplished by an argument of perigee difference and $\delta e = 0$. In this case the maximum separation is

$$y_{\max} \le R_a\left|\delta\theta + \delta\Omega\cos i\right| \tag{4.30}$$

The other scenario is periodic in-plane motion that reduces to the 2-1 ellipse when the chief eccentricity is zero. In this case with $\delta a = 0$ $\delta\theta$ is periodic and to the 1st approximation $\delta\theta_{\max} = 2\delta e$. Since $\delta\Omega$ is constant the maximum amplitude of the in-plane oscillation is

$$y_{\max} \le 2R_a\left|\delta e\right| \tag{4.31}$$

Thus, the relative motion orbits are easily designed with orbital element differences and these differences help provide a visualization of the relative motion orbit. These measures were developed from the linear theory, but they still provide a good approximation when the relative motion orbits are large and the nonlinear terms need to be included. When J_2 is considered differential nodal precession, differential perigee rotation and a differential mean motion can occur. Each of these will cause the formation to drift and/or the size of the formation to grow. The types of orbits that occur in the

presence of differential gravitational perturbations have been classified by Alfriend[43]. The J_2 effects will be considered with the nonlinear effects in the following sections.

4.2.3 Nonlinear Effects

Consider the dimensionless C-W equations with the true anomaly as the independent variable. That is, the motion is referenced to the standard rotating reference frame whose origin is at the target of the Chief and the *x*-axis is in the radial direction, the *y*-axis is in the in-track direction and the *z*-axis in along the orbit normal.

$$\begin{aligned} &u'' - 2v' - 3u = O(e) + O(J_2) + O(L/R) \\ &v'' + 2u' = O(e) + O(J_2) + O(L/R) \\ &w'' + w = O(e) + O(J_2) + O(L/R) \\ &u = x/L,\ v = y/L,\ w = z/L \end{aligned} \tag{4.32}$$

where L is a distance representative of the maximum expected separation distance between the two satellites. The problem with developing perturbation or successive approximation solutions to these equations is the secular term in the in-track direction. The higher order terms in the approximation have t^n terms. For the solution to be uniformly valid it is necessary that

$$\lim_{t\to\infty}\left(\frac{x_{n+1}}{x_n}\right) = O(1) \tag{4.33}$$

where x_n represents the nth order term in the perturbation solution. The t^n terms appear in the solutions in Refs. 95 and 97, thus, the solutions are not uniformly valid. The t^n terms are not a problem in Refs. 95 and 80 as they are looking for the initial conditions

for periodic relative orbits. Karlgard and Lutz[94] avoid this problem with a novel technique of expressing the relative motion in the rotating frame of the deputy, not the chief. However, when transforming back to the chief rotating frame it appears these secular terms will appear. Consider the in-track secular term; it results from the two satellites having different periods, and as shown by Bond[97] the in-track growth is

$$\text{in-track growth} = \frac{\sin(\Delta \text{nt})}{\Delta \text{n}} = t - \frac{(\Delta n)^2}{6} t^3 + \ldots \tag{4.34}$$

where Δn is the difference in the mean motions. A similar $\cos(\Delta nt)$ term exists and these two terms lead to t^2 and t^3 terms in the higher order approximations. Since these t^n terms arise naturally from the expansion process we conclude that the standard approaches of developing a perturbation solution will not produce a uniformly valid solution.

The nonlinear effects cannot be considered in isolation, the other modeling errors must also be considered. There are no circular orbits. Although the mean eccentricity can be zero the osculating eccentricity will be $O(J_2) = O(10^{-3})$. Assuming $R = 7000 km$ for satellites in low earth orbit (LEO) for $L/R < 10^{-3}$ or $L < 7 km$ developing a solution that includes the nonlinear terms without including the effects of J_2 or the eccentricity has little validity since terms of the same order of magnitude have been ignored. Only when the maximum separation distance is much larger, say 100 km, are the effects of the eccentricity and differential J_2 small enough in relation to the nonlinear terms that they can be neglected. Also, carrying the perturbation solution to more than 2nd order is neglecting terms larger than those that have been included.

4.2.4 Nonlinear Theory

The general relative equations of motion in the rotating Hill reference frame that include the reference orbit eccentricity, J_2 and nonlinear effects have been obtained by Kechichian[98]. Developing a perturbation solution to these equations that starts with the C-W equations and contains the reference orbit eccentricity, J_2 and nonlinear effects is a formidable task. This led us to consider a different approach.

The primary criteria for selecting the approach for describing the relative motion in this effort are to have a formulation a) that includes reference orbit eccentricity and J_2 effects, b) which directly describes the relative motion, c) in which the initial conditions that result in bounded relative motion can be determined, d) in which the control of the relative motion can be determined, and e) that minimizes the number of terms required to include the non-linear effects. These criteria led us to use mean orbit elements. From the mean elements the osculating elements are obtained for each satellite and then transformed to the rotating reference frame centered at the Chief to view the relative motion. This approach was used to identify the J_2 *invariant orbits*[89] and control using orbital elements has been demonstrated in Ref. 99.

We start with the Hamiltonian in mean elements. In normalized Delaunay variables with $\mu = 1, R_e = 1$ the averaged Hamiltonian to the second order is[84]

$$M = M_0 + \varepsilon M_1 + 0.5\varepsilon^2 M_2 \tag{4.35}$$

$$M_0 = -\frac{1}{2L^2} \tag{4.36}$$

$$M_1 = \frac{1}{4L^6}\left(\frac{L}{G}\right)^3\left(-1+3\frac{H^2}{G^2}\right) \tag{4.37}$$

$$M_2 = -\frac{15\mu^6 R_e^4}{64L^{10}}\left(\frac{L}{G}\right)^5 \left\{\begin{array}{l}\left[1-\frac{18}{5}\left(\frac{H}{G}\right)^2+\left(\frac{H}{G}\right)^4\right]+\frac{4}{5}\left(\frac{L}{G}\right)\left[1-6\left(\frac{H}{G}\right)^2+9\left(\frac{H}{G}\right)^4\right] \\ -\left(\frac{L}{G}\right)^2\left[1-2\left(\frac{H}{G}\right)^2-7\left(\frac{H}{G}\right)^4\right]\end{array}\right\} \tag{4.38}$$

where $\varepsilon = -J_2$ and J_2 is the gravitational perturbation,

$L = \sqrt{\mu a}, G = L\sqrt{1-e^2} = L\eta, H = G\cos i$

l = mean anomaly

$g = \omega$ = argument of perigee

$h = \Omega$ = right ascension

Mean elements are used because the angle rates are constant, which means the constraints to minimize or prevent drift between the satellites are a function of only the momenta (L,G,H) or (a,e,i). If the starting point is the Hamiltonian in osculating space the constraints would also be a function of the angles and the relative motion orbit more difficult to design. Using the mean argument of latitude $\lambda = l + g$ the angle rates are

$$\dot{l} = \frac{\partial M}{\partial L} = \frac{1}{L^3} + \varepsilon\frac{3}{4L^7\eta^3}\left(1-3\cos^2 i\right) - 0.5\varepsilon^2\frac{15}{64L^{11}} \left[\left(-\frac{5}{\eta^5}-\frac{16}{5\eta^6}+\frac{3}{\eta^7}\right)+\left(\frac{18}{\eta^5}+\frac{96}{5\eta^6}-\frac{6}{\eta^7}\right)\cos^2 i-\left(\frac{5}{\eta^5}+\frac{144}{5\eta^6}+\frac{21}{\eta^7}\right)\cos^4 i\right] \tag{4.39}$$

$$\dot{g} = \frac{\partial M}{\partial G} = \varepsilon\frac{3}{4L^7\eta^4}\left(1-5\cos^2 i\right) - 0.5\varepsilon^2\frac{15}{64L^{11}} \left[\left(-\frac{5}{\eta^6}-\frac{24}{5\eta^7}+\frac{7}{\eta^8}\right)+\left(\frac{126}{5\eta^6}+\frac{192}{5\eta^7}-\frac{18}{\eta^8}\right)\cos^2 i-\left(\frac{9}{\eta^6}+\frac{72}{\eta^7}+\frac{77}{\eta^8}\right)\cos^4 i\right] \tag{4.40}$$

$$\dot{h} = \frac{\partial M}{\partial H} = \varepsilon \frac{3}{2L^7\eta^4}\cos i - 0.5\varepsilon^2 \frac{3}{16L^{11}} \left[\left(-\frac{9}{\eta^6} - \frac{12}{\eta^7} + \frac{5}{\eta^8}\right)\cos i + \left(\frac{5}{\eta^6} + \frac{36}{\eta^7} + \frac{35}{\eta^8}\right)\cos^3 i\right] \tag{4.41}$$

So

$$\dot{\lambda} = \dot{l} + \dot{g} = \frac{1}{L^3} + \varepsilon \frac{3}{4L^7}\left[\left(\frac{1}{\eta^3} + \frac{1}{\eta^4}\right) - \left(\frac{3}{\eta^3} + \frac{5}{\eta^4}\right)\cos^2 i\right] + 0.5\varepsilon^2 \frac{3}{64L^{11}} \left[\left(\frac{25}{\eta^5} + \frac{41}{\eta^6} + \frac{9}{\eta^7} - \frac{35}{\eta^8}\right) - \left(\frac{90}{\eta^5} + \frac{222}{\eta^6} + \frac{162}{\eta^7} - \frac{90}{\eta^8}\right)\cos^2 i + \left(\frac{25}{\eta^5} + \frac{189}{\eta^6} + \frac{465}{\eta^7} + \frac{385}{\eta^8}\right)\cos^4 i\right] \tag{4.42}$$

Eqs (4.39-41) are the mean angle rates with J_2 and J_2^2. We can see from Eq. (4.34), and it was shown in Ref. 89, that there will be secular growth in the relative angles if the momenta (L,G,H) or (a,e,i) of the two satellites are not equal, except for special orbits such as the critical inclination. Since relative orbit design is more direct in terms of (e,i) instead of (G,H) we use (L,e,i)as the momenta variables.

Now consider the differential rates between the satellites. To obtain the differential rates expand in a Taylor series about the Chief satellite.

$$\begin{aligned}\delta\dot{\lambda} = {} & \frac{\partial \dot{\lambda}}{\partial L}\delta L + \frac{\partial \dot{\lambda}}{\partial \eta}\delta\eta + \frac{\partial \dot{\lambda}}{\partial i}\delta i + \frac{1}{2}\frac{\partial^2 \dot{\lambda}}{\partial L^2}\delta L^2 + \frac{1}{2}\frac{\partial^2 \dot{\lambda}}{\partial \eta^2}\delta\eta^2 + \frac{1}{2}\frac{\partial^2 \dot{\lambda}}{\partial i^2}\delta i^2 \\ & + \frac{\partial^2 \dot{\lambda}}{\partial L \partial \eta}\delta L\delta\eta + \frac{\partial^2 \dot{\lambda}}{\partial L \partial i}\delta L\delta i + \frac{\partial^2 \dot{\lambda}}{\partial i \partial \eta}\delta i\delta\eta\end{aligned} \tag{4.43}$$

$$\delta \dot{h} = \frac{\partial \dot{h}}{\partial L}\delta L + \frac{\partial \dot{h}}{\partial \eta}\delta\eta + \frac{\partial \dot{h}}{\partial i}\delta i + \frac{1}{2}\frac{\partial^2 \dot{h}}{\partial L^2}\delta L^2 + \frac{1}{2}\frac{\partial^2 \dot{h}}{\partial \eta^2}\delta\eta^2 + \frac{1}{2}\frac{\partial^2 \dot{h}}{\partial i^2}\delta i^2 + \frac{\partial^2 \dot{h}}{\partial L \partial \eta}\delta L\delta\eta + \frac{\partial^2 \dot{h}}{\partial L \partial i}\delta L\delta i + \frac{\partial^2 \dot{h}}{\partial i \partial \eta}\delta i\delta\eta \tag{4.44}$$

Let

$$\frac{\partial \dot{\lambda}}{\partial L} = a_{10} + \varepsilon a_{11} + 0.5\varepsilon^2 a_{12},\ \frac{\partial \dot{\lambda}}{\partial \eta} = \varepsilon a_{21} + 0.5\varepsilon^2 a_{22},\ \frac{\partial \dot{\lambda}}{\partial i} = \varepsilon a_{31} + 0.5\varepsilon^2 a_{32} \tag{4.45}$$

$$\frac{\partial^2 \dot{\lambda}}{\partial L^2} = a_{40} + \varepsilon a_{41} + 0.5\varepsilon^2 a_{42},\ \frac{\partial^2 \dot{\lambda}}{\partial \eta^2} = \varepsilon a_{51} + 0.5\varepsilon^2 a_{52},\ \frac{\partial^2 \dot{\lambda}}{\partial i^2} = \varepsilon a_{61} + 0.5\varepsilon^2 a_{62} \tag{4.46}$$

$$\frac{\partial^2 \dot{\lambda}}{\partial L \partial \eta} = \varepsilon a_{71} + 0.5\varepsilon^2 a_{72},\ \frac{\partial^2 \dot{\lambda}}{\partial L \partial i} = \varepsilon a_{81} + 0.5\varepsilon^2 a_{82},\ \frac{\partial^2 \dot{\lambda}}{\partial i \partial \eta} = \varepsilon a_{91} + 0.5\varepsilon^2 a_{92} \tag{4.47}$$

$$\frac{\partial \dot{h}}{\partial L} = \varepsilon b_{11} + 0.5\varepsilon^2 b_{12},\ \frac{\partial \dot{h}}{\partial \eta} = \varepsilon b_{21} + 0.5\varepsilon^2 b_{22},\ \frac{\partial \dot{h}}{\partial i} = \varepsilon b_{31} + 0.5\varepsilon^2 b_{32} \tag{4.48}$$

$$\frac{\partial^2 \dot{h}}{\partial L^2} = \varepsilon b_{41} + 0.5\varepsilon^2 b_{42},\ \frac{\partial^2 \dot{h}}{\partial \eta^2} = \varepsilon b_{51} + 0.5\varepsilon^2 b_{52},\ \frac{\partial^2 \dot{h}}{\partial i^2} = \varepsilon b_{61} + 0.5\varepsilon^2 b_{62} \tag{4.49}$$

$$\frac{\partial^2 \dot{h}}{\partial L \partial \eta} = \varepsilon b_{71} + 0.5\varepsilon^2 b_{72},\ \frac{\partial^2 \dot{h}}{\partial L \partial i} = \varepsilon b_{81} + 0.5\varepsilon^2 b_{82},\ \frac{\partial^2 \dot{h}}{\partial i \partial \eta} = \varepsilon b_{91} + 0.5\varepsilon^2 b_{92} \tag{4.50}$$

The partial derivatives are given in the Appendix A. Now consider the size of the relative motion orbit. If $\delta i = O(\varepsilon)$ and/or $\delta e = O(\varepsilon)$ then the size of the relative motion orbit can be several hundred kilometers. Therefore, assume $\delta i = O(\varepsilon)$ and $\delta e = O(\varepsilon)$. If they are smaller that is no problem. Since $\eta\delta\eta = -e\delta e$ the order of magnitude of $\delta\eta$ depends on the value of e and δe. We will assume that $\delta\eta = O(\varepsilon)$. Again, if it is smaller

there is no problem. With these assumptions, and from Ref. 95 and Eqs. (4.43-44) we see that $\delta L = O\left(\varepsilon^2\right)$. Set

$$\begin{aligned} \delta L &= \varepsilon^2 \delta L_2 + \varepsilon^3 \delta L_3 \\ \delta\eta &= \varepsilon\delta\eta_1 + \varepsilon^2 \delta\eta_2 \\ \delta i &= \varepsilon\delta i_1 + \varepsilon^2 \delta i_2 \end{aligned} \tag{4.51}$$

Now substitute Eqs. (4.45-51) into Eqs. (4.43) and (4.44) and equate terms of like order.

$$\begin{aligned} \delta\dot{\lambda} = &\left(a_{10}\delta L_2 + a_{21}\delta\eta_1 + a_{31}\delta i_1\right)\varepsilon^2 + \\ &\left(a_{11}\delta L_2 + a_{10}\delta L_3 + a_{21}\delta\eta_2 + a_{31}\delta i_2 + \frac{1}{2}a_{22}\delta\eta_1 + \frac{1}{2}a_{32}\delta i_1 + \frac{1}{2}a_{51}\delta\eta_1^2 + \frac{1}{2}a_{61}\delta i_1^2 + a_{91}\delta\eta_1\delta i_1\right)\varepsilon^3 \end{aligned} \tag{4.52}$$

$$\begin{aligned} \delta\dot{\Omega} = &\left(b_{21}\delta\eta_1 + b_{31}\delta i_1\right)\varepsilon^2 + \\ &\left(b_{11}\delta L_2 + b_{21}\delta\eta_2 + b_{31}\delta i_2 + \frac{1}{2}b_{22}\delta\eta_1 + \frac{1}{2}b_{32}\delta i_1 + \frac{1}{2}b_{51}\delta\eta_1^2 + \frac{1}{2}b_{61}\delta i_1^2 + b_{91}\delta\eta_1\delta i_1\right)\varepsilon^3 \end{aligned} \tag{4.53}$$

Setting the $O\left(\varepsilon^2\right)$ terms in Eqs. (4.52) and (4.53) to zero gives the conditions for the J_2 *Invariant Orbits*[89]. The condition for no drift at 1st order is[90]

$$\delta\dot{\lambda} + \delta\dot{\Omega}\cos i = 0 \tag{4.54}$$

which leads to

$$\delta L_2 = -\frac{(3\eta + 4)\varepsilon}{4L^3\eta^4}\left[\left(1 - 3\cos^2 i\right)\frac{\delta\eta_1}{\eta} - \sin 2i\,\delta i_1\right] \tag{4.55}$$

To prevent drift out-of-plane drift

$$\delta\eta_1 = -0.25\eta\tan i\,\delta i_1 \tag{4.56}$$

As shown in Ref. 89 for orbits with a specified δi Eq. (4.56) leads to large values for δe for near-polar and near-circular orbits. Thus, invoking the constraint to prevent out-of-plane growth may lead to impractical relative motion orbits. If the desired relative motion orbit only allows one constraint, that constraint should be preventing the in-plane drift. This is called the period matching constraint and to 1st order it is given by Eq. (4.54) with the resulting change in semi-major axis for the deputy given by Eq. (4.55).

The equations for the 2nd order corrections δL_3, $\delta \eta_2$ and δi_2 depend on which of these are independent and whether there are one or two constraints. Consequently, they are not provided and can be derived easily.

An alternative is to use the exact equations for the angle rates and numerically solve using an equation solver, such as exists in Matlab, for the differential elements that satisfy the constraints, e.g., the period matching condition. We have done this and the comparison is provided in the Results Section.

Note that Eq. (4.54) is a necessary condition to suppress the in-track secular growth. To set up bounded relative motions, we still need other initial conditions.

4.2.5 Initial Conditions in Orbital Elements

Our goal is to set up a projected circular orbit (PCO) with the motion projected in the local horizontal plane is a circle. In a chief centered local vertical local horizontal (LVLH) frame, the PCO can be described by

$$\begin{aligned} x &= 0.5\rho \sin(\theta + \alpha_0) \\ y &= \rho \cos(\theta + \alpha_0) \\ z &= \rho \sin(\theta + \alpha_0) \end{aligned} \tag{4.57}$$

where ρ is the relative orbit size and α_0 is the initial phase angle. We want to express Eq. (4.57) in terms of the orbital elements in the mean space. To avoid the singularity at small eccentricity they should be a set of non-singular orbital elements. We have selected the following

$$\boldsymbol{e} = \left[a, q_1, q_2, i, \Omega, \lambda\right] \tag{4.58}$$

$$\begin{aligned} q_1 &= e\cos\omega \\ q_2 &= e\sin\omega \\ \lambda &= g + l = \omega + M \end{aligned} \tag{4.59}$$

Using Eq.(4.28), the initial conditions are[100]

$$\delta q_1 = -\frac{\rho\sin\alpha_0}{2a} \tag{4.60}$$

$$\delta q_2 = -\frac{\rho\cos\alpha_0}{2a} \tag{4.61}$$

$$\delta i = \frac{\rho\cos\alpha_0}{a} \tag{4.62}$$

$$\delta\Omega = -\frac{\rho\sin\alpha_0}{a\sin i} \tag{4.63}$$

$$\delta\lambda = -\delta\Omega\cos i \tag{4.64}$$

From Eq. (4.55) the difference in the semi-major axis is

$$\delta a = -0.5 J_2 a\left(\frac{R_e}{a}\right)^2\left(\frac{3\eta+4}{\eta^4}\right)\left[\left(1-3\cos^2 i\right)\left(\frac{q_1\delta q_1 + q_2\delta q_2}{\eta^2}\right) + \sin 2i\,\delta i\right] \tag{4.65}$$

As mentioned earlier, it is easy to obtain the second order approximation to δa with J_2^2 and without J_2^2. In the Results section, we will compare the accuracy of the first and second order approximation.

4.2.6 Bounded Conditions in Cartesian Frames

It is well known for the Hill's equations

$$\ddot{x} - 2ny - 3n^2 x = 0 \tag{4.66}$$

$$\ddot{y} + 2n\dot{x} = 0 \tag{4.67}$$

$$\ddot{z} + n^2 z = 0 \tag{4.68}$$

that the condition for no secular terms is

$$\dot{y}_0 = -2nx_0 \tag{4.69}$$

This is equivalent to requiring that the semi-major axes be equal. Vaddi, et al[80] obtained bounded solutions for the relative motion problem accommodating the effects of eccentricity and quadratic terms. The modified bounded condition for the PCO is

$$\dot{y}_0 = -\frac{n\rho \sin\alpha_0 (2+e)}{2(1+e)^{\frac{1}{2}}(1-e)^{\frac{3}{2}}} - \left(3\mu/a^4\right)\left(\rho^2/48n\right)(12+6\cos 2\alpha_0) \tag{4.70}$$

In the Results section, we will investigate the effects of the bounded conditions Eq. (4.65), Eq. (4.69) and Eq. (4.70) on suppressing the secular drift in the in-track direction.

4.2.7 Results

4.2.7.1 Chief Orbit and Size of Relative Orbit

The mean elements of the Chief orbit are

$$a = 8000 \text{ (km)},\ i = 50 \text{ (deg)},$$

$$\Omega = 0 \text{ (deg)},\ \omega = 0 \text{ (deg)},\ M_0 = 0 \text{ (deg)}$$

$$e = 1e-4, 0.001, 0.01, 0.1$$

We use these elements and Eqs. (4.60-65) to establish the projected circular orbit (PCO) for a circular Chief orbit. When the Chief orbit is not circular they establish a relative motion orbit that is close to a PCO. Because the period matching condition is used there is very little in-track drift. The radius of the PCO ρ is chosen as 0.16, 0.80, 1.6, 4, 8, 12, 16, 40, 80, 120 and 160 km. The initial phase angle α_0 is set to zero. In each of these cases the out-of-plane motion is created by an inclination change which maximizes the differential nodal precession and out-of-plane drift. Note that they are essentially the same relative motion orbit of increasing size.

4.2.7.2 Accuracy of the First and Second Approximation

Assuming $e = 0.01$, we vary the PCO radius to investigate the accuracy of the approximation of δa. Table 4.1 shows the δa correction for each case from the 1st and 2nd order correction and the δa obtained numerically to satisfy the matching conditions Eq. (4.54). We conclude from Table 4.1:

Table 4.1: δa (m)

ρ *(km)*	1^{st} *Order*	2^{nd} *Order without* J_2^2	2^{nd} *Order including* J_2^2	*Numerical Solutions*
0.1600	-0.3796	-0.3794	-0.3790	-0.3790
0.8000	-1.8979	-1.8968	-1.8948	-1.8948
1.6000	-3.7958	-3.7934	-3.7895	-3.7895
4.0000	-9.4895	-9.4828	-9.4730	-9.4730
8.0000	-18.9790	-18.9632	-18.9435	-18.9435
12.0000	-28.4685	-28.4412	-28.4117	-28.4117
16.0000	-37.9580	-37.9167	-37.8775	-37.8774
40.0000	-94.8950	-94.7189	-94.6218	-94.6199
80.0000	-189.7901	-189.1948	-189.0039	-188.9892
120.0000	-284.6851	-283.4278	-283.1462	-283.0974
160.0000	-379.5801	-377.4179	-377.0487	-376.9339

- As expected the 2nd order is better than the 1st order.
- Inclusion of J_2^2 terms improves the solution.
- As expected the change in semi-major axis to suppress the secular drift is essentially linear with the formation size.

4.2.7.3 Suppression of the In-Track Secular Drift

Orbital elements approach: We use Eqs. (4.60-65) to obtain the mean elements of the Deputy, one of which is the bounded condition Eq. (4.65). Then the mean elements are transformed into the osculating elements for both the Chief and Deputy, and then the initial coordinates in the ECI frame are obtained. The equations of motion

$$\ddot{\mathbf{r}} = -\phi_r \tag{4.71}$$

are then integrated numerically for both the Chief and Deputy where $\boldsymbol{r}$ is the inertial position vector, and ϕ_r is the gravitational potential gradient. The coordinates in the ECI frame are then transformed into the Chief LVLH frame and differenced to obtain the relative orbits.

Hill's approach: The initial conditions for the PCO are

$$x = 0.5\rho \sin\alpha_0 \tag{4.72}$$

$$y = \rho \cos\alpha_0 \tag{4.73}$$

$$z = \rho \sin\alpha_0 \tag{4.74}$$

$$\dot{x} = 0.5\rho n \cos\alpha_0 \tag{4.75}$$

$$\dot{y} = -\rho n \sin\alpha_0 \tag{4.76}$$

$$\dot{z} = \rho n \cos\alpha_0 \tag{4.77}$$

Notice Eq. (4.72) and Eq. (4.76) are satisfied with the bounded condition Eq. (4.69). Using the coordinate transformations, it is easy to get the initial conditions of the Deputy in the ECI frame. Then integrate Eq. (4.71) and transfer the coordinates in the ECI frame into ones in the LVLH frame and obtain the relative orbits.

Vaddi's approach: Substituting Eq. (4.70) for Eq. (4.76) and performing the same procedure as with Hill's approach, the relative orbit is obtained.

Assume $e = 0.01$ and $\rho = 160$ km. Fig. 4.1 illustrates the relative orbits set up by three approaches. The number of the orbits is 10.

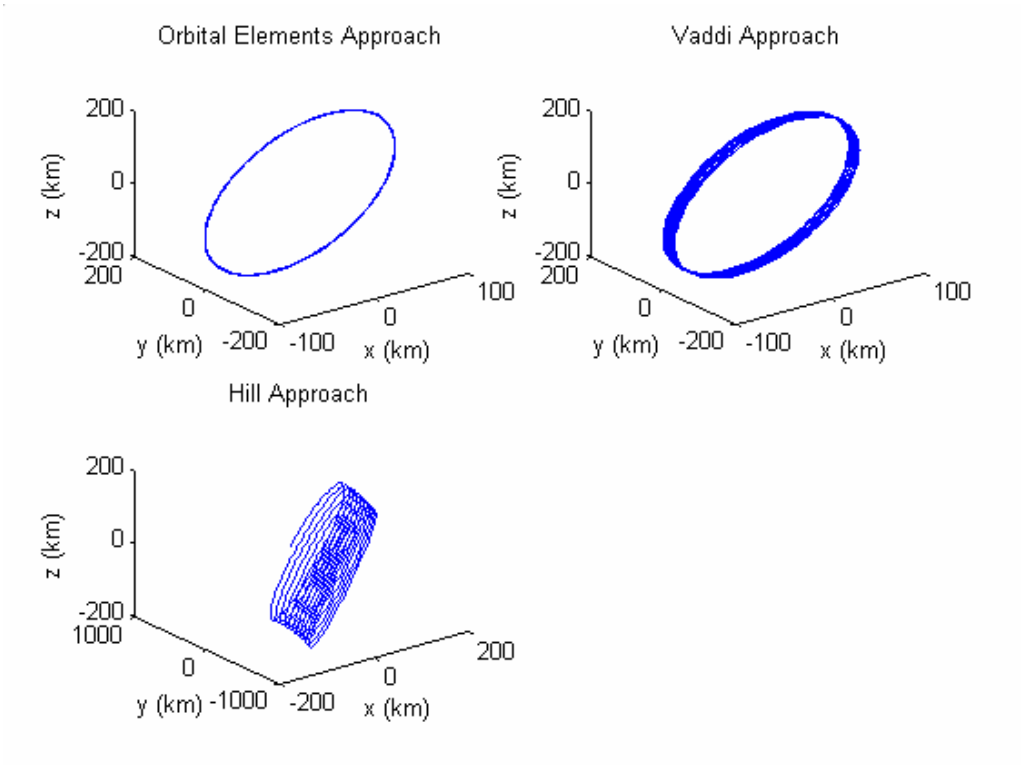

Fig. 4.1 Relative Orbits

Fig. 4.1 shows the bounded relative motion breaks down along the in-track direction using Hill's approach due to the nonlinearity, eccentricity and J_2 perturbations. Vaddi's approach demonstrates the effect of the nonlinearity and eccentricity correction in

suppressing the secular growth in the along track direction, but there is still a significant secular growth caused by J_2 perturbations. The orbital elements approach automatically incorporates the reference or Chief orbit eccentricity and includes 1st and 2nd order J_2 effects, and nonlinearity effects of the transformation can be eliminated by using numerical coordinate transformations. The secular growth is almost removed and the relative orbit is shown in Fig. 4.1.

To investigate the effects of e and ρ on the relative motions, we compute the secular growth at the end of the 10th orbit for each case as shown in Fig.4.2. In the figure, the solid lines represent the solutions from the orbital elements approach, the dotted lines stand for the solutions from Vaddi's approach and ":" lines represent the ones from Hill's approach. Fig. 4.2 shows that the nonlinearity or the relative orbit size ρ has a bigger effect on the secular growth than the eccentricity for Hill's approach. When the eccentricity of the Chief orbit is small Vaddi's approach is close to the orbital elements approach. In any case, the orbital elements approach has a strong effect on suppressing the secular growth.

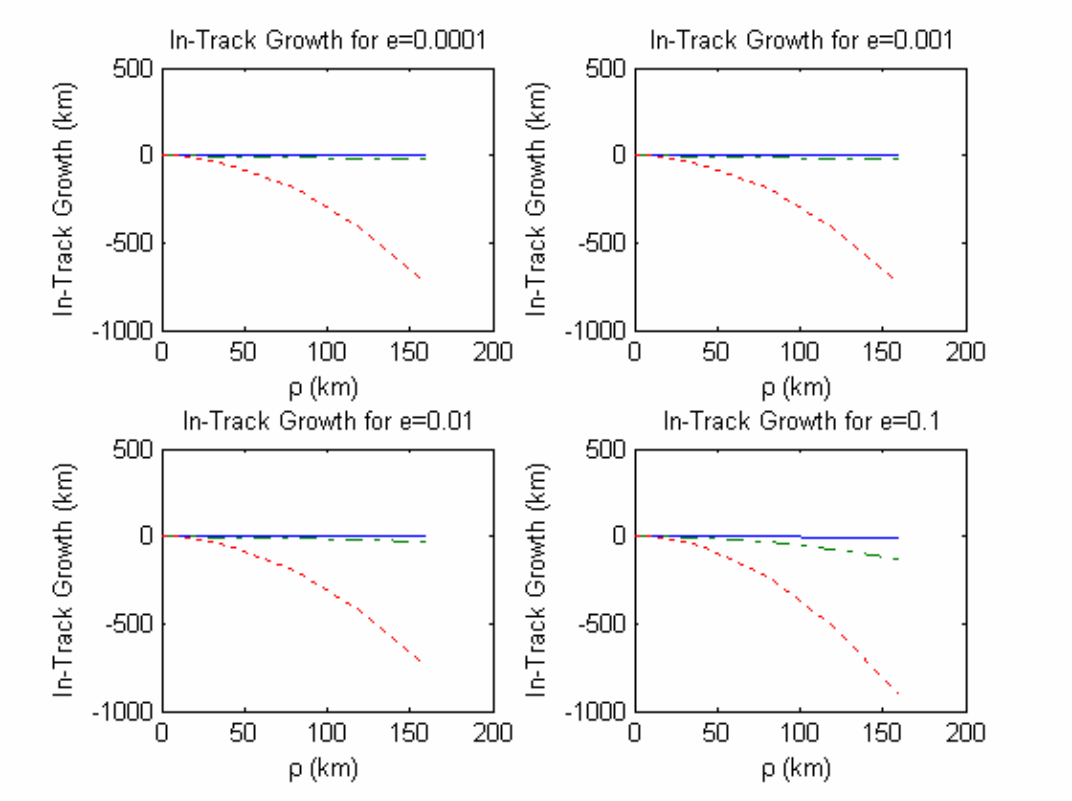

Fig. 4.2 Comparison of Secular Growth for Each Case

4.2.8 Remarks

- A procedure for designing relative motion orbits using orbital element differences has been presented.
- A 2nd order theory including the J_2^2 term for the relative motion of two satellites has been derived using orbital elements. This theory is valid for any eccentricity and contains 1st and 2nd order J_2 effects. It has been shown that for consistency a nonlinear theory for relative motion must also consider eccentricity and gravitational perturbations. Other higher order geopotential terms could easily be included.

- A relative motion theory using orbital elements is more accurate than one using the relative Cartesian or curvilinear coordinates.
- The period matching or bounded condition in the orbital elements has been proposed for the nonlinear problem and compared with the conditions in the Cartesian frame. The results show the orbital elements approach has a strong effect on suppressing the secular growth.

4.3 Development of State Transition Matrix Using Unit Sphere Approach

4.3.1 Introduction

In this section, we use the unit sphere approach, proposed by Vadali[102], to establish a state transition matrix for the perturbed non-circular reference orbit problem. In the unit sphere approach, the relative motion problem is studied by projecting the relative motion of the two satellites onto a unit sphere. This is achieved by normalizing the position vector of each satellite with respect to its radius. This process allows one to study the relative motion using spherical trigonometry so that a kinematically exact description is obtained for the relative positions in terms of the differential orbital elements, without recourse to linearization. In order to obtain time-explicit expressions, the method requires the solution of Kepler's equation or eccentricity expansions to obtain the radial distance and argument of latitude. Taking time derivatives for the relative positions, we obtain analytical expressions for the relative velocities with the help of Gauss' variational equations. However, we do not find the linearly inverse analytical

expressions for the relative motion. This is why we develop the linear STM based on the unit sphere approach. Our numerical evaluations show that the first order STM can be an alternative method to obtain the STM with the same accuracy as the Gim-Alfriend STM. The second order correction developed from the unit sphere approach works well to reduce major errors from the first order STM.

4.3.2 Unit Sphere Approach

The relative position on the unit sphere is given by

$$\begin{Bmatrix} \Delta x \\ \Delta y \\ \Delta z \end{Bmatrix} = \left[C_C C_D^T - I \right] \begin{Bmatrix} 1 \\ 0 \\ 0 \end{Bmatrix} \tag{4.78}$$

where Δx, Δy, and Δz, are respectively, the radial, along-track, and cross-track relative positions on the unit sphere, C_c and C_D are the direction cosine matrices of the Chief and Deputy with respect to the inertial frame, and the subscripts C and D represent the Chief and Deputy, respectively. This results in analytical expressions for the so-called "sub-satellite" points that are functions of the angles only (right ascension Ω, inclination i, and argument of latitude θ). Eq. (4.78) can be expanded as

$$\begin{aligned} \Delta x = & -1 + \mathrm{c}^2\left(0.5 i_C\right) c^2\left(0.5 i_D\right) c\left(\theta_D - \theta_C + \Omega_D - \Omega_C\right) \\ & + s^2\left(0.5 i_C\right) s^2\left(0.5 i_D\right) c\left(\theta_D - \theta_C - \Omega_D + \Omega_C\right) \\ & + s^2\left(0.5 i_C\right) c^2\left(0.5 i_D\right) c\left(\theta_D + \theta_C + \Omega_D - \Omega_C\right) \\ & + c^2\left(0.5 i_C\right) s^2\left(0.5 i_D\right) c\left(\theta_D + \theta_C - \Omega_D + \Omega_C\right) \\ & + 0.5 s\left(i_C\right) s\left(i_D\right) \left[c\left(\theta_D - \theta_C\right) - c\left(\theta_D + \theta_C\right) \right] \end{aligned} \tag{4.79}$$

$$\begin{aligned}\Delta y = {} & c^2(0.5i_C)c^2(0.5i_D)s(\theta_D-\theta_C+\Omega_D-\Omega_C) \\ & +s^2(0.5i_C)s^2(0.5i_D)s(\theta_D-\theta_C-\Omega_D+\Omega_C) \\ & -s^2(0.5i_C)c^2(0.5i_D)s(\theta_D+\theta_C+\Omega_D-\Omega_C) \\ & -c^2(0.5i_C)s^2(0.5i_D)s(\theta_D+\theta_C-\Omega_D+\Omega_C) \\ & +0.5s(i_C)s(i_D)\left[s(\theta_D-\theta_C)-s(\theta_D+\theta_C)\right]\end{aligned} \tag{4.80}$$

$$\Delta z = -s(i_C)s(\Omega_D-\Omega_C)c(\theta_D)-\left[s(i_C)c(i_D)c(\Omega_D-\Omega_C)-c(i_C)s(i_D)\right]s(\theta_D) \tag{4.81}$$

The actual relative positions between the two satellites are

$$\delta x = r_D(1+\Delta x)-r_C \tag{4.82}$$

$$\delta y = r_D\Delta y \tag{4.83}$$

$$\delta z = r_D\Delta z \tag{4.84}$$

Taking time derivatives, we have

$$\delta\dot{x} = \dot{r}_D(1+\Delta x)+r_D\Delta\dot{x}-\dot{r}_C \tag{4.85}$$

$$\delta\dot{y} = \dot{r}_D\Delta y+r_D\Delta\dot{y} \tag{4.86}$$

$$\delta\dot{z} = \dot{r}_D\Delta z+r_D\Delta\dot{z} \tag{4.87}$$

4.3.3 A New State Transformation Matrix

In this section, we derive the transformation matrix using the unit sphere approach. Gauss' variational equations in terms of the nonsingular elements with the perturbing accelerations in the Local-Vertical Local-Horizontal (LVLH) frame are

$$\dot{a} = \frac{2a^2}{h}\left[(q_1\sin\theta-q_2\cos\theta)u_r+\frac{p}{r}u_\theta\right] \tag{4.88}$$

$$\dot{\theta} = \frac{h}{r^2} - \frac{r\sin\theta\cos i}{h\sin i}u_h \tag{4.89}$$

$$\dot{i} = \frac{r\cos\theta}{h}u_h \tag{4.90}$$

$$\dot{q}_1 = \frac{p\sin\theta}{h}u_r + \frac{(p+r)\cos\theta + q_1 r}{h}u_\theta + \frac{q_2 r\sin\theta\cos i}{h\sin i}u_h \tag{4.91}$$

$$\dot{q}_2 = -\frac{p\cos\theta}{h}u_r + \frac{(p+r)\sin\theta + q_2 r}{h}u_\theta - \frac{q_1 r\sin\theta\cos i}{h\sin i}u_h \tag{4.92}$$

$$\dot{\Omega} = \frac{r\sin\theta}{h\sin i}u_h \tag{4.93}$$

where

$$p = a\left(1 - q_1^2 - q_2^2\right) \tag{4.94}$$

$$h = \sqrt{\mu p} \tag{4.95}$$

$$r = \frac{p}{1 + q_1\cos\theta + q_2\sin\theta} \tag{4.96}$$

Considering the gravity perturbation J_2, the accelerations are

$$u_r = -1.5\frac{J_2\mu R_e^2}{r^4}\left(1 - 3\sin^2 i\sin^2\theta\right) \tag{4.97}$$

$$u_\theta = -1.5\frac{J_2\mu R_e^2\sin^2 i\sin 2\theta}{r^4} \tag{4.98}$$

$$u_h = -1.5\frac{J_2\mu R_e^2\sin 2i\sin\theta}{r^4} \tag{4.99}$$

From Eqs. (4.79-81), we have

$$\Delta\dot{x} = \frac{\partial \Delta x}{\partial \theta_C}\dot{\theta}_C + \frac{\partial \Delta x}{\partial \theta_D}\dot{\theta}_D + \frac{\partial \Delta x}{\partial i_C}\dot{i}_C + \frac{\partial \Delta x}{\partial i_D}\dot{i}_D + \frac{\partial \Delta x}{\partial \Omega_C}\dot{\Omega}_C + \frac{\partial \Delta x}{\partial \Omega_D}\dot{\Omega}_D \tag{4.100}$$

$$\Delta\dot{y} = \frac{\partial \Delta y}{\partial \theta_C}\dot{\theta}_C + \frac{\partial \Delta y}{\partial \theta_D}\dot{\theta}_D + \frac{\partial \Delta y}{\partial i_C}\dot{i}_C + \frac{\partial \Delta y}{\partial i_D}\dot{i}_D + \frac{\partial \Delta y}{\partial \Omega_C}\dot{\Omega}_C + \frac{\partial \Delta y}{\partial \Omega_D}\dot{\Omega}_D \tag{4.101}$$

$$\Delta\dot{z} = \frac{\partial \Delta z}{\partial \theta_C}\dot{\theta}_C + \frac{\partial \Delta z}{\partial \theta_D}\dot{\theta}_D + \frac{\partial \Delta z}{\partial i_C}\dot{i}_C + \frac{\partial \Delta z}{\partial i_D}\dot{i}_D + \frac{\partial \Delta z}{\partial \Omega_C}\dot{\Omega}_C + \frac{\partial \Delta z}{\partial \Omega_D}\dot{\Omega}_D \tag{4.102}$$

Since $\boldsymbol{e}_{\mathrm{D}} = \boldsymbol{e}_{\mathrm{C}} + \Delta\boldsymbol{e}$

$$\begin{aligned}\frac{\partial \Delta\dot{x}}{\partial \Delta\mathbf{e}} = {} & \frac{\partial^2 \Delta x}{\partial \theta_C \partial \mathbf{e}_D}\dot{\theta}_C + \frac{\partial^2 \Delta x}{\partial \theta_D \partial \mathbf{e}_D}\dot{\theta}_D + \frac{\partial \Delta x}{\partial \theta_D}\frac{\partial \dot{\theta}_D}{\partial \mathbf{e}_D} \\ & + \frac{\partial^2 \Delta x}{\partial i_C \partial \mathbf{e}_D}\dot{i}_C + \frac{\partial^2 \Delta x}{\partial i_D \partial \mathbf{e}_D}\dot{i}_D + \frac{\partial \Delta x}{\partial i_D}\frac{\partial \dot{i}_D}{\partial \mathbf{e}_D} \\ & + \frac{\partial^2 \Delta x}{\partial \Omega_C \partial \mathbf{e}_D}\dot{\Omega}_C + \frac{\partial^2 \Delta x}{\partial \Omega_D \partial \mathbf{e}_D}\dot{\Omega}_D + \frac{\partial \Delta x}{\partial \Omega_D}\frac{\partial \dot{\Omega}_D}{\partial \mathbf{e}_D}\end{aligned} \tag{4.103}$$

$$\begin{aligned}\frac{\partial \Delta\dot{y}}{\partial \Delta\mathbf{e}} = {} & \frac{\partial^2 \Delta y}{\partial \theta_C \partial \mathbf{e}_D}\dot{\theta}_C + \frac{\partial^2 \Delta y}{\partial \theta_D \partial \mathbf{e}_D}\dot{\theta}_D + \frac{\partial \Delta y}{\partial \theta_D}\frac{\partial \dot{\theta}_D}{\partial \mathbf{e}_D} \\ & + \frac{\partial^2 \Delta y}{\partial i_C \partial \mathbf{e}_D}\dot{i}_C + \frac{\partial^2 \Delta y}{\partial i_D \partial \mathbf{e}_D}\dot{i}_D + \frac{\partial \Delta y}{\partial i_D}\frac{\partial \dot{i}_D}{\partial \mathbf{e}_D} \\ & + \frac{\partial^2 \Delta y}{\partial \Omega_C \partial \mathbf{e}_D}\dot{\Omega}_C + \frac{\partial^2 \Delta y}{\partial \Omega_D \partial \mathbf{e}_D}\dot{\Omega}_D + \frac{\partial \Delta y}{\partial \Omega_D}\frac{\partial \dot{\Omega}_D}{\partial \mathbf{e}_D}\end{aligned} \tag{4.104}$$

$$\begin{aligned}\frac{\partial \Delta\dot{z}}{\partial \Delta\mathbf{e}} = {} & \frac{\partial^2 \Delta z}{\partial \theta_C \partial \mathbf{e}_D}\dot{\theta}_C + \frac{\partial^2 \Delta z}{\partial \theta_D \partial \mathbf{e}_D}\dot{\theta}_D + \frac{\partial \Delta z}{\partial \theta_D}\frac{\partial \dot{\theta}_D}{\partial \mathbf{e}_D} \\ & + \frac{\partial^2 \Delta z}{\partial i_C \partial \mathbf{e}_D}\dot{i}_C + \frac{\partial^2 \Delta z}{\partial i_D \partial \mathbf{e}_D}\dot{i}_D + \frac{\partial \Delta z}{\partial i_D}\frac{\partial \dot{i}_D}{\partial \mathbf{e}_D} \\ & + \frac{\partial^2 \Delta z}{\partial \Omega_C \partial \mathbf{e}_D}\dot{\Omega}_C + \frac{\partial^2 \Delta z}{\partial \Omega_D \partial \mathbf{e}_D}\dot{\Omega}_D + \frac{\partial \Delta z}{\partial \Omega_D}\frac{\partial \dot{\Omega}_D}{\partial \mathbf{e}_D}\end{aligned} \tag{4.105}$$

From Eqs. (4.94-96), we have

$$\dot{r}_D = \frac{\partial r_D}{\partial a_D}\dot{a}_D + \frac{\partial r_D}{\partial \theta_D}\dot{\theta}_D + \frac{\partial r_D}{\partial q_{1D}}\dot{q}_{1D} + \frac{\partial r_D}{\partial q_{2D}}\dot{q}_{2D} \tag{4.106}$$

So,

$$\begin{aligned}\frac{\partial \dot{r}_D}{\partial \Delta \mathbf{e}} &= \frac{\partial^2 r_D}{\partial a_D \partial \mathbf{e}_D}\dot{a}_D + \frac{\partial r_D}{\partial a_D}\frac{\partial \dot{a}_D}{\partial \mathbf{e}_D} + \frac{\partial^2 r_D}{\partial \theta_D \partial \mathbf{e}_D}\dot{\theta}_D \\ &+ \frac{\partial r_D}{\partial \theta_D}\frac{\partial \dot{\theta}_D}{\partial \mathbf{e}_D} + \frac{\partial^2 r_D}{\partial q_{1D} \partial \mathbf{e}_D}\dot{q}_{1D} + \frac{\partial r_D}{\partial q_{1D}}\frac{\partial \dot{q}_{1D}}{\partial \mathbf{e}_D} \\ &+ \frac{\partial^2 r_D}{\partial q_{2D} \partial \mathbf{e}_D}\dot{q}_{2D} + \frac{\partial r_D}{\partial q_{2D}}\frac{\partial \dot{q}_{2D}}{\partial \mathbf{e}_D}\end{aligned} \tag{4.107}$$

Now we obtain the transformation matrix

$$\Sigma(t) = \left(\frac{\partial \delta x}{\partial \Delta \mathbf{e}} \;\; \frac{\partial \delta \dot{x}}{\partial \Delta \mathbf{e}} \;\; \frac{\partial \delta y}{\partial \Delta \mathbf{e}} \;\; \frac{\partial \delta \dot{y}}{\partial \Delta \mathbf{e}} \;\; \frac{\partial \delta z}{\partial \Delta \mathbf{e}} \;\; \frac{\partial \delta \dot{z}}{\partial \Delta \mathbf{e}} \right)^T \tag{4.108}$$

where

$$\frac{\partial \delta x}{\partial \Delta \mathbf{e}} = \frac{\partial r_D}{\partial \Delta \mathbf{e}}(1 + \Delta x) + r_D \frac{\partial \Delta x}{\partial \Delta \mathbf{e}} \tag{4.109}$$

$$\frac{\partial \delta \dot{x}}{\partial \Delta \mathbf{e}} = \frac{\partial \dot{r}_D}{\partial \Delta \mathbf{e}}(1 + \Delta x) + \dot{r}_D \frac{\partial \Delta x}{\partial \Delta \mathbf{e}} + \frac{\partial r_D}{\partial \Delta \mathbf{e}}\Delta \dot{x} + r_D \frac{\partial \Delta x}{\partial \Delta \mathbf{e}} \tag{4.110}$$

$$\frac{\partial \delta y}{\partial \Delta \mathbf{e}} = \frac{\partial r_D}{\partial \Delta \mathbf{e}}\Delta y + r_D \frac{\partial \Delta y}{\partial \Delta \mathbf{e}} \tag{4.111}$$

$$\frac{\partial \delta \dot{y}}{\partial \Delta \mathbf{e}} = \frac{\partial \dot{r}_D}{\partial \Delta \mathbf{e}}\Delta y + \dot{r}_D \frac{\partial \Delta y}{\partial \Delta \mathbf{e}} + \frac{\partial r_D}{\partial \Delta \mathbf{e}}\Delta \dot{y} + r_D \frac{\partial \Delta y}{\partial \Delta \mathbf{e}} \tag{4.112}$$

$$\frac{\partial \delta z}{\partial \Delta \mathbf{e}} = \frac{\partial r_D}{\partial \Delta \mathbf{e}}\Delta z + r_D \frac{\partial \Delta z}{\partial \Delta \mathbf{e}} \tag{4.113}$$

$$\frac{\partial \delta \dot{z}}{\partial \Delta \mathbf{e}} = \frac{\partial \dot{r}_D}{\partial \Delta \mathbf{e}}\Delta z + \dot{r}_D \frac{\partial \Delta z}{\partial \Delta \mathbf{e}} + \frac{\partial r_D}{\partial \Delta \mathbf{e}}\Delta \dot{z} + r_D \frac{\partial \Delta z}{\partial \Delta \mathbf{e}} \tag{4.114}$$

4.3.4 Results

To evaluate the proposed method, the predicted relative motion by the unit sphere STM is compared with that by the Gim-Alfriend STM.

4.3.4.1 Chief and Deputy Orbits

The mean elements of the Chief orbit are

$a = 8000\,(\text{km}),\ i = 50\,(\text{deg}),\ e = 0.01$

$\Omega = 0\,(\text{deg}),\ \omega = 0\ \ (\text{deg}),\ M_0 = 0\ \ (\text{deg})$

The Deputy orbit can be obtained[100] from Eqs. (4.60-65) for the PCO. When the Chief orbit is not circular they establish a relative motion orbit that is close to a PCO. Because the period matching condition is used there is very little in-track drift. The radius of the PCO ρ is chosen as 40 km. The initial phase angle α_0 is set to zero.

4.3.4.2 Comparisons

Figs. 4.3-4.6 compare the position and velocity errors using the unit sphere STM to the Gim-Alfriend STM. The errors are obtained by comparing the solutions from the STMs with the numerical integrations, respectively. The solutions of the numerical integrations are obtained by numerically integrating the equations of motion of both satellites in the ECI frame with a J_2 gravity field, differencing them and transforming to the LVLH frame.

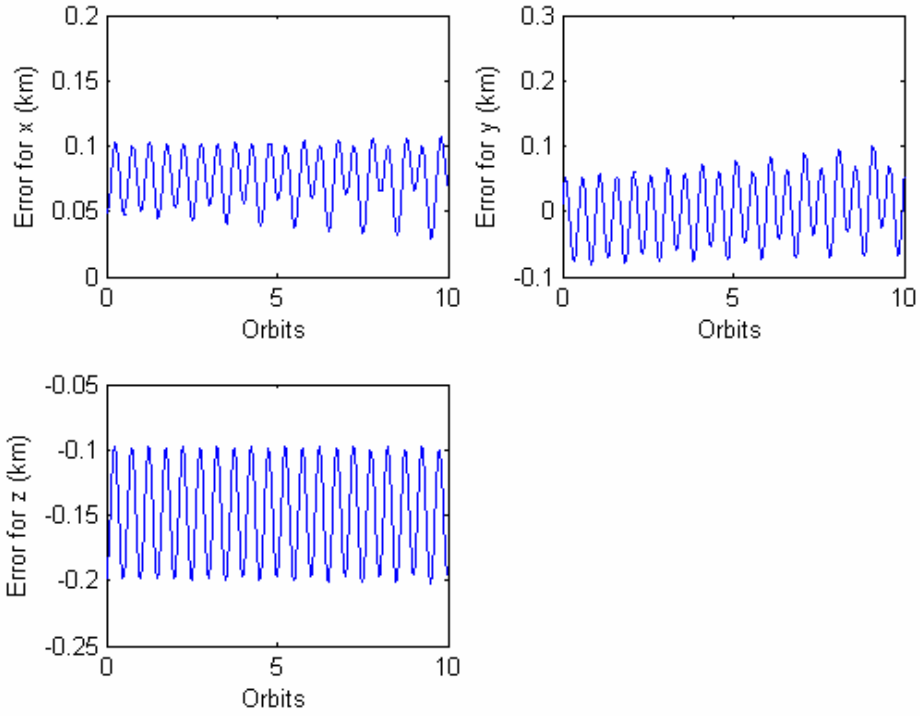

Fig. 4.3 Position Errors by Unit Sphere STM

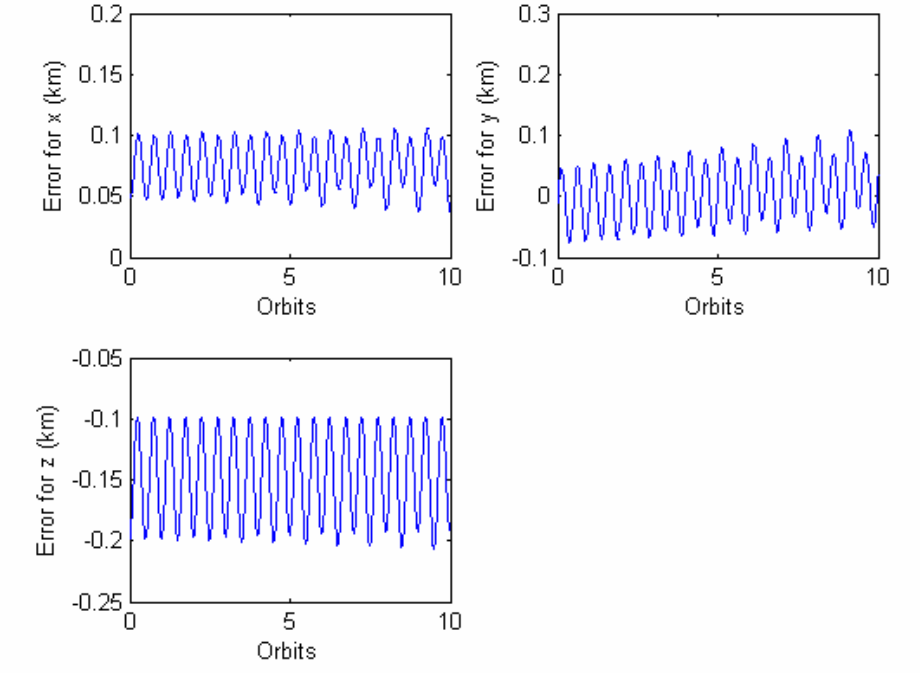

Fig.4.4 Position Errors by Gim-Alfriend STM

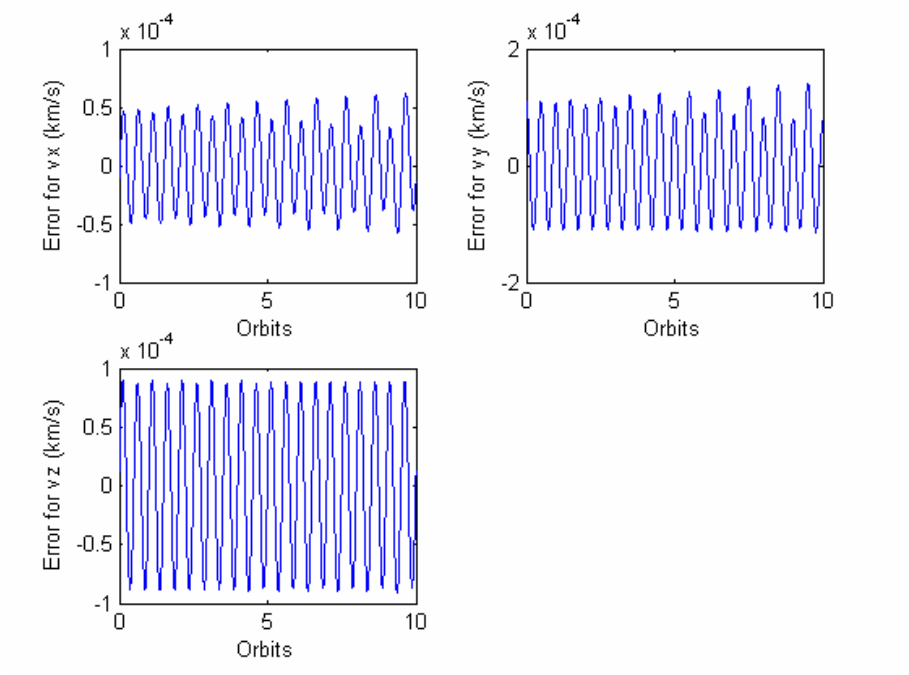

Fig. 4.5 Velocity Errors by Unit Sphere STM

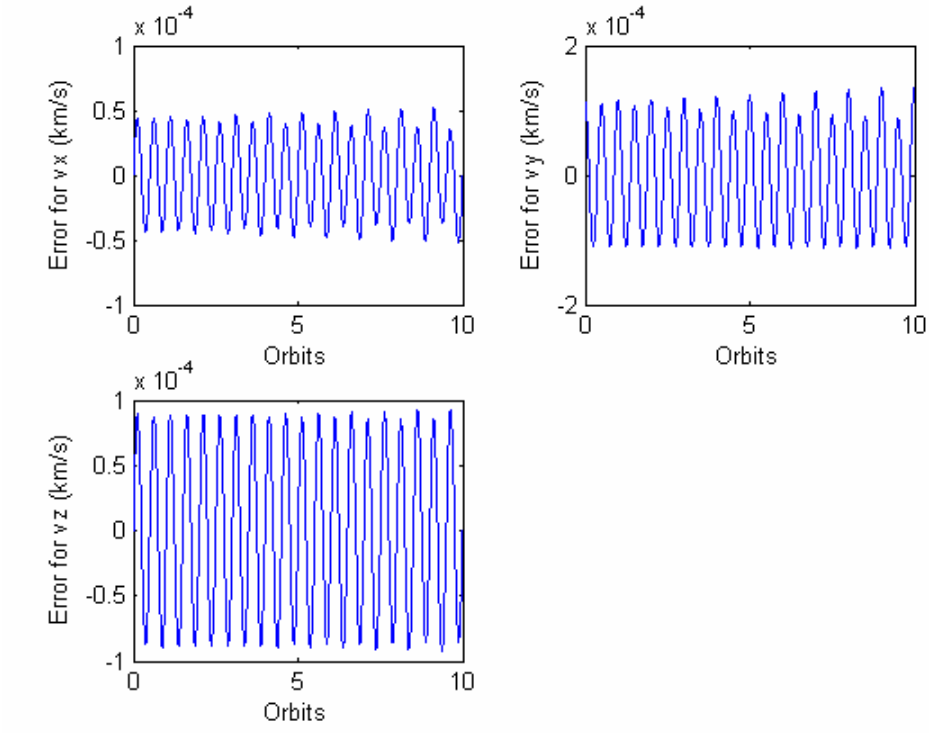

Fig. 4.6 Velocity Errors by Gim-Alfriend STM

The results indicate the STMs are very accurate for describing the relative motion. The STM from the unit sphere has the same accuracy as Gim-Alfriend's STM, which provides an alternative approach for representing relative motion.

One can see there are initial biases in the x and z directions and small drift in the y direction in Figs. 4.3-4.4. The initial bias means the PCO is not centered. The small secular drifts are caused by neglecting J_2^2 in the mean elements propagation and using the linear periodic matching condition Eq. (4.65). To reject these errors, we introduce the second order correction using the unit sphere approach. Expanding Eqs. (4.79-81) in terms of the second order, we have

$$\delta x = \frac{\partial \delta x}{\partial \Delta \mathbf{e}} \Delta \mathbf{e} + \frac{1}{2} \Delta \mathbf{e} \mathbf{H}_x \Delta \mathbf{e}^T \tag{4.115}$$

$$\delta y = \frac{\partial \delta y}{\partial \Delta \mathbf{e}} \Delta \mathbf{e} + \frac{1}{2} \Delta \mathbf{e} \mathbf{H}_y \Delta \mathbf{e}^T \tag{4.116}$$

$$\delta z = \frac{\partial \delta z}{\partial \Delta \mathbf{e}} \Delta \mathbf{e} + \frac{1}{2} \Delta \mathbf{e} \mathbf{H}_z \Delta \mathbf{e}^T \tag{4.117}$$

where $\boldsymbol{e} = \left(a, \theta, i, q_1, q_2, \Omega\right)$. The Hessian matrix is

$$\mathbf{H}_x = \frac{\partial^2 \delta x}{\partial \Delta \mathbf{e}^2} \tag{4.118}$$

$$\mathbf{H}_y = \frac{\partial^2 \delta y}{\partial \Delta \mathbf{e}^2} \tag{4.119}$$

$$\mathbf{H}_z = \frac{\partial^2 \delta z}{\partial \Delta \mathbf{e}^2} \tag{4.120}$$

Introducing the second order term, Fig. 4.3 becomes

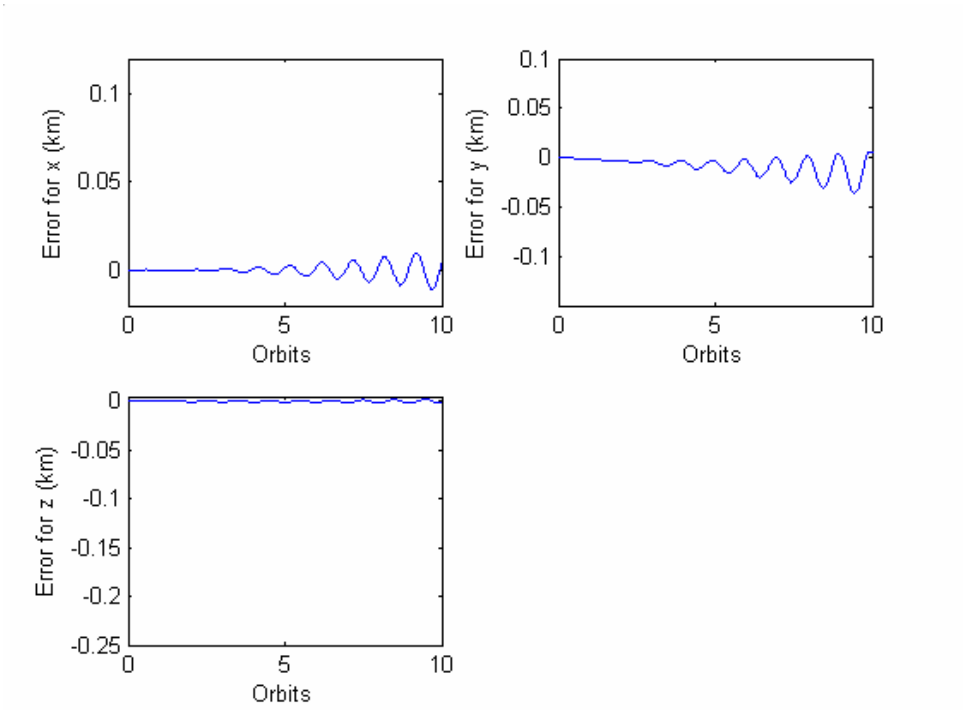

Fig.4.7 Position Errors by Unit Sphere STM Including Second Order

Fig. 4.7 illustrates the biases are removed by the second order term. The amplitudes are greatly reduced when compared with Fig. 4.3. Also one can see the major errors in the state transition matrix come from the second order term of $\sum(t)$. The other sources include the J_2^2 term and numerical integration errors.

4.3.5 Remarks

We develop an alternative STM for describing the relative motion using the unit sphere approach with the same accuracy as Gim-Alfriend's STM. The major errors from the first order STM can be rejected by the second order correction for relative motion.

4.4 An Evaluation and Comparison of Relative Motion Theories

4.4.1 Introduction

The various theories of relative motion are presented in Section 4.1. The complexity of these theories increases as the accuracy improves. Thus, an important question is which theory is needed for a given problem or what needs to be included in the reference orbit model. Since the accuracy is a function of the initial conditions a methodology is needed for comparing the accuracy of the theories for a class of problems. Such a methodology was developed by Junkins, et. al.[83] for comparing linear theories. In Ref. 83 a nonlinear index was introduced for comparing the accuracy of various linearized solutions for the propagation of a debris cloud resulting from a collision or break-up. The analysis showed that when using the linearized equations of motion the most accurate solution is obtained by using differential orbital elements. Recently, Junkins[105] in his tutorial on nonlinearity of orbit and attitude dynamics discussed problems on how to measure nonlinearity and used the nonlinearity index to evaluate several coordinate choices.

In this section we compare various theories for relative motion orbits. The purpose in this research was not just to compare theories, but to provide results that would aid mission designers in deciding what effects need to be included in the reference orbit model for their particular formation. Consequently, we selected theories that include the different effects. The theories selected for comparison are the CW solution[76], the Gim-Alfriend[86] state transition matrix, a small eccentricity state transition matrix, a non-J_2

state transition matrix derived from the Gim-Alfriend state transition matrix, a unit sphere approach proposed by Vadali[102,107] and the Alfriend-Yan nonlinear theory[91,92]. There are numerous other theories in the literature. A new modeling error index derived from the Junkins nonlinearity index is used to compare the theories. The Junkins index cannot be used because it is restricted to linear theories. Comparisons are performed for a spherical Earth and an oblate earth. When $J_2 = 0$ the Gim-Alfriend theory is numerically identical to the Lawden[78] and Tschauner-Hempel[79] theories so their accuracy is captured in these comparisons. The relative motion orbit selected for comparison is the projected circular orbit[90] (PCO) or its equivalent when the reference orbit is not circular. This relative motion orbit was selected because the evaluation of the relative motion theories should include some out-of-plane motion. The two key parameters in the evaluation are the eccentricity of the reference orbit and the relative motion orbit size, e.g., the projected circular orbit radius.

4.4.2 Modeling Error Index

Consider the nonlinear differential equations with the initial conditions

$$\dot{\boldsymbol{x}} = \boldsymbol{f}\left(t, \boldsymbol{x}\right),\ \boldsymbol{x}\left(t_0\right) = \boldsymbol{x}_0 \tag{4.121}$$

In Refs. 83 and 105 the nonlinearity index used was

$$v(t,t_0) = \sup_{i=1\ldots N} \frac{\left\| \Phi_i\left(t,t_0\right) - \bar{\Phi}\left(t,t_0\right) \right\|}{\left\| \bar{\Phi}\left(t,t_0\right) \right\|} \tag{4.122}$$

where $\bar{\Phi}(t,t_0)$ is the state transition matrix that is obtained from Eq. (4.121) with the expected initial conditions $\bar{\boldsymbol{x}}(t_0)$. $\Phi(t,t_0)$ is a state transition matrix that is obtained from Eq. (4.121) with a worst-case distribution of initial conditions neighboring the expected initial conditions. In Ref. 83 this index was used to compare the accuracy of three linear theories for a circular reference orbit, the CW equations, the linear theory using polar coordinates and one obtained from differential orbital elements. The objective was to determine which theory best captured the nonlinear effects. The comparison showed that differential orbital elements were the most accurate.

The nonlinearity index should evaluate modeling error, not just nonlinearity. Since the index in Eq. (4.122) cannot be used with a nonlinear theory a new index is needed. In addition, our objective is to compare the accuracy of the theories for specific types of orbits. For comparison in this paper the projected circular orbit (or its equivalent for a non-circular reference orbit) is used as the baseline orbit. Let $\bar{\boldsymbol{x}}_i(t)$ be the solution for the initial condition $\bar{\boldsymbol{x}}_i(t_0)$ at the corresponding points and let $\boldsymbol{x}_i(t)$ be the solutions for the proposed models. These need not be linearized solutions. It is important that the states be in dimensionless variables or a weighting matrix used. Let $\boldsymbol{W}$ be a weighting matrix that non-dimensionalizes $\boldsymbol{y}$, that is

$$\boldsymbol{y} = \boldsymbol{W}\boldsymbol{x} \tag{4.123}$$

We now propose the following modeling error index

$$v(t) = \max_{i=1\ldots N} |\nu_i| \tag{4.124}$$

$$\nu_i = \frac{\bar{\boldsymbol{y}}_i^T \bar{\boldsymbol{y}}_i}{\boldsymbol{y}_i^T \boldsymbol{y}_i} - 1 \tag{4.125}$$

Note that if there is only one state and we let $y_i = \bar{y}(1+\gamma)$ then the index becomes $\nu = 2|\gamma|$. Therefore, the index is proportional to the percentage error.

4.4.3 Reference Orbits

We use differential orbital elements to set up a reference relative motion orbit or projected circular orbit. Then take many points on the orbit as initial conditions, and propagate them to obtain the model error index as a function of time. The period matching condition for the relative motion at first order is[90]

$$\delta\dot{\lambda} + \delta\dot{\Omega}\cos i = 0 \tag{4.126}$$

In this section we have selected the projected circular relative motion orbit (PCO) for comparing the relative motion theories. In a Chief centered Local Vertical Local Horizontal (LVLH) frame, the PCO can be described by[90]

$$x = 0.5\rho\sin(\theta + \alpha_0) \tag{4.127}$$

$$y = \rho\cos(\theta + \alpha_0) \tag{4.128}$$

$$z = \rho\sin(\theta + \alpha_0) \tag{4.129}$$

where ρ is the relative orbit radius, α_0 is the initial phase angle and θ is the latitude angle of the Chief satellite. We want to express Eqs. (4.127-129) in terms of the orbital

elements in the mean space. To avoid the singularity at small eccentricity they should be a set of non-singular orbital elements. The differential orbital elements are determined from the selected relative motion orbit, as shown in Eqs. (4.60-65).

By choosing values of α_0 between 0 and 360 degree, we obtain a distribution of the initial conditions. Starting with these initial conditions, we evaluate the modeling error index of the approximate methods.

4.4.4 Approximate Methods for Relative Motion

4.4.4.1 Hill's Equations

Hill's equations are established in the LVLH frame by making the assumptions of a circular Chief orbit, spherical Earth, linearizing the differential gravity accelerations and neglecting all other perturbations. Hill's equations are shown in Eqs. (4.1-3).

4.4.4.2 Gim-Alfriend State Transition Matrix

Since Hill's equations have considerable errors and are insufficient for the long term prediction, Alfriend and Gim[86] developed an accurate state transition matrix for the perturbed non-circular reference orbit using a geometrical method, please see Eq. (4.17-18). Realizing the Deputy relative motion is a result of small changes in the orbital elements of the Chief, they used differential orbital elements and then transformed into the LVLH coordinates. The linear approximation using the differential orbital elements is more accurate than that using the Cartesian or curvilinear coordinates as shown in Refs. 83 and 105. Moreover, using the differential orbital elements automatically

includes the reference or Chief orbit eccentricity, which is not included in Hill's equations. Notice this method does not require the solution of differential equations.

4.4.4.3 Small Eccentricity State Transition Matrix

The Gim-Alfriend state transition matrix is valid for any eccentricity. A simpler version for small eccentricity can be derived. The small eccentricity state transition matrix is obtained from the Gim-Alfriend state transition matrix by retaining $O(e)$ terms for the non-J_2 portion and only $O(e^0)$ for the J_2 portion. See Appendix B for the state transition matrix.

4.4.4.4 Non-J_2 state transition matrix

The matrix is obtained from Eq. (4.140) by setting $J_2 = 0$. Its accuracy is numerically identical to those in the Lawden[78] and Tschauner-Hempel[79] theories. Therefore, its evaluation is equally applicable to evaluating either Lawden or Tschauner-Hempel.

4.4.4.5 Unit Sphere Approach

In the unit sphere approach[102,107], the relative motion problem is studied by projecting the motion of the two satellites onto a unit sphere. This is achieved by normalizing the position vector of each satellite with respect to its radius. See Section 4.3 for detail.

4.4.4.6 Yan-Alfriend Nonlinear Method

The geometrical method by Alfriend and Gim is just a transformation from a nonlinear algebra into a linear one. It results in not only a daunting task, but also a nonlinear error. The Yan-Alfriend method extends the earlier work of Schaub and Alfriend[89] in that the Taylor series expansion of the deputy mean orbital elements about the chief is carried to 2nd order. The matching condition to suppress the in-track drift is then determined and the time history of the differential mean elements determined. Since the expansion is carried to 2nd order the J_2^2 terms are included. This constitutes a very simple method for a long term prediction for nonlinear relative motion, that is, we predict mean orbital elements at the given time for the non-circular reference orbit including nonlinear J_2 effects, then transform them into the LVLH coordinates. Details are provided in Refs 91-92.

4.4.5 Numerical Results

Let us define several test cases for which we can evaluate the modeling error index for each approximate method. Let the mean orbital elements of the Chief take on the following values:

$$a = 8000\,(\text{km}),\ i = 50\,(\text{deg}),$$

$$\Omega = 0\,(\text{deg}),\ \omega = 0\ (\text{deg}),\ M_0 = 0\ (\text{deg})$$

$$e = 1e-4, 5e-4, 0.001, 0.005, 0.01, 0.05, 0.1$$

We use these elements and Eqs. (4.60-65) to establish the PCO for a circular Chief orbit. When the Chief orbit is not circular they establish a relative motion orbit that is close to

a PCO. Because the period matching condition is used there is very little in-track drift. The radius ρ of the PCO is chosen as 0.16, 0.80, 1.6, 4, 8, 12, 16, 40, 80, 120 and 160 km. See Fig. 4.8 for the PCO when $e = 0.001$ and $\rho = 12$ km. The objective is to evaluate the index of the approximate methods by varying the eccentricity of the Chief orbit and the PCO radius. For each case (specific value of e and ρ) 100 equally spaced values of the phase angle α_0 between 0 and 360 degree are used. A test was made to calculate the Gim-Alfriend index when the samples are 20, 50, 100, 200 and 500, and 100 samples are enough to get convergence. In Eq. (4.123), $\boldsymbol{x} = [x\ \dot{x}\ y\ \dot{y}\ z\ \dot{z}]$, and select $\boldsymbol{W}$ in terms of the Earth-value units so that $\boldsymbol{y}$ has canonical units. We used for $\boldsymbol{W}$

$$\mathbf{W} = diag\left(\frac{1}{R_e}, \frac{1}{R_e}, \frac{1}{R_e}, \frac{1}{R_e n_0}, \frac{1}{R_e n_0}, \frac{1}{R_e n_0}\right), n_0 = \sqrt{\frac{\mu}{R_e^3}} \tag{4.130}$$

Using Eqs. (4.124-125) the index ν_i is obtained for each of the initial phase angles. Notice $\bar{y}_i$ in Eq. (4.125) is obtained by numerically integrating the equations of motion of both the Chief and Deputy in the ECI reference frame with a J_2 gravity field, and then transforming the position and velocity vectors from the ECI frame to the Chief frame.

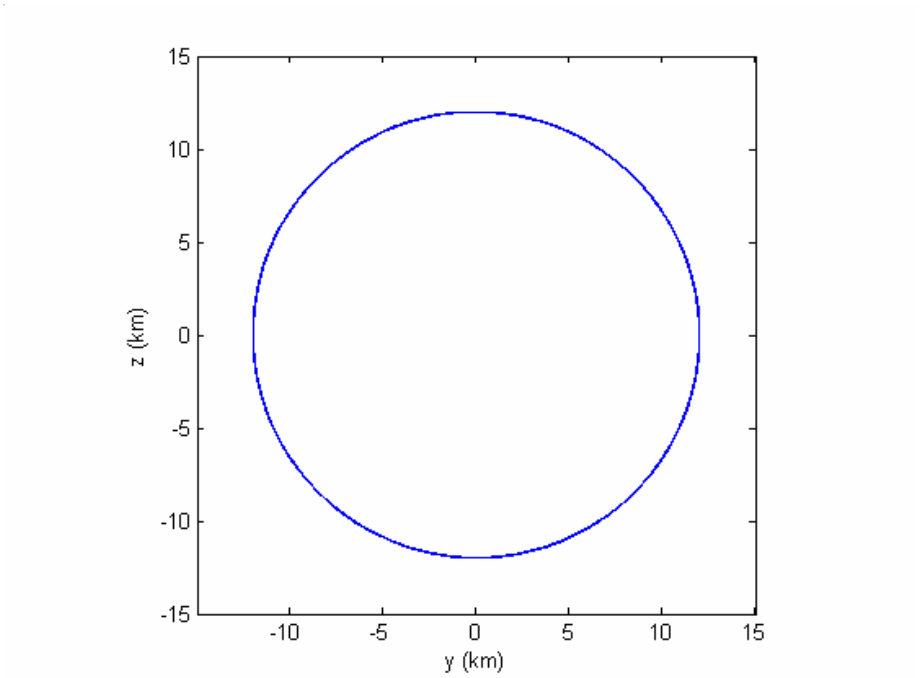

Fig. 4.8 Projected Circular Orbit

Fig. 4.8 illustrates a PCO with the radius of 12 km, as defined in the along-track/cross-track plane. Figs. 4.9-4.16 show the index comparisons as a function of the eccentricity of the Chief orbit and the PCO radius.

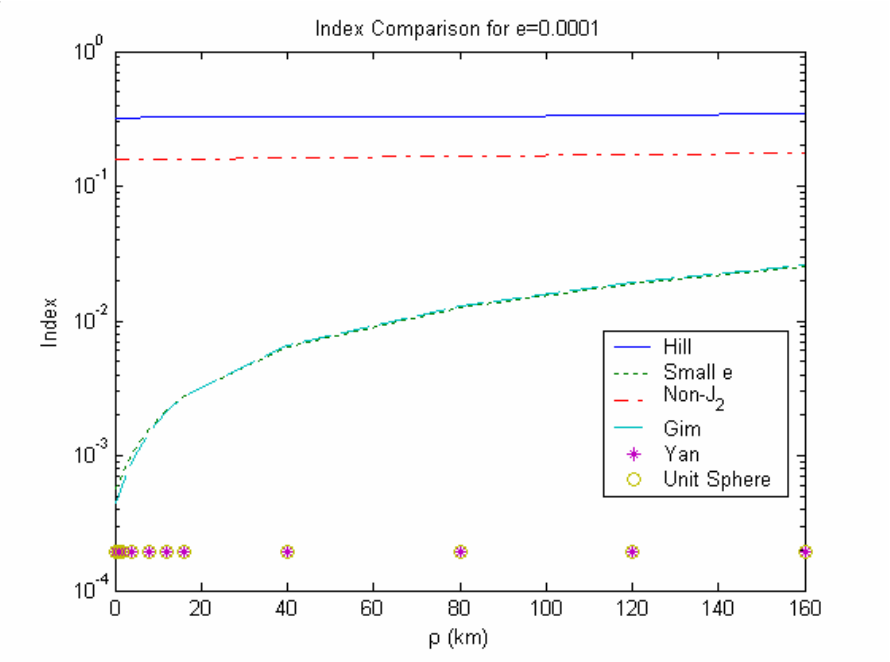

Fig. 4.9 Index Comparison for $e = 0.0001$

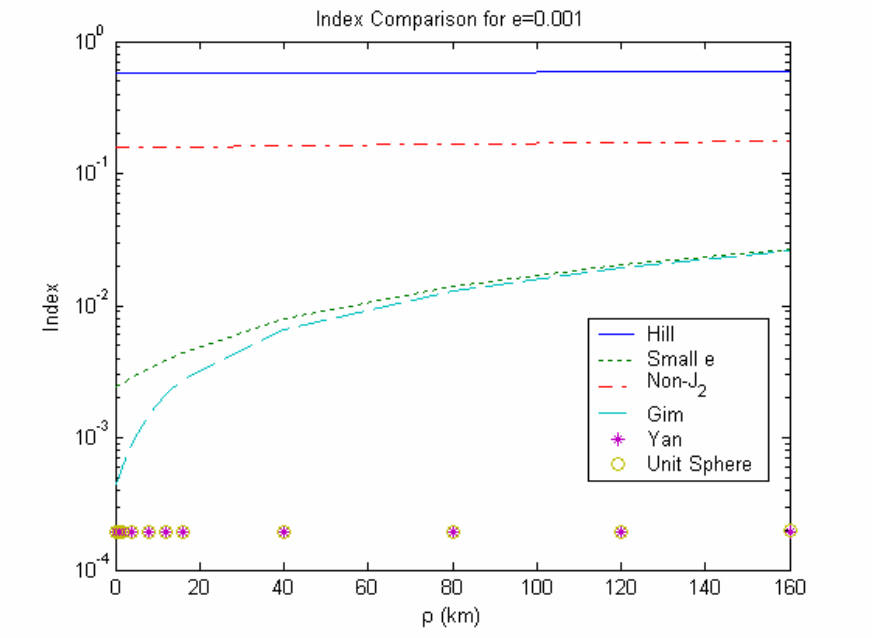

Fig. 4.10 Index Comparison for $e = 0.001$

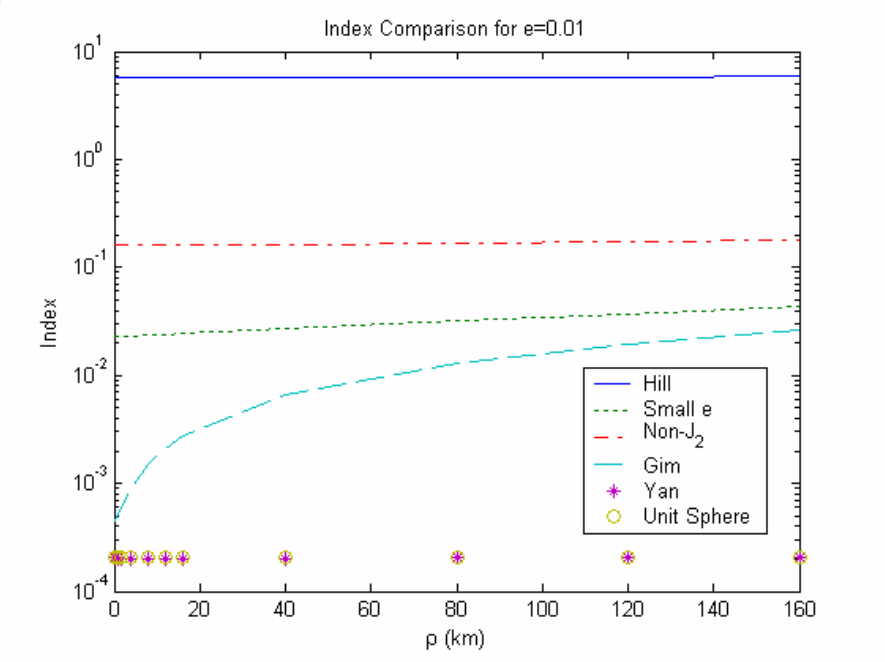

Fig. 4.11 Index Comparison for $e = 0.01$

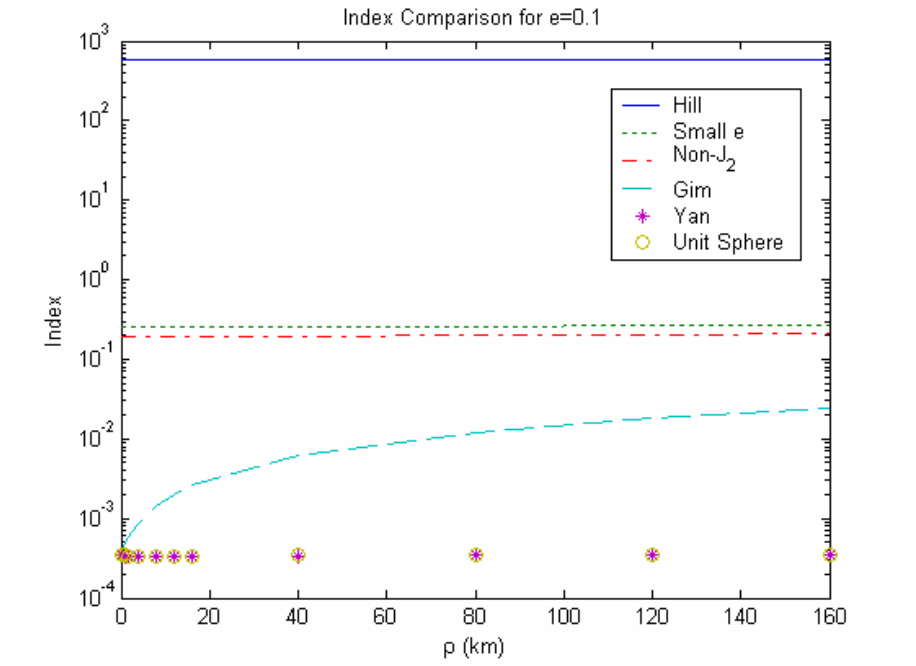

Fig. 4.12 Index Comparison for $e = 0.1$

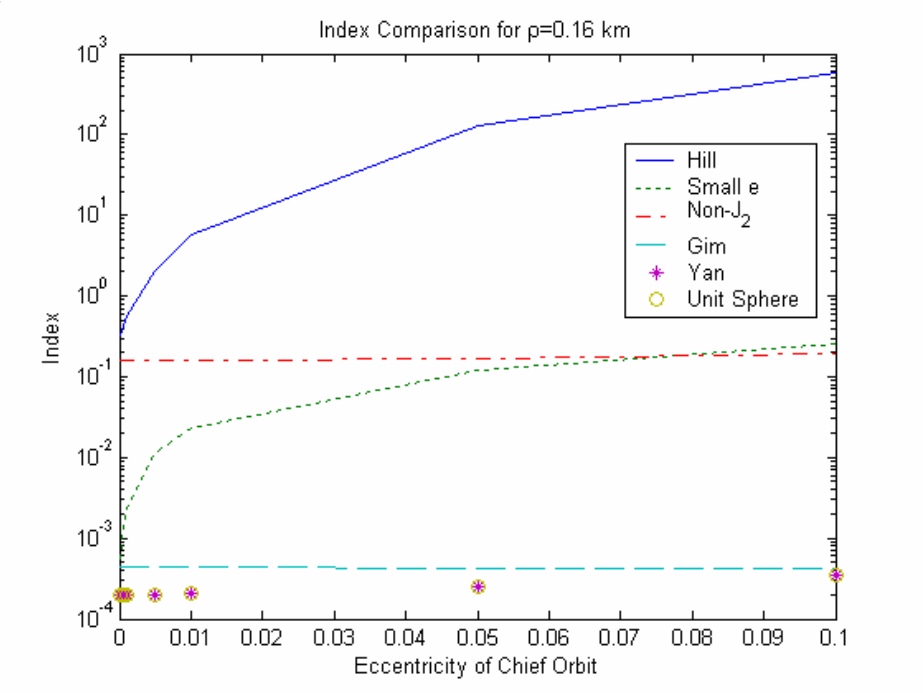

Fig. 4.13 Index Comparison for $\rho = 0.16$ km

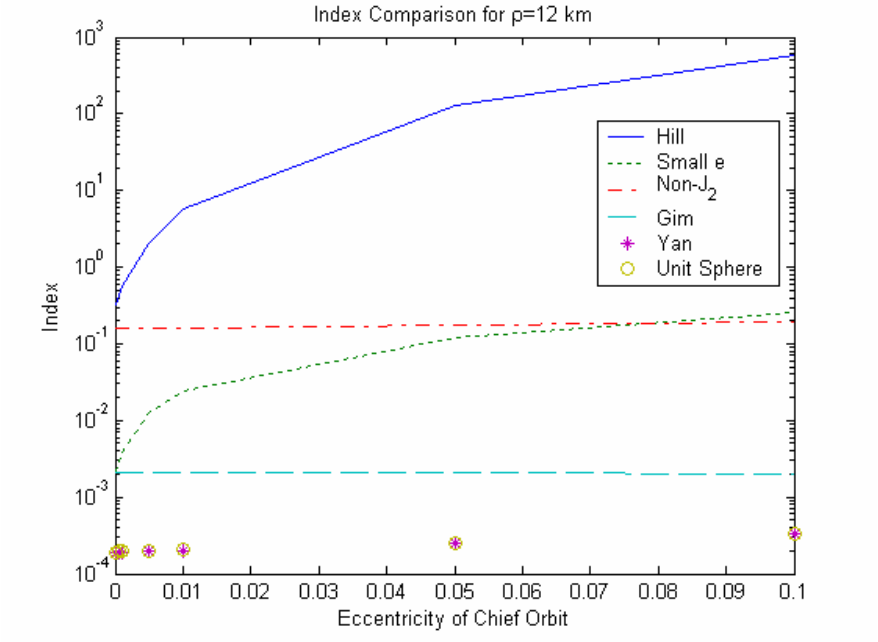

Fig. 4.14 Index Comparison for $\rho = 12$ km

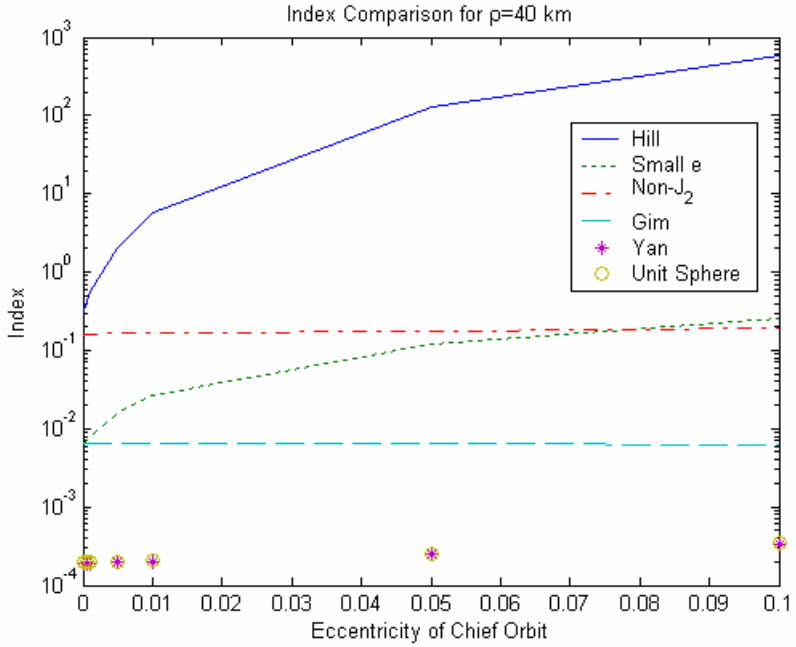

Fig. 4.15 Index Comparison for $\rho = 40$ km

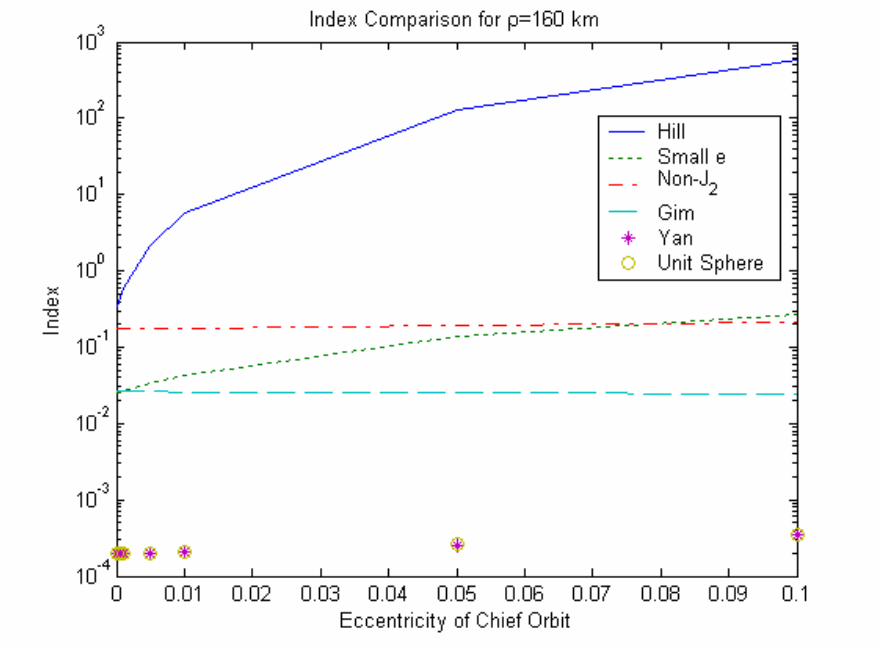

Fig. 4.16 Index Comparison for $\rho = 160$ km

Figs. 4.9-4.16 show the modeling error index at the end of one day for the six theories; Hill's equation, small eccentricity, non-J_2, Gim-Alfriend, unit sphere approach and Yan-Alfriend nonlinear method. Figs. 4.9-4.12 show the effect of the index as a function of the size of the orbit for various eccentricities. Figs. 4.13-4.16 show the effect of the index as a function of eccentricity for various size orbits. The index provides a method for comparing the accuracy of various theories. As shown earlier in the one-dimensional case the index is representative of twice the percentage error. In the n-dimensional case the acceptable value for an index can only be determined by what size errors are acceptable for the mission. Also, keep in mind that the index represents the maximum error over all the initial conditions for the PCO. There are initial conditions for which the modeling errors are minimal. For example, because the differential J_2 effects are caused primarily by the inclination difference the effect of not modeling J_2 is very small if the out of plane motion is created by only a right ascension difference. For a specific set of initial conditions the user would have to compute the index for just those initial conditions.

In Figures 4.9-4.12 the index for Hill's equation and the non-J_2 theory are almost constant. The non-J_2 index is also constant with PCO size as shown in Figs. 4.13-4.16. Since the non-J_2 theory has no eccentricity approximation its index shows the effect of not modeling J_2 for small relative motion orbits. Since it is constant this means the J_2 effects are much larger than the nonlinear effects even for orbits as large as 160 km. The difference between the non-J_2 theory and the Gim-Alfriend index represents the effect of

not modeling J_2; it is significant. Even for $e = 0.001$, there is a factor of four difference between the two indices.

The difference between the Hill index and the non-J_2 index represents the effect of not modeling the eccentricity. Even for $e = 0.001$, it is substantial. Fig. 4.13 shows how it grows with increasing eccentricity.

In Fig. 4.13 the Small e index and non-J_2 index are equal at about e=0.08. This is the point where neglecting 2nd order eccentricity effects is about equal to neglecting the J_2 effects.

For both the Vadali unit sphere and Yan-Alfriend methods, the index is essentially constant for all cases and approximately equal to 10^{-3}. This means they provide an accurate representation of the motion for all eccentricities and relative motion orbits as large as 160 km. As expected the index for the Gim-Alfriend theory is constant with eccentricity since it has no eccentricity approximation. Its sensitivity to the orbit size is evident, but even for PCOs as large as 40 km it is still less than 0.01.

In comparing the Small e and the Gim-Alfriend indices one can see the difference even for e=0.001, even though the index is small. Fig. 4.12 shows that the difference is two orders of magnitude at e=0.01 meaning the Small e theory may not provide sufficient accuracy for e=0.01

4.4.6 Remarks

The modeling error index presented in this paper is an effective tool for evaluating the accuracy of approximate methods of relative motions and should aid designers in

determining what effects need to be included in the reference orbit model. The sequence of the index from high to low is Hill's equation, non-J_2, small eccentricity, Gim-Alfriend index. The unit sphere method and the Yan-Alfriend nonlinear method indices are the lowest, and essentially equal. The numerical results show that a) In general, neglecting J_2 effects is significant even though there are initial conditions for which the effect will be minimal, b) Neglecting eccentricity effects, even for e<0.001 can be significant, c) The Small e theory, which includes the first order eccentricity effects for the non-J_2 terms and 0th order eccentricity for the J_2 terms, provides reasonable results for $e < 0.01$, and d) The unit sphere approach and Yan-Alfriend nonlinear theory are accurate for all eccentricities and relative motion orbits as large as 160 km in low Earth orbit. These results should be valid for any relative motion orbit with out-of-plane motion, such as the circular relative motion orbit. Since the differential J_2 effects are primarily caused by a differential inclination different results would occur for in-plane relative motion orbits.

4.5 Numerical Searches and Real-Time Optimal Control of J_2 Invariant Orbits

4.5.1 Introduction

The J_2 invariant type orbits are relative orbits defined in mean elements that minimize the amount of fuel to maintain[89]. These invariant orbits identify initial conditions that minimize the drift from the desired relative motion orbit, and consequently, reduce the amount of fuel required to maintain the orbit. Using the local

vertical local horizontal LVLH frame there is potentially drift in the in-track, radial and cross-track, or out-of-plane directions. We define drift as secular motion from the desired orbit. This secular motion is actually periodic with a long period, but will appear as secular over a few orbits or days, and this periodic motion will have an amplitude that is much larger than any tolerance on the desired motion. For example, the radial drift is obviously bounded by the maximum distance between the apogees and perigees of the two orbits and its period will be $T = 2\pi / |n_1 - n_2|$. We work in mean elements because in mean elements the Hamiltonian is a function of only the momenta, hence the momenta are constant and the coordinates (angles) are linear with time. This means the differential angular rates or differential momenta define the drift, the initial values of the angles have no effect on the drift.

Numerical optimization methods, such as the pseudospectral methods[11], should provide a more accurate value of the initial conditions to minimize drift, but the disadvantage is they do not provide the functional relationships, only a numerical result. For example, a small differential semi-major axis will negate the in-track drift caused by an inclination difference. If the numerical optimization was performed in the relative Cartesian coordinates then the fact that the initial Cartesian conditions were equivalent to a semi-major axis error would likely not be evident for two reasons: a) in osculating elements the relationship between differential orbital elements and the differential mean semi-major axis is very complex, and b) one would have to make many runs with the correct parameter variations to even potentially find the numerical relationships. Consequently, a secondary objective is to show that the advantage of the numerical

optimization methods is significantly enhanced when combined with the knowledge of the physics of the problem.

Since the J_2 invariant orbit is unable to exactly cancel relative secular drifts, some active control is needed to maintain the invariant orbit. The formation flying maintenance methods can be classified as nonlinear and linear. An excellent survey can be found in Ref. 109. The nonlinear maintenance methods include the Lyapunov method[110,111], feedback linearization[112,113], and state-dependent Riccati equation[114]. Linear quadratic regulators (LQR) have been widely proposed for satellite formation keeping[111,115-116]. The controller is designed to minimize the fuel consumption and reject state errors. In this section we propose an analytical optimal control based on the state transition matrix. We use pseudospectral methods or the Legendre-Gauss-Lobatto (LGL) integration rule to approximate integrals in the state equation and performance index, which transforms the optimal control problem into a parameter optimization which has an analytical solution.

4.5.2 Numerical Searches for Passive J_2 Invariant Orbits

Notice the solutions of Eqs. (4.8-9) and Eq. (4.10) are from the periodic matching conditions and do not provide solutions of the other differential orbit elements. The other elements define the relative motion orbit. In this section, we numerically search all the initial conditions that result in J_2 invariant orbits without using the matching conditions.

For this analysis we will assume that the desired relative motion orbit (RMO) is the projected circular orbit given by

$$\left(y^2+z^2\right)=\rho^2 \tag{4.131}$$

Due to the gravitational perturbations and the orbit eccentricity the RMO will not be a circle so our constraint should be

$$\rho\left(1-\varepsilon_1\right)<\left(y^2+z^2\right)^{1/2}<\rho\left(1+\varepsilon_2\right) \tag{4.132}$$

where $\rho\varepsilon_1$ and $\rho\varepsilon_2$ are the lower and upper limits, respectively. We want to find the initial conditions that minimize the fuel consumption (L1 norm) required to maintain this RMO.

Our searches try to find the minimum $\varepsilon_1+\varepsilon_2$ that satisfy Eq. (4.132) in a given number of orbits. The goal is to determine the accuracy of the invariant orbits in the given number of orbits. We want to compare the initial conditions from the numerical searches to the periodic matching conditions.

We selected the projected circular relative motion orbit (PCO) for reconfiguration. Use Eqs. (4.60-65) to set up a PCO. But we use Eq. (4.132) instead of Eq. (4.65) as the numerical periodic search constraints and set up the following search model:

Find δa to minimize

$$J_{\min}=\left|\varepsilon_1+\varepsilon_2\right| \tag{4.133}$$

and satisfy

$$\rho\left(1-\varepsilon_1\right)<\left(y^2+z^2\right)^{1/2}<\rho\left(1+\varepsilon_2\right) \tag{4.134}$$

where (y,z) are obtained by the unit sphere STM.

We transfer the orbital elements of the Chief and Deputy into ECI coordinates, and integrate them in the ECI frame using the following nonlinear model to verify the linear solutions:

$$\dot{X} = V_X \tag{4.135}$$

$$\dot{Y} = V_Y \tag{4.136}$$

$$\dot{Z} = V_Z \tag{4.137}$$

$$\ddot{X} = -\frac{\mu X}{r^3}\left[1-1.5J_2\left(\frac{R_e}{r}\right)^2\left(5\frac{Z^2}{r^2}-1\right)\right]+u_X \tag{4.138}$$

$$\ddot{Y} = -\frac{\mu Y}{r^3}\left[1-1.5J_2\left(\frac{R_e}{r}\right)^2\left(5\frac{Z^2}{r^2}-1\right)\right]+u_Y \tag{4.139}$$

$$\ddot{Z} = -\frac{\mu Z}{r^3}\left[1-1.5J_2\left(\frac{R_e}{r}\right)^2\left(5\frac{Z^2}{r^2}-3\right)\right]+u_z \tag{4.140}$$

where μ is the gravitational constant, *X*, *Y* and *Z* are the coordinates in the ECI frame, and $r = \sqrt{X^2+Y^2+Z^2}$ For the passive J_2 invariant orbits, we assume control accelerations $u_X = u_Y = u_z = 0$. Eqs (4.141-146) are used to transfer ECI coordinates to LVLH coordinates[90]:

$$x = \frac{\delta r^T r_c}{r_c} \tag{4.141}$$

$$y = \frac{\delta r^T \left(H_c \times r_c\right)}{\left|H_c \times r_c\right|} \tag{4.142}$$

$$z = \frac{\delta r^T H_c}{H_c} \tag{4.143}$$

$$\dot{x} = \frac{\delta v^T r_c + \delta r^T v_c}{r_c} - \frac{\left(\delta r^T r_c\right)\left(r_c^T v_c\right)}{r_c^3} \tag{4.144}$$

$$\begin{aligned} \dot{y} = & \frac{\delta v^T \left(H_c \times r_c\right) + \delta r^T \left(\dot{H}_c \times r_c + H_c \times v_c\right)}{\left|H_c \times r_c\right|} \\ & - \frac{\delta r^T \left(H_c \times r_c\right)\left(H_c \times r_c\right)^T \left(\dot{H}_c \times r_c + H_c \times v_c\right)}{\left|H_c \times r_c\right|^3} \end{aligned} \tag{4.145}$$

$$\dot{z} = \frac{\delta v^T H_c + \delta r^T \dot{H}_c}{H_c} - \frac{\delta r^T H_c \left(H_c^T \dot{H}_c\right)}{H_c^3} \tag{4.146}$$

where $H = r \times v$ is the angular momentum.

4.5.3 Analytical Optimal Control Law Based on STM

In the LVLH frame, the linear model of the relative motion can be set up as

$$\dot{X} = F(t)X + G(t)U \tag{4.147}$$

where

$$U = \begin{pmatrix} u_x & u_y & u_z \end{pmatrix}^T \tag{4.148}$$

$$G(t) = \begin{pmatrix} 0 & 0 & 0 \\ 1 & 0 & 0 \\ 0 & 0 & 0 \\ 0 & 1 & 0 \\ 0 & 0 & 0 \\ 0 & 0 & 1 \end{pmatrix} \tag{4.149}$$

Using the STM the solutions are

$$X(t_f) = \Phi(t_f, t_0)X_0 + \int_{t_0}^{t_f} \Phi_U(t_f, t)U(t)dt \tag{4.150}$$

where

$$\Phi_U(t_f, t) = \Phi(t_f, t)G(t) \tag{4.151}$$

Consider the following optimal control problem. Determine the control function to minimize

$$J = \frac{1}{2}\int_{t_0}^{t_f} U^T U dt \tag{4.152}$$

subject to the final constraints

$$X(t_f) = X_f \tag{4.153}$$

The integral terms can be calculated by the Legendre-Gauss-Lobatto (LGL) integration rule[11]. Assume the number of the LGL points is *N*+1. Eq. (4.150) and Eq. (4.152) become

$$X(t_f) = \Phi(t_f, t_0)X_0 + \frac{t_f - t_0}{2}\sum_{k=0}^{N} \Phi_U(t_f, t_k)U_k w_k \tag{4.154}$$

$$J = \frac{t_f - t_0}{2}\sum_{k=0}^{N} \frac{1}{2} U_k^T U_k w_k \tag{4.155}$$

where w_k are the weights given by

$$w_k = \frac{2}{N(N+1)}\frac{1}{[L_N(t_k)]^2} \qquad k = 0,1,...N \tag{4.156}$$

$L_N(t)$ is the Legendre polynomial of degree *N* on the interval [-1,1]. Notice the continuous controls are equivalent to *N*+1 impulses applied at the LGL time points in Eq. (4.154). Substituting Eq. (4.154) into Eq. (4.153) gives

$$\Phi(t_f,t_0)X_0+\frac{t_f-t_0}{2}\sum_{k=0}^{N}\Phi_U(t_f,t_k)U_k w_k-X_f=0 \tag{4.157}$$

Now the optimal control is changed into a parameter optimization problem. Find the $U_k \quad k=0,1,...N$ that minimize the performance index in Eq. (4.155) and satisfy the equality constraints, Eq. (4.157). Adjoin the constraints Eq. (4.157) to Eq. (4.155) by Lagrange multipliers ξ

$$\bar{J}=\frac{t_f-t_0}{2}\sum_{k=0}^{N}\frac{1}{2}U_k^T U_K w_k+\xi^T\left(\Phi(t_f,t_0)X_0+\frac{t_f-t_0}{2}\sum_{k=0}^{N}\Phi_U(t_f,t_k)U_k w_k-X_f\right) \tag{4.158}$$

Taking the partial derivatives of Eq. (4.158) with respect to $U_k \quad k=0,1,...N$, and setting equal to zero gives for optimality

$$U_K=-\Phi_U^T(t_f,t_k)\xi \tag{4.159}$$

Substituting Eq. (4.159) into Eq. (4.157), we obtain

$$\xi=\frac{2}{t_f-t_0}\left\{\sum_{k=0}^{N}\left[\Phi_U(t_f,t_k)\Phi_U^T(t_f,t_k)w_k\right]\right\}^{-1}\left[\Phi(t_f,t_0)X_0-X_f\right] \tag{4.160}$$

Substituting into Eq. (4.159) gives

$$U_K=-\frac{2}{t_f-t_0}\Phi_U^T(t_f,t_k)\left\{\sum_{k=0}^{N}\left[\Phi_U(t_f,t_k)\Phi_U^T(t_f,t_k)w_k\right]\right\}^{-1}\left[\Phi(t_f,t_0)X_0-X_f\right] \tag{4.161}$$

$$k=0,1,...N$$

or

$$U_K=-K(N)\left[\Phi(t_f,t_0)X_0-X_f\right] \tag{4.162}$$

where the gain is

$$K(N) = -\frac{2}{t_f - t_0}\Phi_U^T(t_f, t_k)\left\{\sum_{k=0}^{N}\left[\Phi_U(t_f, t_k)\Phi_U^T(t_f, t_k)w_k\right]\right\}^{-1} \tag{4.163}$$

The values of the control law between the LGL points can be obtained by interpolation. It should be stressed that the gain expression in Eq. (4.163) only depends on the number of the LGL points *N+1*. As the current states are available, the control law in Eq. (4.162) can be solved analytically. The procedure to derive the control law is similar to the one in the Ref. 34, but here we use the state transition matrix method while the Taylor series expansion was used in Ref. 34. The Gauss quadrature formula is with the maximum degree of precision, compared with the standard trapezoidal formula in Ref. 34. Here we focus on targeting problems while Ref. 34 addressed tracking problems.

4.5.4 Optimal Impulsive Control

Assuming the number of impulsive controls is *n*, we have

$$X(t_f) = \Phi(t_f, t_0)X_0 + \sum_{i=1}^{n}\Phi_U(t_f, t_i)\Delta V_i \tag{4.164}$$

We want to minimize

$$J_1 = \frac{1}{2}\sum_{i=1}^{n}\Delta V_i^T R_i \Delta V_i \tag{4.165}$$

subject to

$$X(t_f) = X_f \tag{4.166}$$

The optimal solutions can be solved by the previous approach, giving

$$\Delta V_i = -\Phi_U^T(t_f, t_i)\left\{\sum_{i=1}^{n}\left[\Phi_U(t_f, t_i)\Phi_U^T(t_f, t_i)/R_i\right]\right\}^{-1}\left[\Phi(t_f, t_0)X_0 - X_f\right]\frac{1}{R_i}, \quad i = 1,...n \tag{4.167}$$

where R_i are the weights.

If the maneuver times are fixed there are six unknowns. Consequently, there is at most one solution for two impulsive controls. Depending on the maneuver times there may be no solution. Consequently, the number of impulsive controls should be greater than two for an optimal solution. For two impulsive controls, we are able to directly get solutions from Eq. (4.164)

$$\begin{pmatrix} \Delta V_1 \\ \Delta V_2 \end{pmatrix} = -\left[\Phi_U(t_2,t_1) \quad \Phi_U(t_2,t_2)\right]^{-1}\left(\Phi(t_2,t_0)X_0 - X_f\right) \tag{4.168}$$

where t_1 and t_2 are the times of applying the first and second impulsive controls, respectively.

4.5.5 Numerical Results

4.5.5.1 Numerical Searches for J_2 Invariant Orbit

The orbital elements of the Chief are

$$a = 7100 \text{ (km)} \quad e = 0.005 \quad i = 70 \text{ (deg)} \quad \omega = \Omega = 0 \quad M = 0.$$

The relative orbit is characterized by two quantities: its radius ρ and initial phase angle α_0. We choose $\rho = 1, 2, 5, 10, 20\,(km)$ and take every 30 degree separation in the 0~360 degree range for the initial phase angle. For each combination of the radius and initial phase angle, we compute an optimal J_2 invariant orbit. The number of the relative orbits is set as 10. Fig. 4.17 illustrates the relationship among the radius, initial phase angle and minimum $\varepsilon = |\varepsilon_1 + \varepsilon_2|$. Fig. 4.17 indicates the accuracy is the best when the

initial phase angles are 90 or 270 degrees and the accuracy is about 2.5%. The peak is at α=0. This is expected because at α=0 the out-of-plane motion is created by an inclination change, which causes both in-track and out-of-plane drift, in contrast to α=90, 270 which results in a right ascension difference that causes no drift.

Fig.4.18 shows comparisons between δa from the numerical searches and δa from the periodic matching conditions. From this figure, one can see numerical searches identify the J_2 invariant orbit.

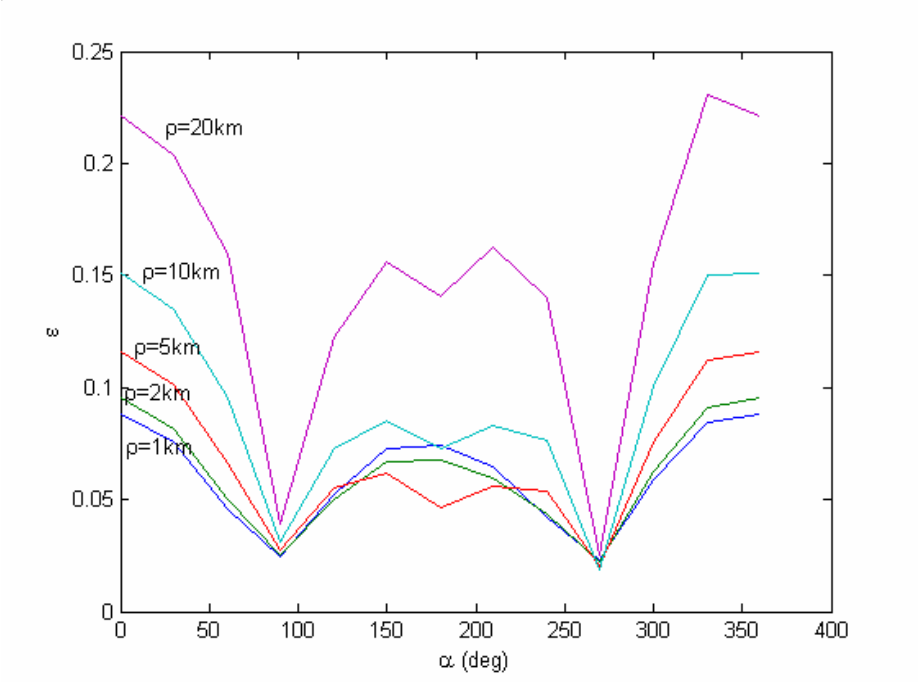

Fig. 4.17 Radius, Initial Phase Angle and Optimal Accuracy

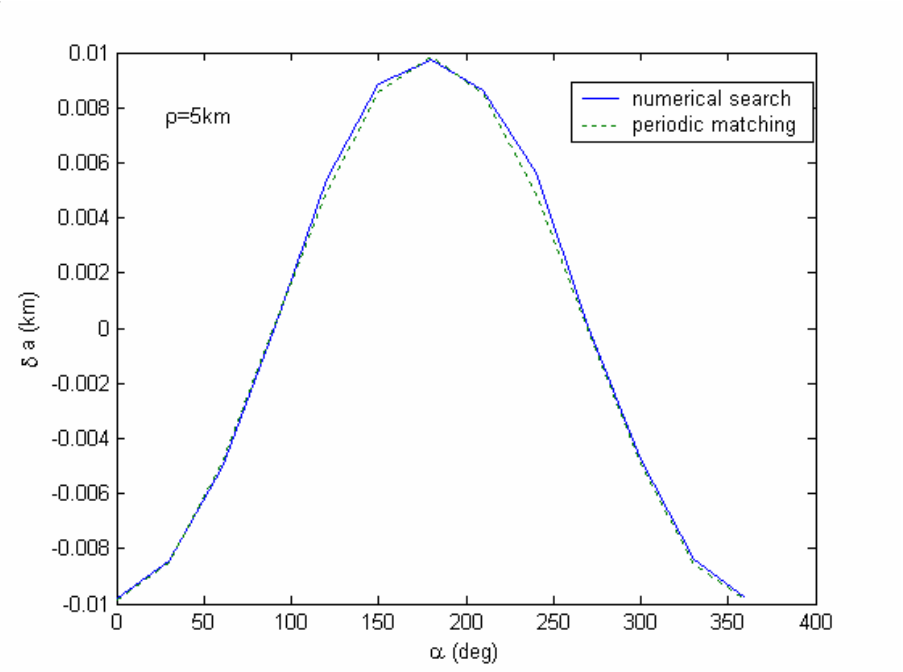

Fig. 4.18 Comparisons

To verify the linear solutions we transfer the orbital elements of Chief and Deputy into ECI coordinates, and integrate them in the ECI frame using the nonlinear model with J_2 perturbations. Select ρ=5 km and α_0=0 degree. The results are shown in Fig. 4.19.

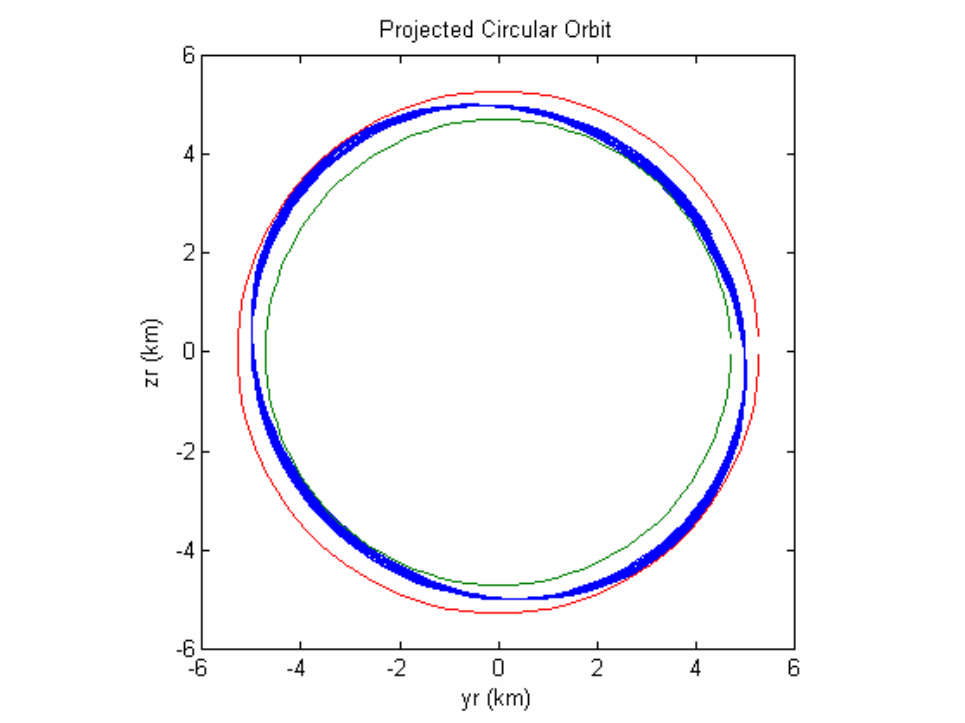

Fig.4.19 Numerical Searches for J_2 Invariant Orbit Keeping

4.5.5.2 J_2 Invariant Orbit Keeping

Fig. 4.19 shows that there is still some drift after the numerical searches. Here we apply optimal control to reset the periodic matching conditions. To do so we force

$$X_f = X_0 \tag{4.169}$$

We use the unit sphere STM to propagate the states,

$$\Phi(t,t_0) = \sum(t) D(t) \bar{\phi}_e(t,t_0) D^{-1}(t_0) \sum(t_0)^{-1} \tag{4.170}$$

Set ρ=5 km and α_0=0 degrees then $\delta a, \delta\lambda, \delta i, \delta q_1, \delta q_2, \delta\Omega$ are obtained from Eqs. (4.60-65). The initial conditions, which satisfy the periodic matching conditions, are solved by

$$\boldsymbol{X}(t) = \sum(t)\delta\boldsymbol{e}(t) \tag{4.171}$$

Choose the LGL points to be 64. The simulation time is 10 orbits. The results are illustrated in Figs. (4.20-4.21). Comparing Fig. 4.20 with Fig. 4.19, the drift in Fig. 4.19 is perfectly rejected. Fig. 4.21 shows the optimal control time histories. The computing time is about 1 second using MATLAB software on a 2.8 GHz PENTIUM 4 computer. The cost is about 1.83e-7 m^2/s^3 according to Eq. (4.152). The control is primarily correcting for two effects; the out-of-plane drift caused by the inclination difference and the rotation of perigee. The rotation of perigee causes there to be a difference in the in-plane and out-of-plane frequencies causing the relative motion orbit to slowly transition from a PCO to a straight line in the *yz* plane and back to a PCO. This is not the differential perigee rotation, but the absolute rotation of the Chief perigee.

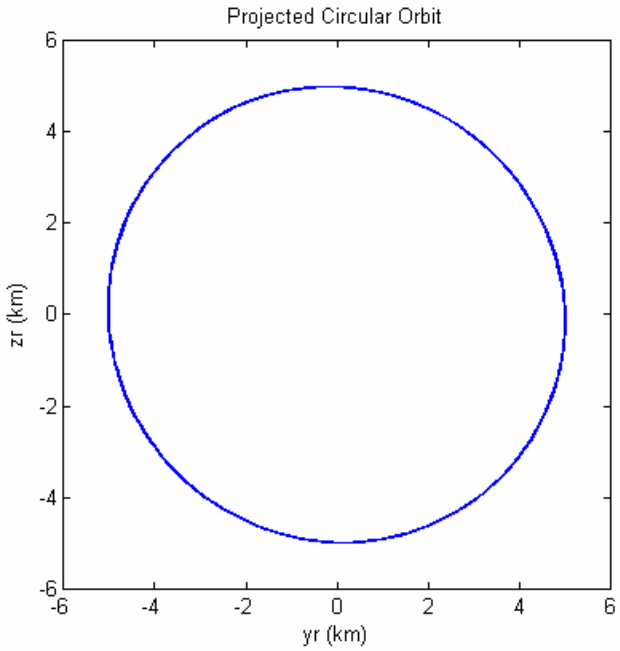

Fig. 4.20 J_2 Invariant Orbit Keeping

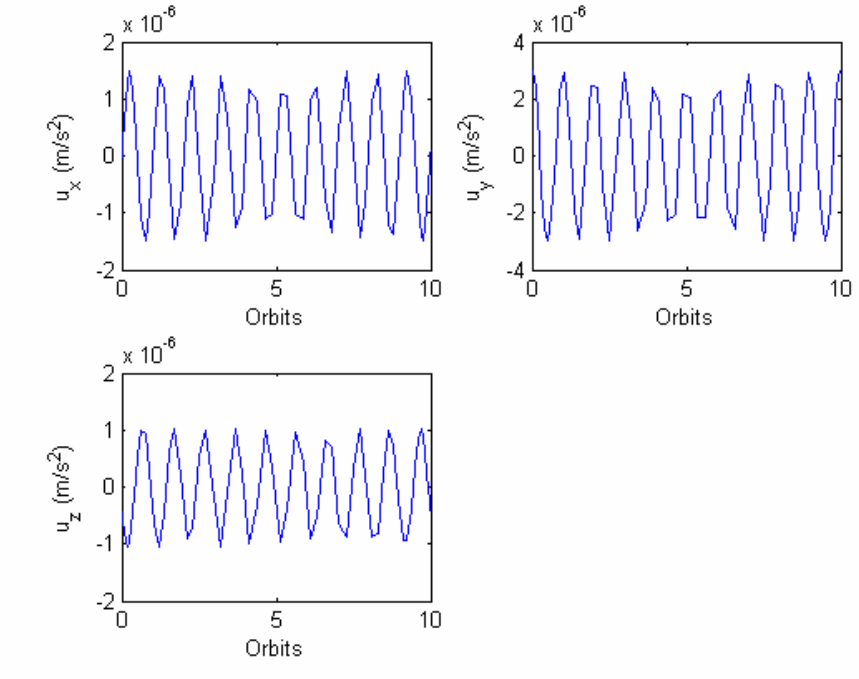

Fig. 4.21 Continuous Control for Keeping

4.5.5.3 J_2 Invariant Orbit Reconfiguration

4.5.5.3.1 Continuous Control

Since the relative orbit is characterized by two quantities ρ and α_0, here we calculate the optimal reconfiguration from $\alpha_0 = 90^\circ$ and $\rho_0 = 2$ km to $\alpha_f = 90^\circ$ and $\rho_f = 20$ km. Figs. 4.22-4.23 illustrate the reconfiguration and continuous control time histories. The transfer time is given as 5 orbits. In Fig. 4.22 the dot lines represent transfer trajectories while the solid lines stand for the initial and final orbits. The reconfiguration is completed through a spiral transfer trajectory. The cost is about $0.0127 m^2/s^3$.

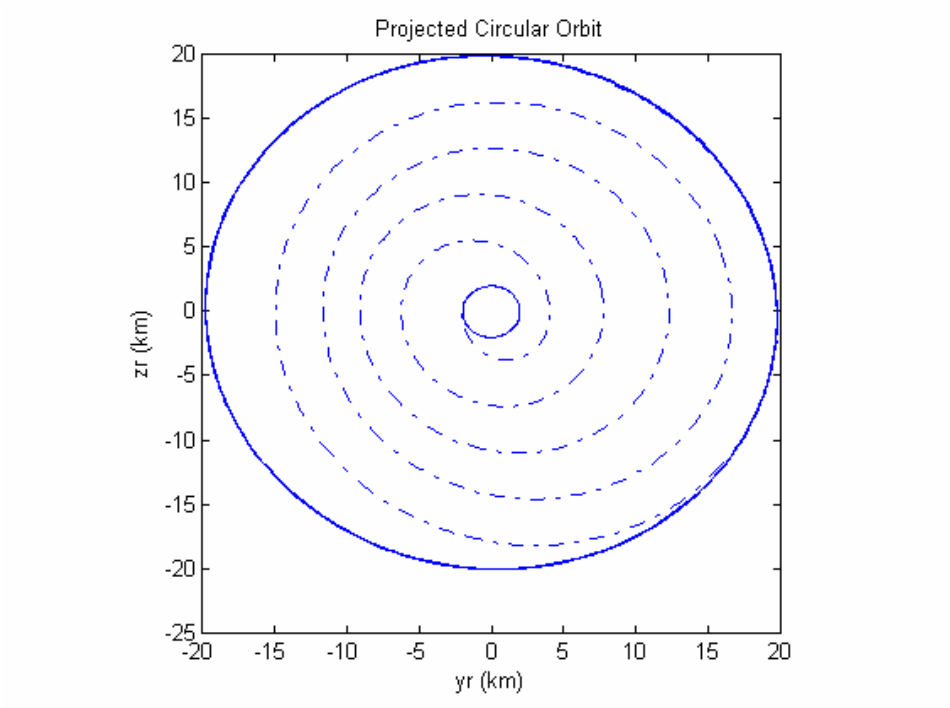

Fig. 4.22 Reconfiguration Using Continuous Control

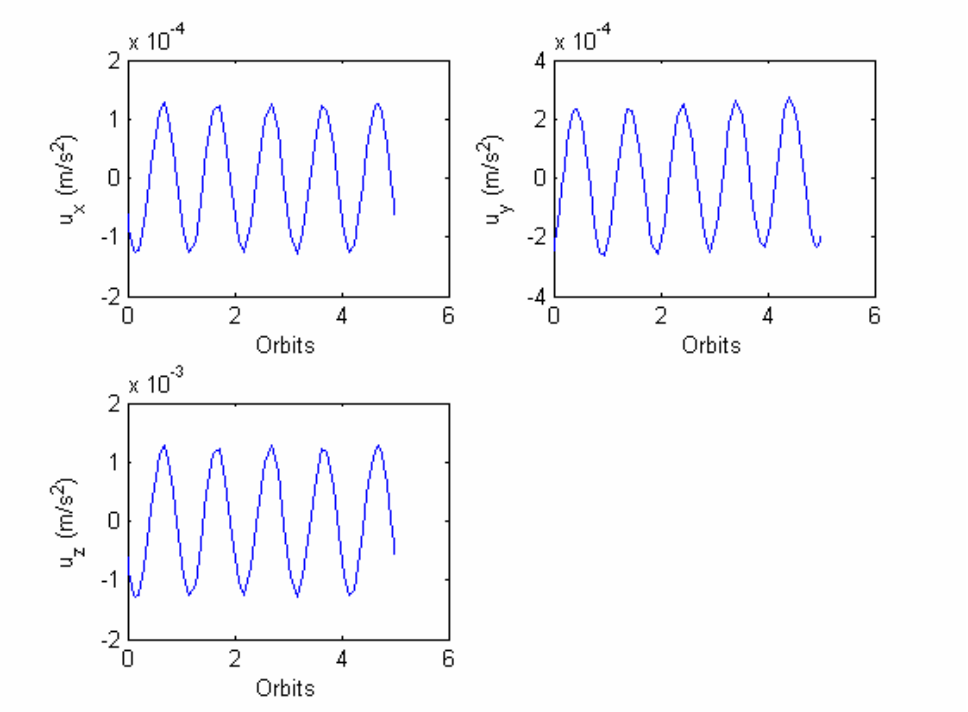

Fig. 4.23 Optimal Control Time Histories for Reconfiguration

4.5.5.3.2 Two Impulsive Controls

Use parameter optimization methods to choose t_1 and t_2 to minimize the cost

$$J_V = \sqrt{\Delta V_1^T \Delta V_1} + \sqrt{\Delta V_2^T \Delta V_2} \tag{4.172}$$

where ΔV_1 and ΔV_2 are obtained from Eq. (4.168). We calculate the same reconfiguration as that in the continuous control case. The optimal impulsive controls are

$$\Delta V_1 = \begin{pmatrix} -7.66 & 0.90 & -19.03 \end{pmatrix}^T \text{ m/s} \tag{4.173}$$

$$\Delta V_2 = \begin{pmatrix} 1.59 & -0.86 & -0.56 \end{pmatrix}^T \text{ m/s} \tag{4.174}$$

The maneuver times are 1454.86 seconds or 0.24 orbits and 5901.58 seconds 0.99 orbits. The cost is 22.43 m/s. The reconfiguration is shown in Fig. 4.24 where the dot lines stand for the transfer orbit.

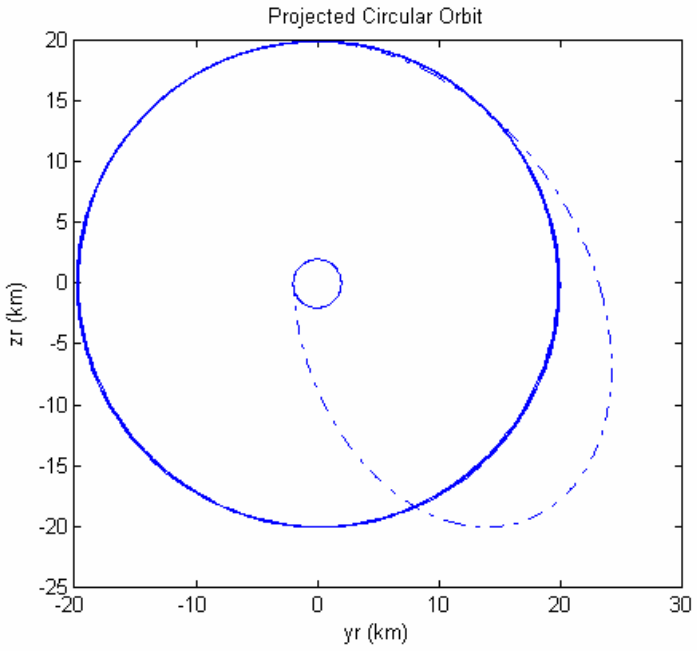

Fig. 4.24 Reconfiguration Using Two Impulsive Controls

4.5.5.4 Numerical Searches for Initial Conditions

The initial conditions X_0 in Eq. (4.169) are determined by $\delta a, \delta\lambda, \delta i, \delta q_1, \delta q_2, \delta\Omega$ where δa is calculated from the periodic matching conditions Eq. (4.65). Now we set δa as a variable and want to search this variable with the optimal model that consists of Eq. (4.154), Eq. (4.155) and Eq. (4.169). Since the optimal control has an analytical solution, the search is just a one dimensional optimization problem. We choose $\rho = 5km$ and take every 30 degree separation in the 0~360 degree range for the initial phase angle. For each combination of the radius and initial phase angle, we perform a one dimensional optimization to determine the optimal δa. All the initial guesses of δa are zero. The solutions are shown in Fig. 4.25 where the solid lines represent the search solutions while the dot lines stand for the analytical periodic conditions. The agreement shown in Fig. 4.25 is not as good as that in Fig. 4.18, since the constraint Eq. (4.132) is much better than the hard constraint Eq. (4.169) to capture the characteristics of the periodic matching condition Eq. (4.132). Fig. 4.25 indicates the "soft" periodic matching conditions Eq. (4.132) are close to the "hard" periodic matching constraints Eq. (4.169).

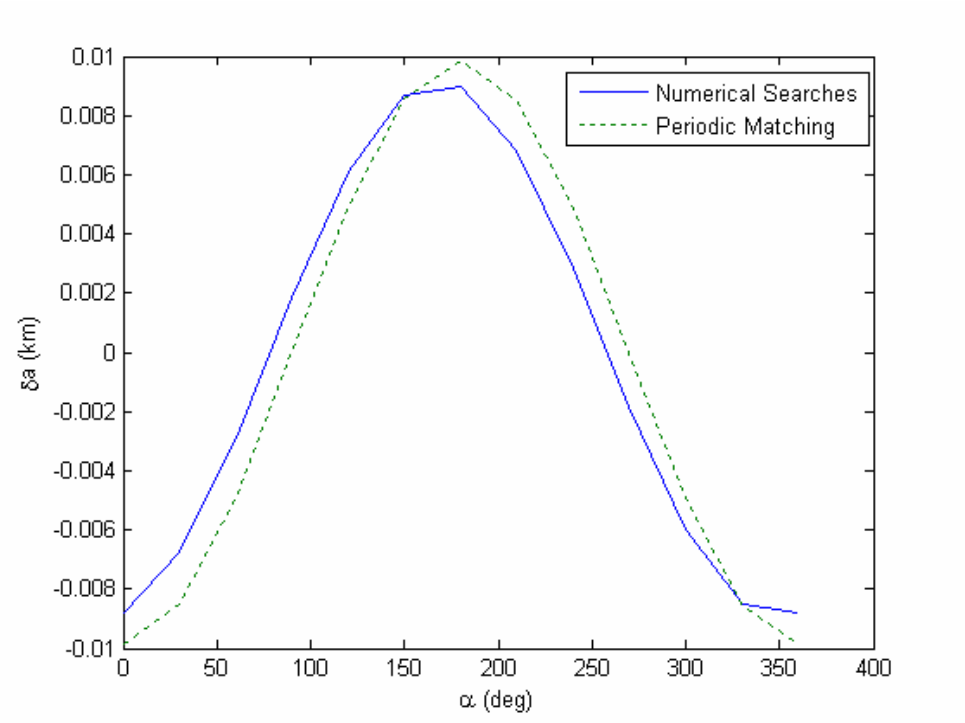

Fig. 4.25 Searches for Periodic Matching Conditions

4.5.5 Remarks

In this section we investigate numerical searches and optimal control of J_2 invariant orbits. For passive J_2 invariant orbits we use linear and nonlinear searches to find the optimal differential elements that minimize the secular drifts. This result agrees with the solution from the periodic matching conditions. We propose an analytical optimal control law based on the state transition matrix for maintenance and reconfiguration of J_2 invariant orbits. Numerical solutions show the control law works well. Based on the control law the initial conditions were searched for hybrid optimality, and the results show the fuel optimal control corresponds to J_2 invariant orbits.

CHAPTER V

CONCLUSIONS

The solutions of the dynamics and real-time optimal control of magnetic attitude control and formation flying system are studied in this dissertation. The dissertation investigates pseudospectral methods for the real-time numerical solution of optimal control problems. Analytical control laws for linear time-varying systems are derived for tracking and targeting problems.

The time optimal attitude rest-to-rest attitude maneuver for a satellite in low Earth orbit with magnetic control is solved. The feasibility of the solutions is verified by numerical integration while the necessary conditions resulting from the Minimum Principle are checked for optimality. The time-optimal magnetic control is bang-bang and the optimal maneuver is not an eigenaxis slew. The minimum slew time is about 232.7 seconds, and it occurs when the maneuver is symmetric about the maximum field strength. For real-time computations, all the tested samples converge to optimal solutions or feasible solutions. We find the average computation time is about 0.45 seconds with the warm start and 19 seconds with the bad initial guess, which means there is great potential for real-time computations. The optimal solutions from the warm start are better than those from the cold start with a bad initial guess. The results show that pseudospectral methods are an excellent method for solving optimal control problems in near real-time.

Three-axis magnetic attitude stabilization is achieved by using a pseudospectral control law via the receding horizon control for satellites in eccentric low Earth orbits. The solutions from the pseudospectral control law are in excellent agreement with those obtained from the Riccati equation, but their computation speed is better by an order of magnitude. The control law indicates the solutions consist of natural and forced responses. The known disturbance is greatly rejected by using a feed forward control. Numerical solutions show natural responses quickly tend to the region where the attitude motion is in the steady state. When the eccentricity is 0.1 the residual librations errors are within 1 degree of nadir pointing. For the problem solved with an eccentricity of 0.1 an interesting result occurs. Less fuel is required for stabilization when the satellite is in an unstable configuration, i.e., when the maximum inertia is along the yaw or roll axis, than when it is in the stable configuration with the maximum inertia along the pitch axis. This occurs because the gravity gradient disturbance torque, which is proportional to eccentricity, is more detrimental in the dynamic stable configuration that the unstable configuration

The dissertation studies formation flying dynamics and real-time optimal control problems. A procedure for designing relative motion orbits using orbital element differences has been presented. A 2nd order theory including the J_2^2 term for the relative motion of two satellites has been derived using orbital elements. This theory is valid for any eccentricity and contains 1st and 2nd order J_2 effects. It has been shown that for consistency a nonlinear theory for relative motion must also consider eccentricity and

gravitational perturbations. Other higher order geopotential terms could easily be included. A relative motion theory using orbital elements is more accurate than one using the relative Cartesian or curvilinear coordinates. The period matching or bounded condition in the orbital elements has been proposed for the nonlinear problem and compared with the conditions in the Cartesian frame. The results show the orbital elements approach has a strong effect on suppressing the secular growth.

The dissertation develops an alternative state transition matrix (STM) to describe relative motion using the unit sphere approach with the same accuracy as the Gim-Alfriend STM. The major errors from the first order STM can be rejected by the second order correction for relative motion.

The modeling error index presented in this dissertation is an effective tool for evaluating the accuracy of approximate methods of relative motions. The sequence of the index from high to low is Hill's equation, non-J_2, small eccentricity, Gim-Alfriend index. The unit sphere method and the Yan-Alfriend nonlinear method indices are the lowest, and essentially equal. The numerical results show that a) In general, neglecting J_2 effects is significant even though there are initial conditions for which the effect will be minimal, b) Neglecting eccentricity effects, even for e<0.001 can be significant, c) The Small e theory, which includes the first order eccentricity effects for the non-J_2 terms and 0th order eccentricity for the J_2 terms, provides reasonable results for $e < 0.01$, and d) The unit sphere approach and Yan-Alfriend nonlinear theory are accurate for all eccentricities and relative motion orbits as large as 160 km in low Earth orbit. The results presented in this paper should be valid for any relative motion orbit

with out-of-plane motion, such as the circular relative motion orbit. Since the differential J_2 effects are primarily caused by a differential inclination different results would occur for in-plane relative motion orbits.

Numerical searches and optimal control of J_2 invariant orbits are studied in the dissertation. For passive J_2 invariant orbits linear and nonlinear searches are used to find the optimal differential elements that minimize the secular drifts. This result agrees with the solution from the periodic matching conditions. The dissertation proposes an analytical optimal control law based on the state transition matrix for maintenance and reconfiguration of J_2 invariant orbits. Numerical solutions show the control law works well. Based on the control law the initial conditions were searched for hybrid optimality, and the results show the fuel optimal control corresponds to J_2 invariant orbits.

REFERENCES

1. Betts, J. T., "Survey of Numerical Methods for Trajectory Optimization," *Journal of Guidance, Control, and Dynamics*, Vol. 21, No.2, 1998, pp. 193-207.

2. Hull, D. G., "Conversion of Optimal Control Problems into Parameter Optimization Problems," *Journal of Guidance, Control, and Dynamics*, Vol. 20, No.1, 1997, pp. 57-60.

3. Yan, H., Fahroo,F., and Ross, I. M., "Accuracy and Optimality of Direct Transcription Methods," *Advances in the Astronautical Sciences*, Vol. 105, 2000, pp. 1613-1630.

4. Williams, P., "A Comparison of Differentiation and Integration Based Direct Transcription Methods," AAS 05-128, *15th AAS/AIAA Space Flight Mechanics Conference*, Copper Mountain, CO, Jan. 23-27, 2005.

5. Conway, B.A., and Larson, K.M., "Collocation Versus Differential Inclusion in Direct Optimization," *Journal of Guidance, Control, and Dynamics*, Vol. 21, No.5, 1998, pp. 780-785.

6. Herman, A.L., and Conway, B.A., "Direct Optimization Using Collocation Based on High Order Gauss-Lobatto Quadrature Rules," *Journal of Guidance, Control, and Dynamics*, Vol. 19, No.3, 1996, pp. 592-599.

7. Elnagar, J., Kazemi, M. A. and Razzaghi, M., " The Pseudospectral Legendre Method for Discretizing Optimal Control Problem," *IEEE Transactions on Automatic Control*, Vol. 40, No. 10, 1995, pp. 1793-1796.

8. Elnagar, J. and Razzaghi, M., "A Collocation-Type Method for Linear Quadratic Optimal Control Problems," *Optimal Control Applications and Methods*, Vol. 18, 1997, pp. 1267-1272.

9. Fahroo, F. and Ross, I.M., "Costate Estimation by a Legendre Pseudospectral Method," *Journal of Guidance, Control, and Dynamics*, Vol.24, No. 2, 2001, pp. 270-277.

10. Ross, I. M., and Fahroo, F., "Pseudospectral Knotting Methods for Solving Optimal Control Problems," *Journal of Guidance, Control, and Dynamics*, Vol. 27, No.3, 2004, pp. 397-405.

11. Ross, I. M., and Fahroo, F., "Legendre Pseudospectral Approximations of Optimal Control Problems," *Lecture Notes in Control and Information Science 295*, edited by Kang, W., Borges, C., and Xiao, M., Springer-Verlag, New York, 2003, pp. 327-342.

12. Ross, I. M., and Fahroo, F., "Pseudospectral Methods for Optimal Motion Planning of Differentially Flat Systems," *IEEE Transactions on Automatic Control*, Vol. 49, No. 8, August 2004, pp. 1410-1413.

13. Ross, I. M., and Fahroo, F., "A Unified Framework for Real-Time Optimal Control," *Proceedings of the IEEE Conference on Decision and Control*, Maui, HI, Dec., 2003.

14. Gong, Q., Ross, I. M., Kang, K., and Fahroo, F., "Dual Convergence of the Legendre Pseudospectral Method for Solving Nonlinear Constrained Optimal Control Problems," *Proceedings of the IASTED International Conference on Intelligent Systems and Control*, Cambridge, MA, Oct. 31-Nov. 2, 2005.

15. Ross, I. M., and Fahroo, F., "User's Manual for DIDO 2002: A MATLAB Application Package for Dynamic Optimization," NPS Technical Report AA-02-002, Department of Aeronautics and Astronautics, Naval Postgraduate School, Monterey, CA, June 2002.

16. Ross, I. M., Gong, Q., and Sekhavat, P., "A Simple Technique for Low-Thrust High-Accuracy Trajectory Optimization," AAS 06-150, *16th AAS/AIAA Space Flight Mechanics Conference*, Tampa, FL, Jan. 22-26, 2006.

17. Gong, Q., and Ross, I. M., "Autonomous Pseudospectral Knotting Methods for Space Mission Optimization," AAS 06-151, *16th AAS/AIAA Space Flight Mechanics Conference*, Tampa, FL, Jan. 22-26, 2006.

18. Mayne, D. Q., Rawlings, J. B., Rao, C. V., and Scokaert, P. O. M., "Constrained Model Predictive Control: Stability and Optimality," *Automatica*, Vol. 36, 2000, pp.789-814.

19. Milam, M. B., "Real-Time Optimal Trajectory Generation for Constrained Dynamical Systems," *Ph.D. Dissertation*, California Institute of Technology, May 2003.

20. Junkins, J. L., and Carrington, C. K., "Time-Optimal Magnetic Attitude Maneuvers," *Journal of Guidance, Control and Dynamics*, Vol. 4, No. 4, pp.363-368, 1981.

21. Junkins, J. L., and Turner, J. D., Optimal Spacecraft Rotational Maneuvers, *Elsevier*, Vol. 3, 1986, pp. 250-267.

22. Qin, S., J., and Badgwell, T. A., "An Overview of Industrial Model Predictive Control Technology," *Fifth International Conference on Chemical Control Process Control*, New York, CACHE, AICHE, May 1997, pp. 232-256.

23. Yan, H., Fahroo, F., and Ross, I. M., "Real –Time Computation of Neighboring Optimal Controls," *Proceedings of the AIAA Guidance, Navigation and Control Conference*, Monterey, CA, August 2002, AIAA 2002-4657.

24. Strizzi, J., Ross, I. M., and Fahroo, F., "Towards Real-Time Computation of Optimal Controls for Nonlinear Systems," *Proceedings of the AIAA Guidance, Navigation and Control Conference*, Monterey, CA, August 2002, AIAA 2002-4945.

25. Yan, H., Fleming, A., Ross, I. M., and Alfriend, K. T., "Real-Time Computation of Time-Optimal Magnetic Attitude Control," AAS 05-233, *15th AAS/AIAA Space Flight Mechanics Conference*, Copper Mountain, CO, Jan., 2005.

26. Yan, H., Lee, D.-J., Ross, I. M., and Alfriend, K. T., "Real-Time Outer and Inner Loop Optimal Control Using DIDO," AAS 05-353, *2005 AAS/AIAA Astrodynamics Specialist Conference*, Lake Tahoe, CA, Aug., 2005.

27. Benson, D., "A Gauss Pseudospectral Transcription for Optimal Control," *Ph.D. Dissertation*, MIT, Cambridge, MA, Feb., 2005.

28. Williams, P., "Real-Time Computation of Optimal Trajectories for Tethered Satellite Systems," AAS 05-320, *2005 AAS/AIAA Astrodynamics Specialist Conference*, Lake Tahoe, CA, August, 2005.

29. Ross, I. M., and Fahroo, F., "Issues in the Real-Time Computation of Optimal Control," *Journal of Mathematical and Computer Modeling*, Vol. 43, 2006, pp. 1172-1188.

30. Hwang, C., and Chen, M. Y., "Analysis and Optimal Control of Time-Varying Linear Systems via Shifted Legendre Polynomials," *Int. J. Control*, Vol. 41, No. 5, 1985, pp. 1317-1330.

31. Chou, J., and Horng, I., "Application of Chebyshev Polynomials to the Optimal Control of Time-Varying Linear Systems," *Int. J. Control*, Vol. 41, No. 1, 1985, pp. 135-144.

32. Razzaghi, M., "Optimal Control of Linear Time-Varying Systems via Fouries Series," *Journal of Optimization Theory and Applications*, Vol. 65, No. 2, 1990, pp. 375-384.

33. Canuto, C., Hussaini, M. Y., Quarteroni, A., and Zang, T. A., *Spectral Methods in Fluid Dynamics*, Springer Verlag, New York, 1988.

34. Lu, P., "Close Form Control Laws for Linear Time-Varying Systems," *IEEE Transactions on Automatic Control*, Vol. 45, No. 3, 2000, pp. 537-542.

35. Williams, P., Blanksby, C., and Trivailo, P., "Receding Horizon Control of Tether System Using Quasilinearisation and Chebyshev Pseudospectral Approximations," Paper AAS 03-535, *AAS/AIAA Astrodynamics Specialists Conference*, Big Sky, MT, Aug. 3-7, 2003.

36. Williams, P., "Guidance and Control of Tethered Satellite Systems Using Pseudospectral Methods" Paper AAS 04-169, *14th AAS/AIAA Space Flight Mechanics Conference*, Maui, HI, Feb. 8-12, 2004.

37. Fahroo, F., and Ross, I. M., "Trajectory Optimization by Indirect Spectral Collocation Methods," the *Proceedings of the AIAA/AAS Astrodynamics Specialist Conference*, Denver, CO, Aug., 2000, pp. 123-129.

38. He, S., and Unbehauen, R., "Pseudospectral Technique for Continuation Methods with Application to Nonlinear Control Problems," *IEE Proceedings -Control Theory Applications*, Vol. 151, No. 5, Sept 2004, pp. 531-538.

39. Yan, H., Fahroo, F., and Ross, I.M., "Optimal Feedback Control Laws by Pseudospectral Approximations", *2001 American Control Conference*, Arlington, VA, June 2001.

40. Yan, H., Ross, I. M., and Alfriend, K. T., "Three-Axis Magnetic Attitude Control Using Pseudospectral Control Law," AAS 05-417, *2005 AAS/AIAA Astrodynamics Specialist Conference*, Lake Tahoe, CA, August, 2005.

41. Yan, H. and Alfriend, K. T., "Three-Axis Magnetic Attitude Control Using Pseudospectral Control Law in Eccentric Orbits," AAS 06-103, *AAS/AIAA Space Flight Mechanics Conference* , Tampa, FL, Jan 2006.

42. Leonard, B. S., "NPSAT1 Magnetic Attitude Control System," Paper SSC02-V-7, *16th Annual AIAA/USU Conference on Small Satellites*, Logan, UT, Aug. 2002.

43. Alfriend, K. T., Gim, D. W., and Vadali, S. R., "The Characterization of Formation Flying Satellite Relative Motion Orbits," AAS 02-143, 12th *AAS/AIAA Space Flight Mechanics Meeting*, San Antonio, TX, Jan., 2002.

44. Hargraves, C. R., and Paris, S. W., "Direct Trajectory Optimization Using Nonlinear Programming and Collocation," *Journal of Guidance, Control, and Dynamics*, Vol. 10, No.4, 1987, pp. 338-342.

45. Seywald, H., and Kumar, R., *EZopt: An Optimal Control Toolkit*, Analytical Mechanics Associate, Inc., Hampton, VA, 1997.

46. Seywald, H. and Kumar, R. R., "Method for Automatic Costate Calculation," *Journal of Guidance, Control and Dynamics*, Vol. 19, No.6, 1996, pp. 1252-1261.

47. Shen, H., and Tsiotras, P., "Time-Optimal Control of Axisymmetric Rigid Spacecraft Using Two Controls," *Journal of Guidance, Control, and Dynamics*, Vol. 22, No.5, 1999, pp. 682-694.

48. Fornberg, B., *A Practical Guide to Pseudospectral Methods*, Cambridge University Press, New York, 1998.

49. Kwon, W. H., and Pearson, A. E., "A Modified Quadratic Cost Problem and Feedback Stabilization of a Linear Systems," *IEEE Transactions on Automatic Control*, Vol. 22, pp 838-842.

50. Holmstrom, K., Goran, A. O., and Edvall, M., *User's Guide for Tomlab/SNOPT*, Tomlab Optimization Inc., San Diego, CA, 2003.

51. Crassidis, J. L., and Junkins, J. L, *Optimal Estimation of Dynamic Systems*, CRC Press Company, Boca Raton, FL, 2004.

52. Alfriend, K. T., "Magnetic Attitude Control System for Dual-Spin Satellites," *AIAA Journal*, Vol. 13, June 1975, pp.817-822.

53. Makovec, K. L., Turner, A. J., and Hall, C. D., "Design and Implementation of a Nanosatellite Attitude Determination and Control System," AAS Paper 01-311, Feb, 2001.

54. Hur, P., Melton, R. G., and Spencer, D. B., "Attitude Determination and Control of a Nanosatellite Using the Geomagnetic Field Data and Sun Sensors," AAS Paper 04-144, Feb., 2004.

55. Psiaki, M. L., "Magnetic Torquer Attitude Control via Asymptotic Periodic Linear Quadratic Regulation," *Journal of Guidance, Control and Dynamics*, Vol. 24, No. 2, 2001, pp. 386-394.

56. Bilimoria, K.D., and Wie,B., "Time-Optimal Three-Axis Reorientation of a Rigid Spacecraft ," *Journal of Guidance, Control, and Dynamics,* Vol.16, No.3, 1993, pp. 446-452.

57. Shen, H., and Tsiotras, P., "Time-Optimal Control of Axisymmetric Rigid Spacecraft Using Two Controls," *Journal of Guidance, Control, and Dynamics,* Vol. 22, No.5, 1999, pp. 682-694.

58. Liang, J., Fullmer, R., and Chen, Y., "Time-Optimal Magnetic Attitude Control for Small Spacecraft," *Proceedings of the 43rd IEEE Conference on Decision and Control*, Vol. 1, Bahamas, FL, Dec. 2004, pp. 255 – 260.

59. Fleming, A. "Real-time Optimal Slew Maneuver Design and Control." Astronautical Engineer's Thesis, US Naval Postgraduate School, Monterey, CA, 2004.

60. Wertz, J. R. (ed.), *Spacecraft Attitude Determination and Control*, D. Reidel, Boston, 1978, pp. 779-786.

61. Bryson, A. E., and Ho., Y. C., *Applied Optimal Control*, Hemisphere, New York, 1975.

62. Wisniewski, R., "Linear Time Varying Approach to Satellite Attitude Control Using Only Electromagnetic Actuation," *Proceedings of the AIAA Guidance, Navigation, and Control Conference*, Vol. 23, AIAA, Reston, VA, 1997, pp.243-251.

63. Wang, P., and Shtessel, Y. B., "Satellite Attitude Control Using Only Magnetic Torquers," *Proceedings of the AIAA Guidance, Navigation, and Control Conference*, Vol. 23, AIAA, Reston, VA, 1998, pp.1490-1498.

64. Martel, F., Pal, P. K., and Psiaki, M. L., "Active Magnetic Control System for Gravity Gradient Stabilized Spacecraft," *Proceedings of the 2nd Annual AIAA/USU Conference on Small Satellites*, Utah State Univ., Logan, UT, 1988.

65. Kulkarni, J., and Campbell, M., "An Approach to Magnetic Torque Attitude Control of Satellites via 'H_∞' Control for LTV Systems," *43rd IEEE Conference on Decision and Control*, Paradise Island, Bahamas, Dec., 2004.

66. Hughes, P. C., *Spacecraft Attitude Dynamics*, Dover Publications, Inc., New York, 2004, pp. 281-353.

67. Chobotov, V. A., *Spacecraft Attitude Dynamics and Control*, Krieger Publishing Company, Malabar, FL, 1991, pp. 91-104.

68. Baker, R. M., "Librations on a Slightly Eccentric Orbit," *ARS Journal*, Vol., 30, No. 1, Jan. 1960, pp.124-126.

69. Busch, R., and Flugge-Lotz, I., "Attitude Control of Stable and Unstable Satellites in an Elliptic Orbit," *Journal of Spacecraft and Rockets*, Vol. 6, No. 6, June 1969, pp. 685-691.

70. Boykon, W., and Flugge-Lotz, I., "Attitude Control of a Satellite in an Elliptic Orbit," *Journal of Spacecraft and Rockets*, Vol. 4, No. 4, Apr. 1967, pp. 436-442.

71. Sorensen, J., A., "A Magnetic Attitude Control System for an Axisymmetric Spinning Spacecraft," *Journal of Spacecraft and Rockets*, Vol. 8, No. 5, May 1971, pp. 441-448.

72. Schmidt, G. E., "The Application of Magnetic Attitude Control to a Momentum Biased Synchronous Communications Satellite," *AIAA Guidance and Control Conference*, Boston, MA, August 20-22 1975.

73. Sticker, A. C., and Alfriend, K. T., "Elementary Magnetic Attitude Control System," *Journal of Spacecraft and Rockets*, Vol. 13, No. 5, May 1976, pp. 282-287.

74. Schaub, H., and Junkins, J. L., *Analytical Mechanics of Space Systems,* AIAA Education Series, 2003, pp. 160-170.

75. Arduini, C., and Baiocco, P., "Active Magnetic Damping Attitude Control for Gravity Gradient Stabilized Spacecraft," *Journal of Guidance, Control and Dynamics*, Vol. 20, No. 1, 1997, pp. 117-122.

76. Clohessy, W. H. and Wiltshire, R. S., "Terminal Guidance System for Satellite Rendezvous," *Journal of the Astronautical Sciences*, Vol. 27, No. 9, Sept. 1960, pp. 653-678.

77. Hill, G. W., "Researches in the Lunar Theory," *American Journal of Mathematics*, Vol. 1, 1878, pp. 5-26.

78. Lawden, D. F., *Optimal Trajectories for Space Navigation*, Butterworths, London, 1963.

79. Tschauner, J. and Hempel, P., "Optimale Beschleunigeungsprogramme fur das Rendezvous-Manover," *Astronautica Acta*, Vol. 10, 1964, pp. 296-307.

80. Vaddi, S. S., Vadali, S. R., and Alfriend, K. T., "Formation Flying: Accommodating Nonlinearity and Eccentricity Perturbations", *Journal of Guidance, Control and Dynamics,* Vol. 26, No. 2, 2003, pp. 214-223.

81. Schweighart, S. A., and Sedwick, R. J., "High-Fidelity Linearized J_2 Model for Satellite Formation Flight," *Journal of Guidance, Control, and Dynamics*, Vol. 25, No. 6, 2002, pp. 1073-1080.

82. Garrison, J. L., Gardner, T. G., and Axelrad, P., "Relative Motion in Highly Elliptical Orbits", Paper AAS-95-194, *AAS/AIAA Spaceflight Mechanics 1995*, Vol. 89, 1995, pp. 1359-1376.

83. Junkins, J. L., Akella, M. R., and Alfriend, K. T., "Non-Gaussian Error Propagation in Orbital Mechanics," *Journal of the Astronautical Sciences*, Vol. 44, Oct.-Dec. 1996, pp. 541-563.

84. Brouwer, D., "Solution of the Problem of Artificial Satellite Theory Without Drag," *The Astronomical Journal*, Vol. 64, No. 1274, 1959, pp378-397.

85. Alfriend K. T., Schaub, H., and Gim, D.-W, "Gravitational Perturbations, Nonlinearity and Circular Orbit Assumption Effects on Formation Flying Control Strategies" Paper AAS 00-012, AAS Guidance and Control 2000, Vol. 104, 2000, pp. 139-158.

86. Gim, D.-W. and Alfriend, K. T., "State Transition Matrix of Relative Motion for the Perturbed Noncircular Reference Orbit," *Journal of Guidance, Control and Dynamics*, Vol. 26, No. 6, Nov.-Dec. 2003, pp. 956-971.

87. Alfriend, K. and T., Yan, H., "An Evaluation and Comparison of Relative Motion Theories," *Journal of Guidance, Control, and Dynamics*, Vol. 28, No. 2, 2005, pp. 254-261.

88. Inalhan, G., Tillerson, M., and How, J. P., "Relative Dynamics and Control of Spacecraft Formations in Eccentric Orbits," *Journal of Guidance, Control, and Dynamics*, Vol. 25, No. 1, January-February 2002, pp. 48-59.

89. Schaub, H. and Alfriend, K.T., "J_2 Invariant Orbits for Spacecraft Formations," *Celestial Mechanics and Dynamical Astronomy*, Vol. 79, 2001, pp. 77-95.

90. Vadali, S. R., Vaddi, S. S., and Alfriend, K. T., "An Intelligent Control Concept for Formation Flying Satellites," *International Journal of Robust and Nonlinear Control,* Vol. 12, 2002, pp.97-115.

91. Alfriend, K. T., Yan, H. and Vadali, S. R., "Nonlinear Considerations in Satellite Formation Flying," Paper No. AIAA 02-4741, *AIAA/AAS Astrodynamics Specialist Conference*, Monterey, CA, August 2002.

92. Alfriend, K. T. and Yan, H., "An Orbital Elements Approach to the Nonlinear Formation Flying Problem," *International Formation Flying Conference: Missions and Technologies*, Toulouse, France, October 2002.

93. Carter, T. E., "New Form for the Optimal Rendezvous Equations Near a Keplerian Orbit," *AIAA J. of Guidance, Control and Dynamics*, Vol. 13, No. 1, Jan.-Feb. 1990.

94. Karlgard, C. D., and Lutze, F. H., " Second Order Relative Motion Equations," AAS 01-464, AAS/AIAA Astrodynamics Conference, Quebec City, Quebec, July 2001.

95. Mitchell, J., W., and Richardson, D. L., "A Third Order Analytical Solution for Relative Motion with a Circular Reference Orbit", Paper AAS 02-147, *AAS/AIAA 2002 Space Flight Mechanics Conference*, San Antonio, TX, January 2002.

96. Schaub, H., "Spacecraft Relative Orbit Geometry Description Through Orbit Element Differences," *AIAA Guidance and Control Conference*, Denver, CO, August 2001.

97. Bond, V. R., "A New Solution for the Rendezvous Problem," Paper AAS 99-178, *AAS/AIAA Space Flight Mechanics Meeting*, Breckenridge, CO, Feb. 1999.

98. Kechichian, J., "The Analysis of the Relative Motion in General Elliptic Orbit with Respect to a Dragging and Precessing Coordinate Frame," Paper AAS 97-733, *AAS/AIAA Astrodynamics Specialist Conference*, Sun Valley, ID, Aug. 1997.

99. Schaub, H., and Alfriend, K. T., "Impulsive Feedback Control to Establish Specific Mean Elements of Spacecraft Formations," *Journal of Guidance, Control and Dynamics,* Vol. 24, No. 4, July 2001, pp. 739-745.

100. Vaddi, S. S., Alfriend, K. T., Vadali, S. R., and Sengupta, P., " Formation Establishment and Reconfiguration Using Impulsive Control," *Journal of Guidance, Control, and Dynamics*, Vol. 28, No. 2, 2005, pp. 262-268.

101. Melton, R. G., "Time-Explicit Representation of Relative Motion Between Elliptical Orbits," *Journal of Guidance, Control and Dynamics*, Vol. 23, No.4, 2000, pp. 604-610.

102. Vadali, S. R., "An Analytical Solution for Relative Motion of Satellites," *DCSSS Conference*, *Cranfield University*, Cranfield, UK, July 2002.

103. Anthony, M. L. and Sasaki, F. T., "Rendezvous Problem for Nearly Circular Orbits," *AIAA Journal*, Vol. 3, No. 9, Sept. 1965, pp.1666-1673.

104. London, H. S., "Second Approximation to the Solution of the Rendezvous Equations," *AIAA Journal*, Vol. 1, No. 7, July 1963, pp.1691-1693.

105. Junkins, J. L., "How Nonlinear Is It?" Paper AAS 03-286, *John L. Junkins Astrodynamics Symposium,* College Station, TX, 23-24 May 2003.

106. Vallado, D. A., *Fundamentals of Astrodynamics and Applications*, McGraw-Hill, New York, 1997, pp. 343-368.

107. Sengupta, P., Vadali, S. R., and Alfriend, K. T., "Modeling and Control of Satellite Formations in High Eccentricity Orbits," Paper AAS 03-277, *John L. Junkins Astrodynamics Symposium,* College Station, TX, 23-24 May 2003.

108. Yan, H, Sengupta, P., Vadali, S. R., and Alfriend, K. T., "Development of a State Transition Matrix for Relative Motion Using the Unit Sphere Approach," Paper No. AAS 04-163, *14th AAS/AIAA Space Flight Mechanics Meeting*, Maui, Hi, Feb. 8-12, 2004.

109. Scharf, D. P., Hadaegh, F. Y., and Ploen, S. R., "A Survey of Spacecraft Formation Flying Guidance and Control (Part II): Control," *Proceedings of the American Control Conference*, Boston, MA, June 2004.

110. H. Schaub, S. R. Vadali, J. L. Junkins and K. T. Alfriend, ``Spacecraft Formation Flying Control Using Mean Orbit Elements, " AAS Journal of Astronautical Sciences, Vol. 48, No. 1, Jan.–March, 2000, pp. 69–87.

111. Vaddi, S. S., and Vadali, S. R., "Linear and Nonlinear Control Laws for Formation Flying," AAS 03-109, *13th AAS/AIAA Space Flight Mechanics Conference*, Ponce, Puerto Rico, February 9-13, 2003.

112. Yan, Q., Yang, G., Kapila, V., and de Queiroz, M. S., "Nonlinear Dynamics and Output Feedback Control of Multiple Spacecraft in Elliptical Orbits," *Proceedings of the American Control Conference*, Chicago IL, June 2000.

113. Abdelkhalik, O., and Alberts, T. E., "Interval Control of Formations in Eccentric Orbits," AAS 04-255, *14th AAS/AIAA Space Flight Mechanics Conference*, Maui, HI, Feb. 8-12, 2004.

114. Won, C. –H., and Ahn, H,-S, "Nonlinear Orbital Dynamics Equations and State-Dependent Riccati Equation Control of Formation Flying Satellites," *The Journal of Astronautical Sciences*, Vol. 51, No. 4, 2003, pp. 433-449.

115. Naasz, B. J., Karlgaard, C. D., and Hall, C. D., "Application of Serval Control Techniques for the Ionospheric Observation Nanosatellite Formation," AAS 02-188, *12th AAS/AIAA Space Flight Mechanics Conference*, San Antonio, TX, Jan. 27-30, 2002.

116. Vignal, P., and Pernicka, H., "Close Spacecraft Formation Keeping," AAS 04-296, *14th AAS/AIAA Space Flight Mechanics Conference*, Maui, HI, Feb. 8-12, 2004.

APPENDIX A

PARTIAL DERIVATIVES

$$a_{10} = -\frac{3}{L^4}$$

$$a_{11} = -\frac{21}{4L^8}\left[\left(\frac{1}{\eta^3}+\frac{1}{\eta^4}\right)-\left(\frac{3}{\eta^3}+\frac{5}{\eta^4}\right)\cos^2 i\right]$$

$$a_{12} = -\frac{33}{64L^{12}}\left[\begin{array}{l}\left(\frac{25}{\eta^5}+\frac{41}{\eta^6}+\frac{9}{\eta^7}-\frac{35}{\eta^8}\right)-\left(\frac{90}{\eta^5}+\frac{222}{\eta^6}+\frac{162}{\eta^7}-\frac{90}{\eta^8}\right)\cos^2 i \\ +\left(\frac{25}{\eta^5}+\frac{189}{\eta^6}+\frac{465}{\eta^7}+\frac{385}{\eta^8}\right)\cos^4 i\end{array}\right]$$

$$a_{21} = -\frac{3}{4L^7}\left[\left(\frac{3}{\eta^4}+\frac{4}{\eta^5}\right)-\left(\frac{9}{\eta^4}+\frac{20}{\eta^5}\right)\cos^2 i\right]$$

$$a_{22} = \frac{3}{64L^{11}}\left[\begin{array}{l}\left(-\frac{125}{\eta^6}-\frac{246}{\eta^7}-\frac{63}{\eta^8}+\frac{280}{\eta^9}\right)+\left(\frac{450}{\eta^6}+\frac{1332}{\eta^7}+\frac{1134}{\eta^8}-\frac{720}{\eta^9}\right)\cos^2 i \\ -\left(\frac{125}{\eta^6}+\frac{1134}{\eta^7}+\frac{3255}{\eta^8}+\frac{3080}{\eta^9}\right)\cos^4 i\end{array}\right]$$

$$a_{31} = \frac{3\sin 2i}{4L^7}\left(\frac{3}{\eta^3}+\frac{5}{\eta^4}\right)$$

$$a_{32} = \frac{3\sin 2i}{64L^{11}}\left[\left(\frac{90}{\eta^5}+\frac{222}{\eta^6}+\frac{162}{\eta^7}-\frac{90}{\eta^8}\right)-2\left(\frac{25}{\eta^5}+\frac{189}{\eta^6}+\frac{465}{\eta^7}+\frac{385}{\eta^8}\right)\cos^2 i\right]$$

$$a_{40} = \frac{12}{L^5}$$

$$a_{41} = \frac{42}{L^9}\left[\left(\frac{1}{\eta^3}+\frac{1}{\eta^4}\right)-\left(\frac{3}{\eta^3}+\frac{5}{\eta^4}\right)\cos^2 i\right]$$

$$a_{42} = \frac{99}{16L^{13}}\left[\begin{array}{l}\left(\frac{25}{\eta^5}+\frac{41}{\eta^6}+\frac{9}{\eta^7}-\frac{35}{\eta^8}\right)-\left(\frac{90}{\eta^5}+\frac{222}{\eta^6}+\frac{162}{\eta^7}-\frac{90}{\eta^8}\right)\cos^2 i \\ +\left(\frac{25}{\eta^5}+\frac{189}{\eta^6}+\frac{465}{\eta^7}+\frac{385}{\eta^8}\right)\cos^4 i\end{array}\right]$$

$$a_{51} = \frac{3}{L^7}\left[\left(\frac{3}{\eta^5}+\frac{5}{\eta^6}\right)-\left(\frac{9}{\eta^5}+\frac{25}{\eta^6}\right)\cos^2 i\right]$$

$$a_{52} = \frac{3}{64L^{11}}\left[\begin{array}{l}\left(\frac{750}{\eta^7}+\frac{1722}{\eta^8}+\frac{504}{\eta^9}-\frac{2520}{\eta^{10}}\right)-\left(\frac{2700}{\eta^7}+\frac{9324}{\eta^8}+\frac{9072}{\eta^9}-\frac{6480}{\eta^{10}}\right)\cos^2 i \\ +\left(\frac{750}{\eta^7}+\frac{7938}{\eta^8}+\frac{26040}{\eta^9}+\frac{27720}{\eta^{10}}\right)\cos^4 i\end{array}\right]$$

$$a_{61} = \frac{3\cos 2i}{2L^7}\left(\frac{3}{\eta^3}+\frac{5}{\eta^4}\right)$$

$$a_{62} = \frac{3}{32L^{11}}\left[\left(\frac{90}{\eta^5}+\frac{222}{\eta^6}+\frac{162}{\eta^7}-\frac{90}{\eta^8}\right)\cos 2i - 2\left(\frac{25}{\eta^5}+\frac{189}{\eta^6}+\frac{465}{\eta^7}+\frac{385}{\eta^8}\right)\left(4\cos^4 i - 3\right)\right]$$

$$a_{71} = \frac{21}{4L^8}\left[\left(\frac{3}{\eta^4}+\frac{4}{\eta^5}\right)-\left(\frac{9}{\eta^4}+\frac{20}{\eta^5}\right)\cos^2 i\right]$$

$$a_{72} = -\frac{33}{64L^{12}}\left[\begin{array}{l}\left(-\frac{125}{\eta^6}-\frac{246}{\eta^7}-\frac{63}{\eta^8}+\frac{280}{\eta^9}\right)+\left(\frac{450}{\eta^6}+\frac{1332}{\eta^7}+\frac{1134}{\eta^8}-\frac{720}{\eta^9}\right)\cos^2 i \\ -\left(\frac{125}{\eta^6}+\frac{1134}{\eta^7}+\frac{3255}{\eta^8}+\frac{3080}{\eta^9}\right)\cos^4 i\end{array}\right]$$

$$a_{81} = -\frac{21\sin 2i}{4L^8}\left(\frac{3}{\eta^3}+\frac{5}{\eta^4}\right)$$

$$a_{82} = -\frac{33\sin 2i}{64L^{12}}\left[\left(\frac{90}{\eta^5}+\frac{222}{\eta^6}+\frac{162}{\eta^7}-\frac{90}{\eta^8}\right)-2\left(\frac{25}{\eta^5}+\frac{189}{\eta^6}+\frac{465}{\eta^7}+\frac{385}{\eta^8}\right)\cos^2 i\right]$$

$$a_{91} = -\frac{3\sin 2i}{4L^7}\left(\frac{9}{\eta^4}+\frac{20}{\eta^5}\right)$$

$$a_{92} = -\frac{3\sin 2i}{64L^{11}}\left[\left(\frac{450}{\eta^6}+\frac{1332}{\eta^7}+\frac{1134}{\eta^8}-\frac{720}{\eta^9}\right)-2\left(\frac{125}{\eta^6}+\frac{1134}{\eta^7}+\frac{3255}{\eta^8}+\frac{3080}{\eta^9}\right)\cos^2 i\right]$$

$$b_{11} = -\frac{21}{2L^8\eta^4}\cos i$$

$$b_{12} = \frac{33\cos i}{16L^{12}}\left[\left(-\frac{9}{\eta^6}-\frac{12}{\eta^7}+\frac{5}{\eta^8}\right)+\left(\frac{5}{\eta^6}+\frac{36}{\eta^7}+\frac{35}{\eta^8}\right)\cos^2 i\right]$$

$$b_{21} = -\frac{6}{L^7\eta^5}\cos i$$

$$b_{22} = -\frac{3\cos i}{16L^{11}}\left[\left(\frac{54}{\eta^7}+\frac{84}{\eta^8}-\frac{40}{\eta^9}\right)-\left(\frac{30}{\eta^7}+\frac{252}{\eta^8}+\frac{280}{\eta^9}\right)\cos^2 i\right]$$

$$b_{31} = -\frac{3}{2L^7\eta^4}\sin i$$

$$b_{32} = -\frac{3\sin i}{16L^{11}}\left[\left(\frac{9}{\eta^6}+\frac{12}{\eta^7}-\frac{5}{\eta^8}\right)-3\left(\frac{5}{\eta^6}+\frac{36}{\eta^7}+\frac{35}{\eta^8}\right)\cos^2 i\right]$$

$$b_{41} = \frac{84}{L^9\eta^4}\cos i$$

$$b_{42} = -\frac{99\cos i}{4L^{13}}\left[\left(-\frac{9}{\eta^6}-\frac{12}{\eta^7}+\frac{5}{\eta^8}\right)+\left(\frac{5}{\eta^6}+\frac{36}{\eta^7}+\frac{35}{\eta^8}\right)\cos^2 i\right]$$

$$b_{51} = \frac{30}{L^7\eta^6}\cos i$$

$$b_{52} = -\frac{3\cos i}{16L^{11}}\left[\left(-\frac{378}{\eta^8}-\frac{672}{\eta^9}+\frac{360}{\eta^{10}}\right)+\left(\frac{210}{\eta^8}+\frac{2016}{\eta^9}+\frac{2520}{\eta^{10}}\right)\cos^2 i\right]$$

$$b_{61} = -\frac{3}{2L^7\eta^4}\cos i$$

$$b_{62} = -\frac{3\cos i}{16L^{11}}\left[\left(\frac{9}{\eta^6}+\frac{12}{\eta^7}-\frac{5}{\eta^8}\right)-3\left(\frac{5}{\eta^6}+\frac{36}{\eta^7}+\frac{35}{\eta^8}\right)\left(1-3\sin^2 i\right)\right]$$

$$b_{71} = \frac{42}{L^8\eta^5}\cos i$$

$$b_{72} = \frac{33\cos i}{16L^{12}}\left[\left(\frac{54}{\eta^7}+\frac{84}{\eta^8}-\frac{40}{\eta^9}\right)-\left(\frac{30}{\eta^7}+\frac{252}{\eta^8}+\frac{280}{\eta^9}\right)\cos^2 i\right]$$

$$b_{81} = \frac{21}{2L^8\eta^4}\sin i$$

$$b_{82} = \frac{33\sin i}{16L^{12}}\left[\left(\frac{9}{\eta^6}+\frac{12}{\eta^7}-\frac{5}{\eta^8}\right)-3\left(\frac{5}{\eta^6}+\frac{36}{\eta^7}+\frac{35}{\eta^8}\right)\cos^2 i\right]$$

$$b_{91} = \frac{6}{L^7\eta^5}\sin i$$

$$b_{92} = \frac{3\sin i}{16L^{11}}\left[\left(\frac{54}{\eta^7}+\frac{84}{\eta^8}-\frac{40}{\eta^9}\right)-3\left(\frac{30}{\eta^7}+\frac{252}{\eta^8}+\frac{280}{\eta^9}\right)\cos^2 i\right]$$

APPENDIX B

SMALL ECCENTRICITY STATE TRANSITION MATRIX

In this Appendix the relative motion state transition matrix (STM) for small eccentric Chief orbits is derived. This STM will include $O(e)$ terms for the non-J_2 portion and only $O(e^0)$ for the J_2 portion. The STM is obtained from[8] by setting $q_1 = q_2 = 0$ in all the terms multiplied by J_2 and retaining only the first order terms in q_1 and q_2 in the non-J_2 terms. The notation of Ref. 86 will be used. Assume $\Sigma = A(t) + \alpha B(t)$, R is radius of the Chief orbit, p is a semi-parameter, V_r and V_t are the radial and transversal velocity of the Chief, respectively.

Σ and Σ^{-1}

Σ **Matrix** (refer to APPENDIX A of Ref. 86)

The matrices as they are. $O(e)$ approximations for R, V_r, V_t and p could be made but this does not shorten the calculations so they are not changed.

Mean to Osculating (refer to APPENDIX E of Ref.86)

Since no eccentricity terms are retained the mean to osculating transformation for zero eccentricity is;

$$
\begin{aligned}
&e_{osc} = e_m + \varepsilon\left[e^{(lp)} + e^{(sp1)} + e^{(sp2)} \right] \\
&e = \left(a, \theta, i, q_1, q_2, \Omega\right)^T \\
&\overline{a} = a / R_e, \theta = f + \omega, q_1 = e\cos\omega, q_2 = e\sin\omega \\
&\varepsilon = -J_2
\end{aligned}
\tag{1}
$$

$$
e^{(lp)} = 0 \tag{2}
$$

$$
\begin{aligned}
&a^{(sp1)} = \theta^{(sp1)} = i^{(sp1)} = \Omega^{(sp1)} = 0 \\
&q_1^{(sp1)} = \frac{3\left(1-3\cos^2 i\right)}{4\overline{a}^2}\cos\theta \\
&q_2^{(sp1)} = \frac{3\left(1-3\cos^2 i\right)}{4\overline{a}^2}\sin\theta
\end{aligned}
\tag{3}
$$

$$
\begin{aligned}
&a^{(sp2)} = -\left(\frac{3R_e \sin^2 i}{2\overline{a}}\right)\cos 2\theta \\
&\lambda^{(sp2)} = -\frac{3\left(3-5\cos^2 i\right)}{8\overline{a}^2}\sin 2\theta \\
&\theta^{(sp2)} = \lambda^{(sp2)} + \left(\frac{\sin^2 i}{\overline{a}^2}\right)\sin 2\theta \\
&i^{(sp2)} = -\left(\frac{3\sin 2i}{8\overline{a}^2}\right)\cos 2\theta \\
&q_1^{(sp2)} = -\left(\frac{\sin^2 i}{8\overline{a}^2}\right)\left(3\cos\theta + 7\cos 3\theta\right) \\
&q_2^{(sp2)} = \left(\frac{\sin^2 i}{8\overline{a}^2}\right)\left(3\sin\theta - 7\sin 3\theta\right) \\
&\Omega^{(sp2)} = -\left(\frac{3\cos i}{4\overline{a}^2}\right)\sin 2\theta
\end{aligned}
\tag{4}
$$

***D* Matrix** (refer to APPENDIX E of Ref. 86)

Only the non-zero terms are presented. Assume $\Theta = \dfrac{1}{1-5\cos^2 i}$.

$$D = \frac{\partial e_{osc}}{\partial e_m} = I - J_2\left[D^{(lp)} + D^{(sp1)} + D^{(sp2)}\right] \tag{5}$$

$$D_{24}^{(lp)} = -\frac{\sin^2 i}{8\bar{a}^2}\left(1-10\Theta\cos^2 i\right)\sin\theta, D_{25}^{(lp)} = -\frac{\sin^2 i}{8\bar{a}^2}\left(1-10\Theta\cos^2 i\right)\cos\theta \tag{6a}$$

$$D_{44}^{(lp)} = -\frac{\sin^2 i}{16\bar{a}^2}\left(1-10\Theta\cos^2 i\right), \Theta = \left(1-5\cos^2 i\right)^{-1} \tag{6b}$$

$$D_{55}^{(lp)} = \frac{\sin^2 i}{16\bar{a}^2}\left(1-10\Theta\cos^2 i\right) \tag{6c}$$

$$D_{14}^{(sp1)} = \frac{3R_e\left(1-3\cos^2 i\right)}{2\bar{a}}\cos\theta,\ D_{15}^{(sp1)} = \frac{3R_e\left(1-3\cos^2 i\right)}{2\bar{a}}\sin\theta \tag{7a}$$

$$D_{24}^{(sp1)} = \frac{9}{4\bar{a}^2}\left(1-5\cos^2 i\right)\sin\theta, D_{25}^{(sp1)} = -\frac{9}{4\bar{a}^2}\left(1-5\cos^2 i\right)\cos\theta \tag{7b}$$

$$D_{41}^{(sp1)} = -\frac{3\left(1-3\cos^2 i\right)}{2R_e\bar{a}^3}\cos\theta, D_{42}^{(sp1)} - \frac{3\left(1-3\cos^2 i\right)}{4\bar{a}^2}\sin\theta, D_{43}^{(sp1)} = \frac{9\sin 2i}{4\bar{a}^2}\cos\theta \tag{7c}$$

$$D_{44}^{(sp1)} = \frac{3\left(1-3\cos^2 i\right)}{8\bar{a}^2}\left(2+\cos 2\theta\right),\ D_{45}^{(sp1)} = \frac{3\left(1-3\cos^2 i\right)}{8\bar{a}^2}\sin 2\theta \tag{7d}$$

$$D_{51}^{(sp1)} = -\frac{3\left(1-3\cos^2 i\right)}{2R_e\bar{a}^3}\sin\theta, D_{52}^{(sp1)} = \frac{3\left(1-3\cos^2 i\right)}{4\bar{a}^2}\cos\theta, D_{53}^{(sp1)} = \frac{9\sin 2i}{4\bar{a}^2}\cos\theta \tag{7e}$$

$$D_{54}^{(sp1)} = \frac{3\left(1-3\cos^2 i\right)}{8\bar{a}^2}\sin 2\theta, D_{55}^{(sp1)} = \frac{3\left(1-3\cos^2 i\right)}{8\bar{a}^2}\left(2-\cos 2\theta\right) \tag{7f}$$

$$D_{64}^{(sp1)} = \frac{9\cos i}{2\overline{a}^2}\sin\theta, D_{65}^{(sp1)} = -\frac{9\cos i}{2\overline{a}^2}\cos\theta \tag{7g}$$

$$D_{11}^{(sp2)} = \left(\frac{3\sin^2 i}{2\overline{a}^2}\right)\cos 2\theta, D_{12}^{(sp2)} = \left(\frac{3R_e \sin^2 i}{\overline{a}}\right)\sin 2\theta, D_{13}^{(sp2)} = -\left(\frac{3R_e \sin 2i}{2\overline{a}}\right)\cos 2\theta \tag{8a}$$

$$D_{14}^{(sp2)} = -\left(\frac{9R_e \sin^2 i}{4\overline{a}}\right)\left(\cos\theta + \cos 3\theta\right), D_{15}^{(sp2)} = \left(\frac{9R_e \sin^2 i}{4\overline{a}}\right)\left(\sin\theta - \sin 3\theta\right) \tag{8b}$$

$$D_{21}^{(sp2)} = -\left(\frac{6-7\sin^2 i}{4R_e\overline{a}^3}\right)\sin 2\theta, D_{22}^{(sp2)} = \left(\frac{6-7\sin^2 i}{4\overline{a}^2}\right)\cos 2\theta, D_{23}^{(sp2)} = -\left(\frac{7\sin 2i}{8\overline{a}^2}\right)\sin 2\theta \tag{8c}$$

$$D_{24}^{(sp2)} = \left(\frac{24-47\sin^2 i}{32\overline{a}^2}\right)\sin\theta + \frac{\cos^2 i}{4\overline{a}^2}\sin 3\theta, D_{25}^{(sp2)} = \left(\frac{24-47\sin^2 i}{32\overline{a}^2}\right)\cos\theta - \frac{\cos^2 i}{4\overline{a}^2}\cos 3\theta \tag{8d}$$

$$D_{31}^{(sp2)} = \left(\frac{3\sin 2i}{4R_e\overline{a}^3}\right)\cos 2\theta, D_{32}^{(sp2)} = \left(\frac{3\sin 2i}{4\overline{a}^2}\right)\sin 2\theta, D_{33}^{(sp2)} = -\left(\frac{3\cos 2i}{4\overline{a}^2}\right)\cos 2\theta \tag{8e}$$

$$D_{34}^{(sp2)} = -\left(\frac{\sin 2i}{8\overline{a}^2}\right)\left(3\cos\theta + \cos 3\theta\right), D_{35}^{(sp2)} = \left(\frac{\sin 2i}{8\overline{a}^2}\right)\left(3\sin\theta - \sin 3\theta\right) \tag{8f}$$

$$D_{41}^{(sp2)} = \left(\frac{\sin^2 i}{4R_e\overline{a}^3}\right)\left(3\cos\theta + 7\cos 3\theta\right), D_{42}^{(sp2)} = \left(\frac{3\sin^2 i}{8\overline{a}^2}\right)\left(\sin\theta + 7\sin 3\theta\right) \tag{8g}$$

$$D_{43}^{(sp2)} = -\left(\frac{\sin 2i}{8\overline{a}^2}\right)\left(3\cos\theta + 7\cos 3\theta\right) \tag{8h}$$

$$\begin{aligned} D_{44}^{(sp2)} &= -\left(\frac{3\sin^2 i}{16\overline{a}^2}\right)\left(3 + 10\cos 2\theta + 3\cos 4\theta\right) \\ D_{45}^{(sp2)} &= \frac{3\left(3-5\cos^2 i\right)}{8\overline{a}^2}\sin 2\theta - \left(\frac{9\sin^2 i}{16\overline{a}^2}\right)\sin 4\theta \end{aligned} \tag{8i}$$

$$D_{51}^{(sp2)} = -\left(\frac{\sin^2 i}{4R_e\bar{a}^3}\right)\left(3\sin\theta - 7\sin 3\theta\right), D_{52}^{(sp2)} = \left(\frac{3\sin^2 i}{8\bar{a}^2}\right)\left(\cos\theta - 7\cos 3\theta\right) \tag{8j}$$

$$D_{53}^{(sp2)} = \left(\frac{\sin 2i}{8\bar{a}^2}\right)\left(3\sin\theta - 7\sin 3\theta\right) \tag{8k}$$

$$D_{54}^{(sp2)} = -\frac{3\left(3-5\cos^2 i\right)}{8\bar{a}^2}\sin 2\theta - \left(\frac{9\sin^2 i}{16\bar{a}^2}\right)\sin 4\theta, D_{55}^{(sp2)} = \left(\frac{3\sin^2 i}{16\bar{a}^2}\right)\left(3-10\cos 2\theta + 3\cos 4\theta\right) \tag{8l}$$

$$D_{61}^{(sp2)} = \left(\frac{3\cos i}{2R_e\bar{a}^3}\right)\sin 2\theta, D_{62}^{(sp2)} = -\left(\frac{3\cos i}{2\bar{a}^2}\right)\cos 2\theta, D_{63}^{(sp2)} = \left(\frac{3\sin i}{4\bar{a}^2}\right)\sin 2\theta \tag{8m}$$

$$D_{64}^{(sp2)} = -\left(\frac{\cos i}{4\bar{a}^2}\right)\left(3\sin\theta + \sin 3\theta\right), D_{65}^{(sp2)} = -\left(\frac{\cos i}{4\bar{a}^2}\right)\left(3\cos\theta - \cos 3\theta\right) \tag{8n}$$

$\bar{\phi}_{\bar{e}}$ **Matrix** (refer to APPENDIX D of Ref. 86)

Again, only the non-zero terms are supplied.

$$\begin{aligned}
&\alpha = 3J_2R_e^2 \\
&G_\theta = \frac{nR}{V_t}, G_{\theta_0} = -G_\theta\left(t = t_0\right) \\
&G_{q_1} = -\left(\frac{R}{a}\right)\left(1+\frac{R}{a}\right)\sin\theta, G_{q_{10}} = -G_{q_1}\left(t = t_0\right) \\
&G_{q_1} = \left(\frac{R}{a}\right)\left(1+\frac{R}{a}\right)\cos\theta, G_{q_{10}} = -G_{q_1}\left(t = t_0\right)
\end{aligned} \tag{9}$$

$$\bar{\phi}_{\bar{e}11} = 1 \tag{10}$$

$$\bar{\phi}_{\bar{e}21} = -\frac{3n_0\left(t-t_0\right)}{2a_0 G_\theta}\left[1+\left(\frac{7\alpha}{6a_0^2}\right)\left(4\cos^2 i_0 - 1\right)\right], \bar{\phi}_{\bar{e}22} = -\frac{G_{\theta_0}}{G_\theta} \tag{11a}$$

$$\bar{\phi}_{\bar{e}23} = -\frac{2\alpha n_0\left(t-t_0\right)\sin 2i_0}{a_0^2 G_\theta} \tag{11b}$$

$$\bar{\phi}_{\bar{e}24} = -\frac{1}{G_\theta}\left[G_{q_{10}} + G_{q_1}\cos\left(\Delta\omega\right) + G_{q_2}\sin\left(\Delta\omega\right)\right], \Delta\omega = \dot{\omega}^{(s)}\left(t-t_0\right) \tag{11c}$$

$$\bar{\phi}_{\bar{e}25} = -\frac{1}{G_\theta}\left[G_{q_{20}} - G_{q_1}\sin\left(\Delta\omega\right) + G_{q_2}\cos\left(\Delta\omega\right)\right] \tag{11d}$$

$$\bar{\phi}_{\bar{e}33} = 1 \tag{12}$$

$$\bar{\phi}_{\bar{e}44} = \cos\left(\Delta\omega\right), \bar{\phi}_{\bar{e}45} = -\sin\left(\Delta\omega\right) \tag{13a}$$

$$\bar{\phi}_{\bar{e}54} = \sin\left(\Delta\omega\right), \bar{\phi}_{\bar{e}55} = \cos\left(\Delta\omega\right) \tag{13b}$$

$$\bar{\phi}_{\bar{e}61} = \left(\frac{7\alpha}{4a_0^2}\right)\left(\frac{n_0\cos i_0}{a_0}\right)\left(t-t_0\right), \bar{\phi}_{\bar{e}63} = \left(\frac{\alpha}{2a_0^2}\right)\left(n_0\sin i_0\right)\left(t-t_0\right), \bar{\phi}_{\bar{e}66} = 1 \tag{13c}$$

VITA

Hui Yan is a Ph.D. candidate in the Department of Aerospace Engineering, Texas A&M University. He obtained his B.Eng. in Beijing Institute of Technology in 1984, M.Eng. in Northwestern Polytechnical University in 1990, and D.Eng. in Northwestern Polytechnical University in 1996. His current research interest includes: attitude control, formation flying and real-time optimal control.

Hui Yan may be reached at 200 Charles Haltom Ave., 3H, College Station, TX 77840. His email address is hyan@tamu.edu.